INFORMATION TO USERS

This manuscript has been reproduced from the microfilm master. UMI films the text directly from the original or copy submitted. Thus, some thesis and dissertation copies are in typewriter face, while others may be from any type of computer printer.

The quality of this reproduction is dependent upon the quality of the copy submitted. Broken or indistinct print, colored or poor quality illustrations and photographs, print bleedthrough, substandard margins, and improper alignment can adversely affect reproduction.

In the unlikely event that the author did not send UMI a complete manuscript and there are missing pages, these will be noted. Also, if unauthorized copyright material had to be removed, a note will indicate the deletion.

Oversize materials (e.g., maps, drawings, charts) are reproduced by sectioning the original, beginning at the upper left-hand corner and continuing from left to right in equal sections with small overlaps.

Photographs included in the original manuscript have been reproduced xerographically in this copy. Higher quality 6" x 9" black and white photographic prints are available for any photographs or illustrations appearing in this copy for an additional charge. Contact UMI directly to order.

Bell & Howell Information and Learning
300 North Zeeb Road, Ann Arbor, MI 48106-1346 USA
800-521-0600

Université d'Ottawa · University of Ottawa

The Effect of Sodium Dodecyl Sulfate Solutions as Gelation Media on The Formation of PES Membranes

by

Alsdeg M. Alsari

A thesis submitted to the Faculty of Graduate and Postdoctoral Studies
in partial fulfillment of the requirements for the degree of
MASTER OF APPLIED SCIENCE
in the Department of Chemical Engineering
University of Ottawa

1999

Abstract

Sodium Dodecyl Sulfate (SDS) aqueous solutions have been used as gelation media in the preparation of polyethersulfone (PES) membranes. The casting solution composition was the same for all casted membranes. Two temperatures were applied to the gelation media: 4°C and 20°C. The concentration of the SDS was changed from 0 to 3.0 g/L at 4°C and from 0 to 1.6 g/L at 20°C.

The surface tension of the gelation media was measured by the drop weight method and their electrical conductivities were measured by CDM 80 conductivity meter. The membranes were characterized by solute transport parameters obtained from separation experiments and roughness parameters obtained by the atomic force microscope technique (AFM).

The molecular weight cut-off (MWCO) of the studied membranes was found between 9,000 and 88,000 Daltons for membranes gelled at 4°C, and between 28,000 and 85,000 Daltons for membranes gelled at 20°C. For both temperatures, the lowest MWCO was obtained for membranes gelled in gelation media with a surface tension slightly lower than the critical micelles concentration (CMC). The pore sizes were found to be between 3.04 and 10.37 nm for membranes gelled at 4°C and between 4.48 and 10.74 nm for membranes gelled at 20°C. The pore density ranged from 4.79 to 939 pores/μm^2 for membranes gelled at 4°C and from 8.14 to 109.6 pores/μm^2 for membranes gelled at 20°C. In general, MWCO and pore size decreased with an increase of SDS concentration in gelation media below CMC, and increased with an increase in SDS concentration in gelation media above CMC.

Images of membranes surfaces, by AFM technique, showed that nodules and depressions decreased with a decrease in pore size. The roughness of membranes increased with an increase in pore size and MWCO.

Résumé

Des solutions aqueuses de dodécylsulfate de sodium (D.S.S.) ont été utilisées comme milieux de gélification dans la préparation de membranes de polyethersulfone (P.E.S.). La composition de la solution de moulage était la même pour toutes les membranes moulées. Deux températures ont été appliquées aux milieux de gélification: 4°C et 20°C. La concentration de D.S.S. a été changée de 0 à 4°C et de 0 à 1.6 g/L à 20°C.

La tension superficielle des milieux de gélification a été mesurée en utilisant la méthode par chute de poids, et leur conductivité a été calculée avec un conductimètre CDM 80. Les membranes se caractérisaient par le transport du soluté et par les paramètres de rugosité obtenus par la technique du microscope à force atomique (AFM).

La limite du poids moléculaire des membranes étudiées se situait entre 9 000 et 88 000 Daltons pour les membranes gélifiées à 4°C, et entre 28 000 et 85 000 Daltons pour les membranes gélifiées à la 20°C. Le poids moléculaire limite le plus bas a été obtenu pour des membranes gélifiées dans des milieux de gélification ayant une tension superficielle légèrement inférieure à la concentration critique pour la formation de micelles (CCM). La dimension des pores variait entre 3,04 et 10,37 nm pour les membranes gélifiées à 4°C, et entre 4,48 et 10,74 nm pour les membranes gélifiées à 20°C. La densité des pores variait de 4,79 à 939 pores/μm^2 pour les membranes gélifiées à 4°C, et de 8,14 à 109,6 pores/μm^2. En règle générale, la limite du poids moléculaire et la dimension des pores diminuaient avec l'augmentation de D.S.S. dans la composition des milieux de gélification inférieurs à la CCM, et augmentaient avec l'augmentation de D.S.S. dans des milieux de gélification supérieurs à la CCM. Grâce à la technique AFM, des images de la surface des membranes ont permis de démontrer que les nodules et les dépressions diminuaient avec la diminution

de la dimension des pores. La rugosité des membranes augmentait avec une augmentation de la dimension des pores et de la limite du poids moléculaire.

ACKNOWLEDGMENTS

I would like to thank Prof. T. Matsuura for his supervision and guidance throughout this research work. Thanks are also due to Dr. K.C. Khulbe for his time and technical help.

The author is grateful for the financial support of the ministry of high education of Libya.

Technical support provided by the machine shop in the Department of Chemical Engineering is also appreciated. Finally, I would like to take this opportunity to thank all the fellow students and researchers at Industrial Membrane Research Institute for their help and valuable discussions.

Table of Contents

LIST OF TABLES

LIST OF FIGURES

Nomenclature

Symbols

A	permeability coefficient (mol/m2.s.Pa)
A_0	intercept of linear regression on log-normal probability paper
A_1	slope of linear regression on log-normal probability paper
A	area (m^2)
a	Stoke radius (cm)
a_w	water activity
B	mobility coefficient ($mol.m^2/ J.s$)
B	solute permeability coefficient (m/s)
c	concentration (mol/m^3)
c_f	solute concentration in the feed solution (mol/m^3)
c_p	solute concentration in the permeat (mol/m^3)
c_j	salt concentration (mol/m^3)
Δc_s	solute concentration difference across the membrane (mol/m^3)
D_i	diffusion coefficient of component i (m^2/s)
D_{AB}	diffusivity (m^2/s)
D_w	water diffusivity (m^2/s)
d_{max}	maximum pore size (nm)
d_{min}	minimum pore size (nm)
d_p	pore size (nm)
d_s	solute size (nm)
dE/dt	the rate of mass transfer in solvent extraction (mol/s)

f solute separation (%)

f_i fraction of pores of diameter d_i

f_i^s activity coefficient referring to the pure phase

G surface Gibbs free energy (mJ)

ΔG free enthalpy of mixing (J/mole)

J total solvent flux through all the pores (m^3/m^2s)

J_i solvent flux through the pores of diameter d_i (m^3/m^2s)

J_s solute flux through the membrane ($mol/m^2.s$)

J_w water flux through the membrane (m^3/m^2s)

Ks distribution coefficient of solute

K_{01}, K_{02} overall mass transfer coefficients based on phases 1 and 2 (m/s)

k Boltzmann's constant

Lx, Ly dimensions of the surface $f(x, y)$

M molecular weight (kg/mol)

N total number of pores per unit area

N_i number of pores (per unit area) having diameter of d_i

N number of molecules

ΔP pressure drop cross pores/membrane (kPa)

R universal gas constant (J/mol.K)

R_a mean roughness (nm)

R_q root mean square of Z data (nm)

R_z mean difference between five highest peaks and five lowest valleys (nm)

R rejection coefficient

r	coefficient of correlation
r_B	capillary tip diameter (cm)
S_p	surface porosity (%)
T	absolute temperature (K)
T_k	Kraft point (K)
V	drop volume (ml)
v	molar volume of the solute (cm^3/mol)
w	work (J)
W	drop weight (g)
X_i	mole fraction of component i
X_m	mole fraction of the solute in the micelles
Z	the vertical distance that the tip moves on the membrane surface
Z_{avg}	average of the Z value (nm)
Z_i	current Z value (nm)
δ	skin layer thickness (m, μm)
η	solvent (water) viscosity ($N\ s/m^2$)
μ_p	geometric mean pore size of the membrane (nm)
μ_s	geometric mean solute size (nm)
μ_i	chemical potential of component i (J/kg)
μ_b^o	chemical potential of solute in the bulk organic phase (J/kg)
μ_m	chemical potential of solute in the micellar solution (J/kg)
μ_m^o	chemical potential in micelles (J/kg)

σ_g geometric standard deviation of solute size

σ_p geometric standard deviation of pore size

$\Delta\pi$ osmotic pressure difference (kPa)

γ interfacial tension (mN/m)

$[\eta]$ intrinsic viscosity of PEG/PEO (dL/g)

Γ_i surface excess of component i

Abbreviations

AFM	atomic force microscopy
CMC	critical micelles concentration
NF	nanofiltration
MWCO	molecular weight cut-off
NMP	N-methylpyrrolidone
NF	nanofiltration
PEG	polyethylene glycol
PEO	polyethylene oxide
PVP	polyvinylpyrrolidone
PWP	pure water permeation
RO	reverse osmosis
SEM	scanning electron microscope
TEM	transmission electron microscope
TOC	total organic carbon
UF	ultrafiltration

CHAPTER 1

1. INTRODUCTION

1.1 Definition and Classification of Membranes

Membrane is a semipermeable barrier that separates two phases and membrane processes are generally separation processes. A membrane process requires two bulk phases physically separated by the membrane.

In a membrane separation process, the feed is a mixture of phases (liquid-liquid, liquid-solid, liquid-gas, or gas-gas). The membrane is preferentially selective to one or more of the species in the feed mixture. The result will be two new phases, one is enriched with the selected species and the other is depleted. The enriched phase is called retentate or concentrate stream and the depleted phase is called the permeate stream (Figure 1.1), which implies that either the concentrate or permeate stream is the product. If the aim is concentration, the retentate will usually be the product stream. However, in the case of purification, both the retentate or permeate can yield the desired product.

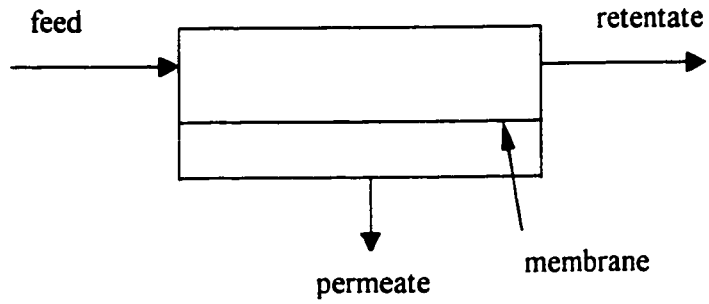

Figure 1.1. Schematic representation of a membrane process where the feed is separated into a retentate and a permeate stream.

One or more driving forces cause the movement of the species across the membrane. These driving forces arise from a gradient in chemical or electrical potential. A gradient in chemical potential may be due to a concentration or pressure gradient.

Membranes can be biological or synthetic, organic or inorganic, liquid or solid, symmetric or asymmetric, homogenous or heterogeneous, and porous or non-porous (Mulder, 1996).

The principal characteristics of commercialised membrane separation processes can be specified based on the following aspects (Kesting, 1985):

- Separation goal.
- Size of species retained.
- Nature of species transported through the membrane (electrolytic or volatile).
- Driving force.

- Mechanism for transportation.

- Phase of feed and permeate streams.

Table 1.1 shows different types of membranes and membrane processes that have been developed for different applications (Franken and Fane, 1990).

1.2 Filtration Membranes

Various pressure-driven membrane processes can be used to concentrate or purify a dilute (aqueous or non-aqueous) solution. The characteristic of these processes is that the solvent is the continuous phase and that the concentration of the solute is relatively low. The size and chemical properties of the solute determine the structure (i.e., pore size and pore size distribution) necessary for the membrane employed.

Various processes can be distinguished depending on the size of the solute and consequently on the membrane structure. These processes are microfiltration, ultrafiltration, nanofiltration and reverse osmosis. Because of a driving force (i.e., the applied pressure) the solvent and various solute molecules permeate through the membrane, whereas other molecules or particles are rejected to various extents depending on the structure of the membrane.

As we go from microfiltration through ultrafiltration and nanofiltration to reverse osmosis, the size (or molecular weight) of the particles or molecules to be separated diminishes and consequently the pore size in the membrane must become smaller.

Table 1.1 Membrane processes and their applications (Franken and Fane, 1990).

Process	Driving force	Applications
Electrodialysis (ED)	Electrical potential difference	desalination of brackish water removal of metals in wastewater
Microfiltration (MF)	Pressure difference (10-100 kPa)	removal of colloids from waste streams removal of dust particles from air
Ultrafiltration (UF)	Pressure difference (0.1-1 MPa)	separation of oil/water emulsions recovery of proteins recovery of electrophoretic paints
Nanofiltration (NF)	Pressure difference (0.5-2 MPa)	treatment of electroplating rinse water
Reverse Osmosis (RO)	Pressure difference (2-10 MPa)	desalination of sea water removal of nitrate from ground water
Liquid Membranes (LM)	Concentration difference	recovery of plating chemicals
Gas Separation (GS)	Pressure difference (2-10 MPa)	air separation removal of CO_2 from methane
Vapor Permeation (VP)	Partial pressure difference	removal of condensable solvents from air
Pervaporation (PV)	Partial pressure difference	dehydration of solvents removal of organics from waste water
Membrane Distillation (MD)	Temperature difference	desalination of brine

This implies that the resistance of the membrane to mass transfer increases and hence the applied pressure (driving force) has to be increased to obtain the same flux. However, no sharp distinction can be drawn between the various processes. A schematic drawing of the separation range involved in these various processes is given in Figure 1.2. It is possible to distinguish between the various processes in terms of membrane structure. In the case of microfiltration, the complete membrane thickness may contribute towards transport resistance, when a symmetrical porous structure is involved. The membrane thickness can extend from 10 μm to more than 150 μm. In ultrafiltration and hyperfiltration, on the other hand, asymmetric membranes are used in which a thin, relatively dense top layer (thickness 0.1-1.0 μm) is supported by a porous substructure (thickness ≈ 50-150 μm). The hydraulic resistance is almost completely located in the top-layer, the sub-layer having only a supporting function. The flux through these and other membranes is inversely proportional to the effective thickness.

1.3 Historical Developments

According to Cheryan (1986), the phenomenon of membrane separation was first observed by La Hire. He showed that the pork bladder is more permeable to water than to alcohol. In 1748, Abbe Nollet reported the discovery of osmosis, when he observed that water diffused from a dilute solution to a more concentrated one when separated by a semipermeable membrane. In 1865, Fick developed the first synthetic membrane, made of nitrocellulose. Two years later, Traube reported an artificial membrane.

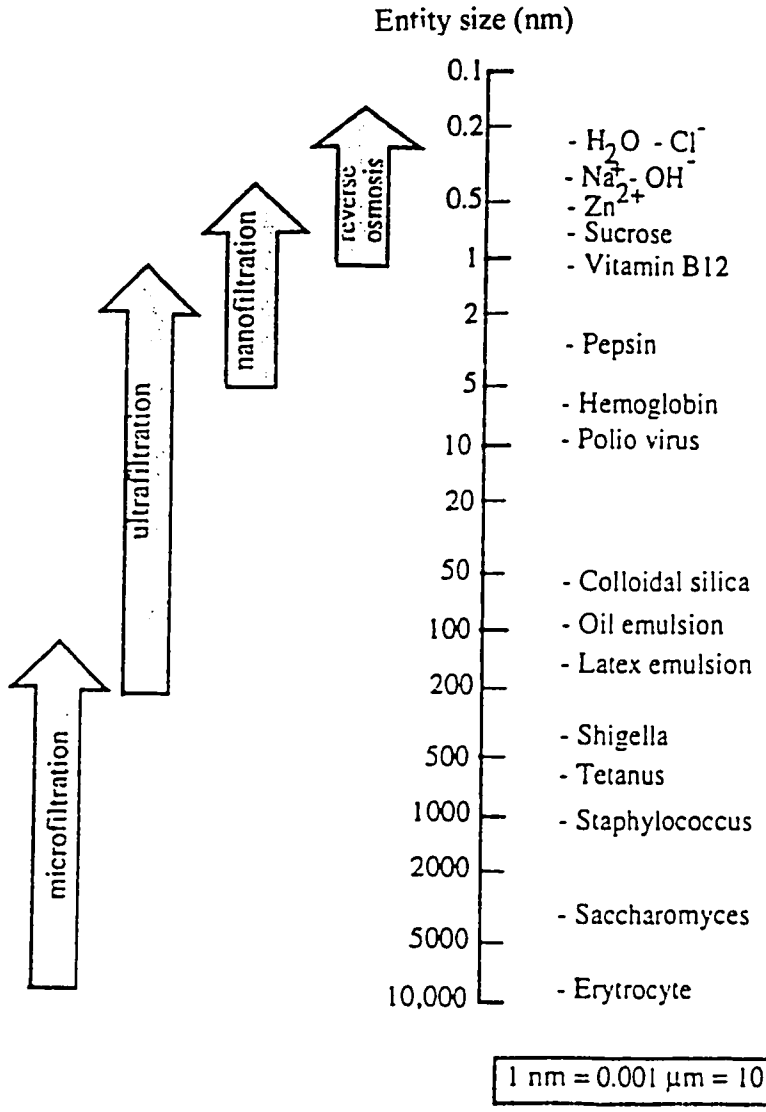

Figure 1.2. Application range of microfiltration, ultrafiltration, nanofiltration and reverse osmosis (Mulder, 1996).

The development of membrane separation processes in the early stages was very slow. The major problems of early membranes were their insufficient selectivity and low flux, making them costly and uncompetitive compared with other separation processes. The intrinsic characteristic of all membranes, high selectivity comes at the cost of low permeability, was behind the poor performance of the early membranes.

In 1961, Loeb and Sourirajan reported the invention of the first integrally-skinned membrane. This invention was considered the key to the emergence of the current worldwide interest in membrane separations. This membrane is known as the Loeb-Sourirajan membrane (Kesting, 1985).

An asymmetric integrally-skinned membrane is a bilayer consisting of a thin (~0.2 μm) dense skin and a thick (~ 100 μm) porous substructure (Figure 1.3). The term integral means that both layers are of the same material and are formed more or less simultaneously as a result of the gelation of a single solution by the general process known as phase inversion (Kesting, 1985).

1.4 Phase Inversion Process of Membrane Making

Many methods are used for membrane preparation, but most of the asymmetric membranes are prepared by the Loeb technique (Matsuura, 1993). To obtain a membrane, polymer is dissolved in a solvent, which can be a single component solvent or a mixture of solvents and nonsolvents.

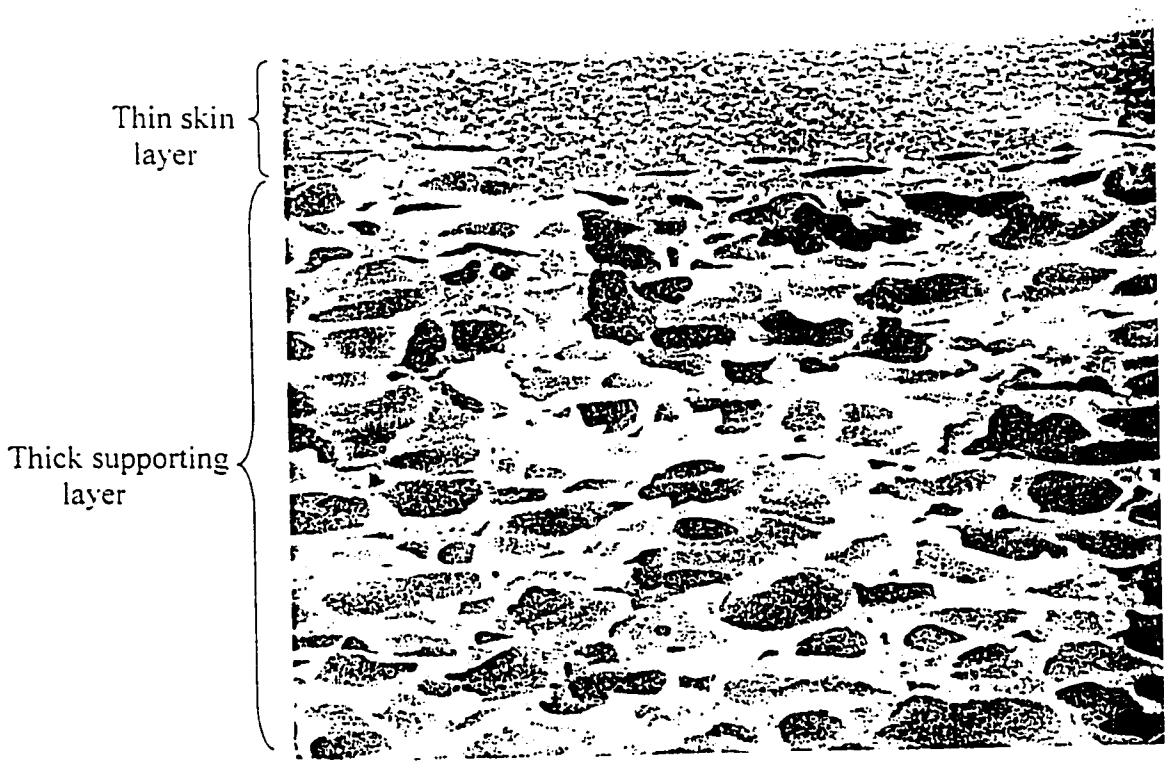

Figure 1.3. Cross-section of an asymmetric cellulose acetate membrane (Kesting, 1985).

The solution is then cast to a thin film. A change in composition of the polymer solution occurs either by solvent evaporation (dry process), or by solvent and nonsolvent (gelation media) exchange in the gelation bath (wet process). The result is two phases: a polymer-rich solid phase, the membrane, and a solvent-rich liquid phase, which forms the liquid-filled membrane pores.

1.5 Surfactants

Surfactants are a class of industrially important amphiphilic substances. Amphiphilic substances are those that possess both hydrophilic and hydrophobic parts at the same time (i.e., water-attracting and water-repelling parts, respectively). A surfactant (a contraction of the term *surface-active agent*) is a substance that, when present at low concentration in a system, has the property of adsorbing onto the surfaces or interfaces of the system and of altering to a marked degree the surface or interfacial free energies of those surfaces (or interfaces). The hydrophilic (the head-group) and hydrophobic (the tail) parts of the surfactant are linked together by a chemical bond and consequently cannot separate as they would if the two parts were free. Surfactants are categorised into four groups depending on the charge of the head-group: nonionic (0), anionic (-), cationic (+) and zwitterionic (±) surfactants (Jonsson and Jonsson, 1991). The surfactant used in this work, Sodium Dodecyl Sulfate (SDS), is classified as an anionic surfactant.

1.5.1 Sodium Dodecyl Sulphate (SDS)

SDS is classified as an alcohol sulphate (AS) anionic surfactant. Alcohol sulphates are now generally made from primary linear alcohols, which can be natural or synthetic. Organic sulphates are the esters of sulphuric acid:

$$ROH + H_2SO_4 \rightarrow ROSO_3H$$

"The sulphur atom is joined to the carbon atom of the hydrophobic chain via an oxygen atom. The acid ester is unstable and can revert back readily to the alcohol and sulphuric acid (particularly in acidic conditions), whereas the neutralised salts are stable at neutral pH. In the manufacture of sulphates the neutralisation must be carried out quickly to avoid the break down of the acid ester. In practice, sulphuric acid is very seldom used and chlorsulphonic acid or sulphur trioxide/air mixtures (in continuous reactors) tend to be the most common methods of sulphating alcohols. The neutralisation is usually carried out continuously with sulphation" (Porter, 1994).

As an anionic surfactant, SDS consists of a hydrophobic tail ($C_{12}H_{25}$) and a polar hydrophilic head (SO_4 Na) (Figure 1.4).

1.5.2 Adsorption and Critical Micelle Concentration (CMC)

It is known that pure hydrocarbons are rather insoluble in water, while polar materials are soluble in water, since water itself is a highly polar material.

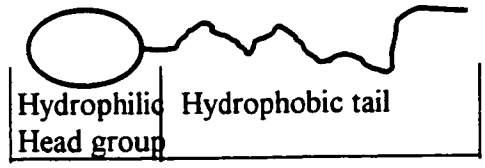

Figure 1.4. The basic chemical nature of an ionic surfactant molecule.

We might ask what might happen to a material such as sodium dodecyl sulfate (SDS) ($C_{12}H_{25}SO_4Na$) which has both a hydrocarbon chain and a polar group, when it is added to water. When such molecules are put in water, they prefer the (water/air) surface, where the hydrophilic "head" and hydrophobic "tail" lie, respectively, in and out of the water. As shown in Figure 1.5, this ideal condition is achieved by adsorbing the surfactant molecule at the interface of water and adjacent fluid as a monomolecular layer or "monolayer."

Surfactants have another important property. It too is a consequence of the reluctance of water to incorporate hydrocarbon chains. At very low concentrations dissolved surfactants exist as individual molecules, as for most other solutes. But at a certain concentration it becomes more favorable for the surfactant molecules to form aggregates called micelles. This particular concentration is called the critical micelle concentration (CMC). As illustrated in Figure 1.5, the polar groups are all in contact with water while the hydrocarbon chains form the interior of the micelle.

1.5.3 Formation of Micelles

The bulk properties of surfactant solutions are unusual and can change dramatically over very small concentration ranges. The measurement of bulk solution properties such

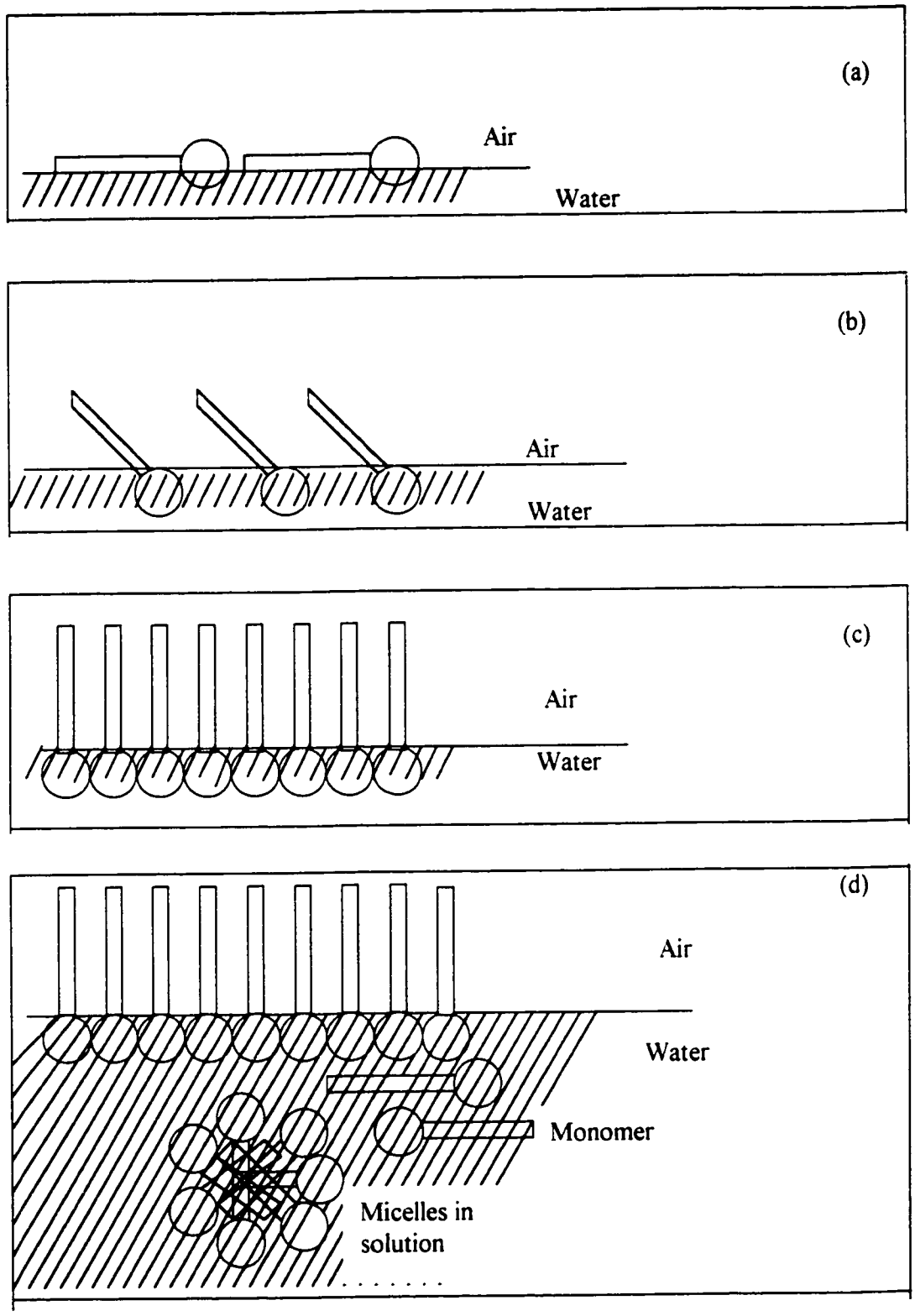

Figure 1.5. State of surfactant at different concentrations : (a) at very low concentration (b) at low concentration (c) at CMC (d) higher than CMC.

as surface tension, electrical conductivity, or light scattering as a function of surfactant concentration will produce curves that normally exhibit relatively sharp discontinuities at comparatively low concentration (Figure 1.6). The sudden change in any measured property is interpreted as indicating a significant change in the nature of the solute species affecting the measured quantity. These changes occur at the critical micelle concentration (CMC) (Rosen, 1989).

The determination of the value of the CMC can be made by use of any of these physical properties, but most commonly the breaks in the electrical conductivity, surface tension, light scattering, or refractive index concentration curves have been used for this purpose (Rosen, 1989).

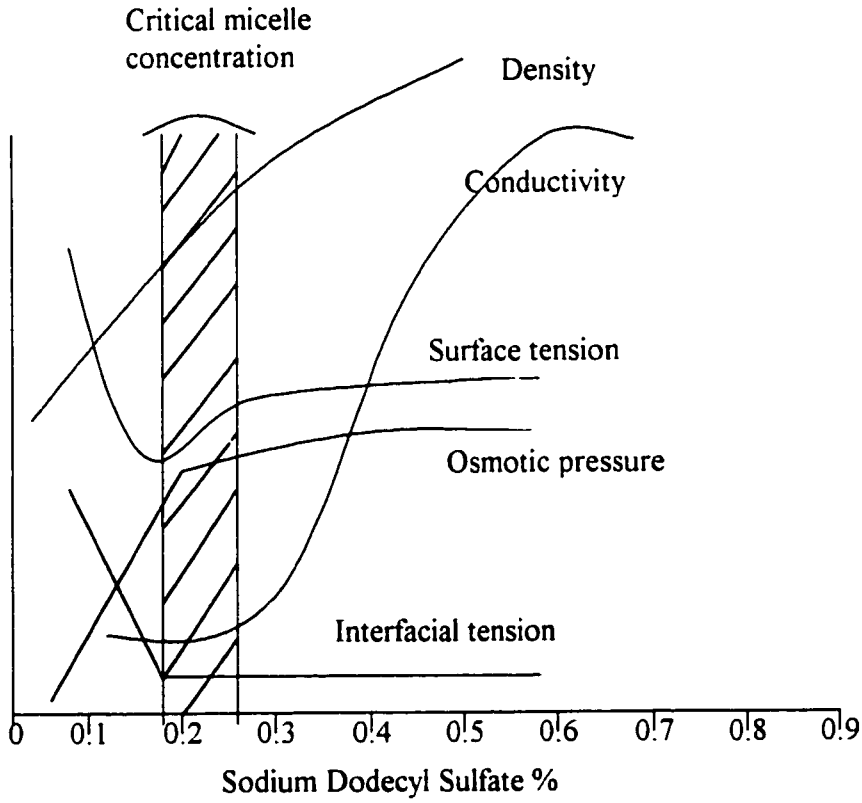

Figure 1.6. Change in some physical properties of an aqueous solution of sodium dodecyl sulfate in the neighborhood of the CMC (Rosen, 1989).

1.5.4 The Kraft Point (T_k)

The Kraft point is defined as the temperature at which the solubility of an ionic surfactant becomes equal to the CMC. Above the Kraft temperature, the solubility of a surfactant increases sharply with the temperature as the surfactant solutes can now form micelles.

1.6 Previous Works

Tweddle and Sourirajan (1978) used ethanol-water mixtures as gelation media over a wide range of alcohol concentrations and temperatures. Two different casting solutions involving cellulose acetate, acetone, and aqueous magnesium perchlorate (composition I) or formamide (composition II) were used. Their work was concerned with the porous structure of the surface layer, which is primarily responsible for solute separation in reverse osmosis. On the basis that the rate of solvent-nonsolvent exchange in the nascent membrane during gelation governs the overall porous structure of the resulting membrane, it is reasonable to expect that the gelation environment and, more specifically, the composition and the temperature of the gelation medium must have significant effects on the porous structure of the membrane surface.

The experimental data on membrane performance fell into four distinct regions with progressive increase in ethanol concentration in the gelation medium. In the initial region (region 1), the rate of membrane-permeated product decreased and the corresponding solute separation increased with increase in ethanol concentration in the gelation medium. In the next region (region 2), the product rate increased and solute separation decreased.

With further increase in ethanol concentration in the gelation medium, in the regions 3 and 4, the product rates obtained were relatively high, and they passed through successive maxima and minima while the corresponding solute separations were relatively low or practically zero.

Frommer et al. (1971) observed a similar behaviour for the membrane performance in region 1. Frommer et al. (1971) and Tweddle and Sourirajan (1978) attributed the changes to the decrease in water activity with increase in alcohol concentration in the gelation medium. Consequently, the rate of water penetration into the membrane decreased, resulting in finer precipitation of polymer material in the skin layer of the membrane, and ultimately in a smaller average pore size on the membrane surface. In addition, as the alcohol concentration in the gelation medium increased further beyond region 1 into regions 2, 3 and 4, the polymer precipitating power of alcohol and its interactions with the polymer, solvent, and nonsolvent swelling agent in the membrane matrix became progressively more important. These factors could affect both the precise instant of phase inversion and also the size, number, and distribution of nonsolvent droplets (incipient voids) in the interdispersed phase during gelation, which ultimately determined the surface pore structure of the resulting membrane. The general increase in product rate with increase in alcohol concentration in the gelation medium in regions 2, 3 and 4, and the existence of maxima and/or minima in product rates indicate that the above factors include those having tendencies in the direction of change of size, number and distribution of pores in the membrane surface and the effective thickness of the membrane.

Gildert et al. (1979) used five different alcohol-water mixtures as gelation media. The alcohol component in the gelation medium was either methyl alcohol, ethyl alcohol, propyl

alcohol, isopropyl alcohol, or ethylene glycol. Their results were very similar to the previous work. With respect to all alcohols studied, in region 1, the product rates decreased and the corresponding solute separations increased with increase in alcohol concentration in the gelation medium. To explain the behaviour of the membrane in region 1, they considered that the water-acetone exchange that primarily governs the porous structure on the surface layer of the resulting membrane. The kinetics of such change may be expected to be a function of the rate of the water penetration into the incipient membrane phase during gelation. This rate in turn may be expected to be governed both by the activity of water in the gelation medium and the diffusivity of water in the membrane phase. Numerical values for the activity (a_w) and diffusivity (D_w) of water in the alcohol-water gelation medium at the composition corresponding to the initial minimum in product rate were calculated. These results showed that, the effect of a_w on the membrane performance was less than that of D_w in region 1. Further, as the value of $a_w D_w$ decreased, there was a corresponding decrease in solute separation.

Okada and Matsuura (1988) used sodium chloride solutions as gelation media to study the effect of the change in the water activity on the pattern formation on the surface of cellulose acetate membranes prepared by the phase inversion technique. A series of sodium chloride solutions of different concentrations were prepared for the experiment. Sodium chloride concentrations were 0, 1.8, 3.9,and 4.3 mol/L, which correspond to water activities of 1.0, 0.94, 0.86, and 0.80 respectively, at 25°C. Images of the membrane showed that the patterns on the membrane surface changed with the change in sodium chloride concentration in the gelation bath. The results showed that the amplitude of the

wavy pattern decreased with decrease in water activity, while the wave length was almost unchanged. They explained their results on the basis of the exchange of the solvent and nonsolvent at the interface between the gelation bath and the casting solution during the gelation process. When water activity decreases, by an increase in sodium chloride concentrations, swelling of the membrane decreases, which in turn results in the decrease of amplitude of the pattern decrease.

No surfactants have been added to gelation media used in the preparation of asymmetric membranes. Adding alcohol to the water will result in a gradual decrease in in the surface tension of the solution. The surface tension will decrease with increasing the alcohol concentration and then it levels off at a certain value of alcohol concentration (Figure 1.7). This behaviour of alcohols in water is the same the behaviour of surfactants when they added to water (Mayers, 1988).

All the previous studies a greed that the solvent/nonsolvent exchange rate governs the pore size, porosity and roughness of the resulted membranes. None of the previous studies were concerned, however, with the changes that happen to the interface due to the addition of alcohols to the gelation bath.

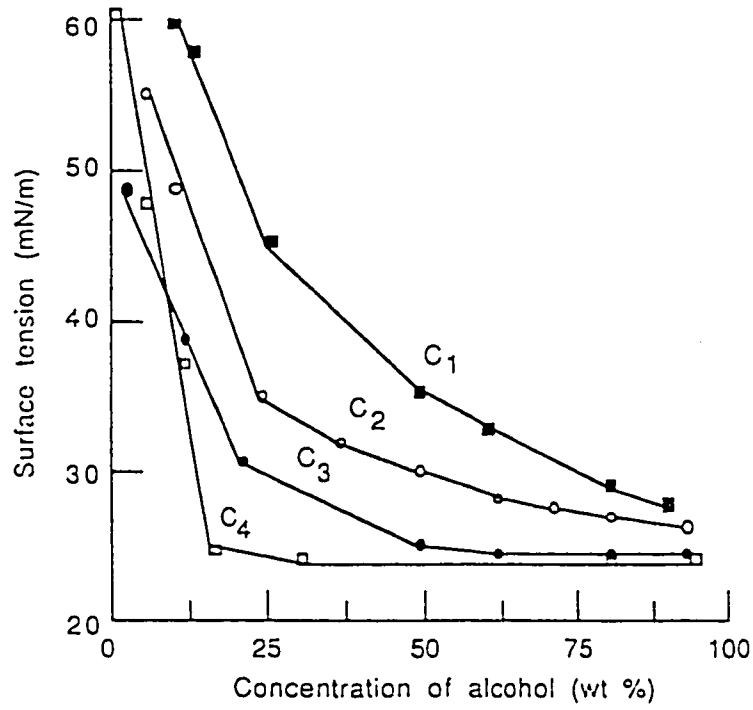

Figure 1.7. The effect of added alcohols on the surface tension of aqueous solution. (C1) methanol, (C2) ethanol, (C3) propanol and (C4) butanol (Myers, 1988).

1.7 Scope of the Research

It is clear from the previous work that the change of the gelation bath composition and temperature had a considerable effect on the performance and morphology of the tested membranes. No one has, however, paid attention to the interfacial phenomena that take place in the phase inversion process. Adding SDS to the gelation bath in the preparation of PES membranes was motivated by the following reasons:

- Surfactants have an interesting and unusual effect on the surface of their solutions, which will form the interface with the polymer solution film in the gelation process.
- Surfactants have never been added to the gelation media despite the fact that the behavior of surfactant solutions is well known and studied.
- Polyethersulfone (PES) is a widely used material for preparing ultrafiltration membranes due to its superior charac teristics such as chemical and thermal stability and mechanical strength.
- Sodium dodecyl sulfate (SDS) is an ionic alcohol sulfate surfactant and, according to Porter (1994), it is the most studied surfactant.

Hence, the objectives of this work were:

(i) To prepare PES ultrafiltration membranes by the phase inversion technique using SDS aqueous solutions as gelation media.

(ii) To study the effect of SDS concentration on the performance and morphology of PES membranes so prepared.

CHAPTER 2

2. THEORETICAL BACKGROUND

In the early stages after the invention of the Loeb-Sourirajan membrane, the parameters controlling the formation of asymmetric membranes were a mystery. The laboratory experiments, measuring the flux and separation, were useful but not enough to give a final picture. Improvement of these membranes depended on trial and error technique. By using the scanning electron microscope (SEM), which gives a relatively clear picture of the general membrane structure (Figure 1.4), it was possible to rationalize the factors affecting the formation of integrally-skinned membranes. It was thought that the asymmetric structure is a characteristic of cellulose acetate membranes, but in fact, the whole process of precipitating a polymer solution is just a type of a general process known as phase inversion (Strathmann, 1983).

2.1 Formation of Asymmetric Membranes by Phase Inversion

The majority of the commercially available membranes are produced by the phase inversion process, in which the structure of polymer in a membrane is determined when the polymer gel is immobilized prior to complete solvent evaporation or depletion.

There are four types of phase inversion; (i) Thermal Phase Inversion, (ii) Dry Phase Inversion, (iii) Vapour Phase Inversion, (iv) Wet Phase Inversion (Strathmann, 1983). In this work, the wet phase inversion process was used for making the membranes.

2.1.1 Wet Phase Inversion

The wet-phase inversion technique is also known as "Immersion Precipitation". It was first used successfully by Loeb and Sourirajan for the preparation of reverse osmosis membranes.

In this process, a polymer cast film is immersed in a nonsolvent bath (the gelation bath). The precipitation of the polymer is caused by an increase in nonsolvent/solvent ratio in the cast film as a result of solvent/nonsolvent exchange. In other words, both liquid-liquid (L-L) phase separation and polymer precipitation take place in the process of solvent/nonsolvent exchange. This technique can be rationalized with the aid of a three-component phase diagram shown schematically in Figure 2.1.

Suppose a nonsolvent is added to a homogenous solution consisting of polymer and solvent, the composition of which is indicated by point A on the solvent-polymer line. If the solvent is removed from the mixture and the nonsolvent enters, the composition of the mixture will change following the path ABDC. At point B, the composition of the system will reach the phase boundary line and two separate phases will begin to form, a polymer-rich phase represented by the upper phase boundary line and a polymer-poor phase represented by the lower phase boundary line. The space between the polymer-solvent axis and the phase boundary curve is called the homogenous liquid phase. At a certain composition of the three-component mixture, the polymer concentration in the polymer-

rich phase will be enough to be considered solid. This composition is represented by point D in Figure 2.1. At this point, the membrane structure is more or less determined. Further exchange of solvent and nonsolvent will lead to the final composition of the membrane, the porosity of which is determined by point C. Point C represents a mixture of the solid polymer-rich phase and the liquid nonsolvent rich phase as represented by points S and L, respectively.

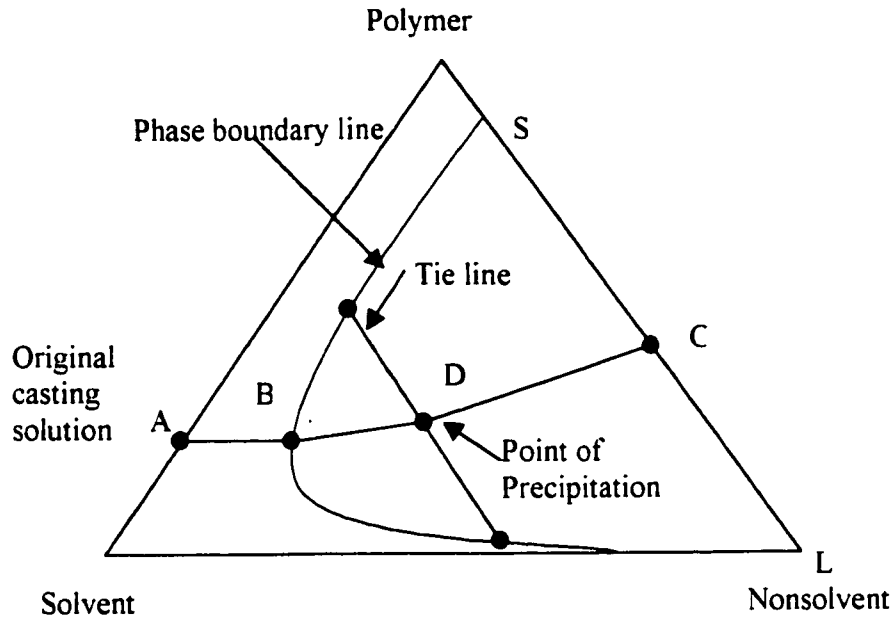

Figure 2.1. Schematic phase diagram of the system polymer-solvent-nonsolvent showing the gelation pathway of the casting solution during membrane formation.

It should be appreciated that the phase diagram is the description of an equilibrium state. It reflects the conditions under which a multicomponent mixture is either stable as a homogeneous phase, or decays into two phases. According to Strathman and Koch (1977), "In macromolecular systems, however, equilibrium is frequently never reached and the phase separation is largely governed by kinetics parameters".

The wet phase inversion process can be divided into two types:

- Instantaneous liquid-liquid demixing.
- Delayed onset of liquid-liquid demixing.

Instantaneous demixing means that the membrane is formed immediately after immersion in the gelation bath whereas it takes some time before the ultimate membrane is formed in the case of delayed demixing (Mulder, 1996).

2.1.2 Mathematical Description of Phase Separation

For simplicity, the basic thermodynamic relations of the phase separation or precipitation processes are discussed for a binary system at constant pressure and temperature.

2.1.2.1 Thermodynamic Description of a Binary System with Limited Miscibility

The thermodynamic interpretation of a system with limited miscibility can be given in terms of the free energy of mixing. At constant pressure and temperature, three different states can be distinguished:

- A stable state, with a homogeneous solution in a single phase, which meets the thermodynamic conditions

$$\Delta G > 0 \text{ and } \left(\frac{\partial \mu_i}{\partial X_i}\right)_{P,T} > 0. \qquad (2.1)$$

- An unstable state, where the homogeneous solution separates spontaneously into two phases, which are in equilibrium. This state, which is always located within the phase boundary line, is thermodynamically given by

$$\Delta G < 0 \text{ and } \left(\frac{\partial \mu_i}{\partial X_i}\right)_{P,T} < 0 \qquad (2.2)$$

- An equilibrium state, located on the phase-boundary, whose composition is thermodynamically given by

$$\Delta G = 0 \text{ and } \left(\frac{\partial \mu_i}{\partial X_i}\right)_{P,T} = 0 \qquad (2.3)$$

Here, ΔG is the free enthalpy of mixing, μ_i is the chemical potential of component i, and X_i is its mole fraction.

2.1.2.2 Kinetic Description of a Binary System with Limited Miscibility

The kinetic interpretation of a system with limited miscibility can be given in terms of the diffusion coefficient, D, of the system. At constant pressure and temperature, again three different states can be distinguished (Strathmann and Koch, 1977).

- A stable state with the homogeneous solution in one phase which is kinetically determined by

$$D_i > 0. \qquad (2.4)$$

- An unstable state, where the homogeneous solution decays spontaneously into two different phases. This state is determined by

$$D_i < 0. \qquad (2.5)$$

- An equilibrium state given by the phase-boundary composition. Here the diffusion coefficient becomes

$$D_i = 0. \qquad (2.6)$$

The physical significance of these three states becomes clear when it is realized that the diffusion coefficient is defined in Fick's law in terms of a concentration gradient as

the driving force. However, the actual driving force for the flux of a component is not the gradient in its concentration but the gradient in its chemical potential, and it is possible to produce situations when the gradients in concentration and chemical potential are of different sign. In this case the diffusion coefficient as defined by Fick's law will be negative.

The diffusion coefficient can be related to the chemical potential driving force by

$$D_i=B_i\left(\frac{\partial \mu_i}{\partial X_i}\right)_{P,T} \tag{2.7}$$

Here D_i is the diffusion coefficient of component i, μ_i is its chemical potential, and X_i is its mole fraction, and B_i is a mobility term, which is always positive. Introducing the chemical potential of a non ideal solution, which is given by

$$\mu = \mu_i^{\circ} + RT \ln f_i^s X_i \tag{2.8}$$

into Eq. (2.7) leads to

$$D_i = \frac{B_i RT}{X_i}\left(1+\frac{\partial \ln f_i^s}{\partial \ln X_i}\right) \tag{2.9}$$

Here μ_i^0 is a standard chemical potential, f_i^s is an activity coefficient referring to the pure phase, R is the gas constant, and T is the absolute temperature. The last term in Eq. 2.9 determines whether the diffusion coefficient is positive, negative, or zero according to the following three possibilities:

$$\frac{\partial \ln f_i^s}{\partial \ln X_i} > -1, < -1, \text{ or } = -1 \tag{2.10}$$

Combining Eqs. 2.9 and 2.10, it can be concluded that D_i will become positive, negative or zero, depending on whether $0 < n < 1$, $n > 1$ and $n = 1$, respectively, in the following

equation

$$f_i^s = \frac{1}{X_i^n} \tag{2.11}$$

Eqs. 2.8 to 2.11 indicate that, if for any reason the activity coefficient of a component i in a binary solution is raised to the extent that the product $f_i^s X_i$ becomes larger than unity, phase separation will occur and the component i will flow from an area of lower concentration into an area of higher concentration. Thus the flux of the component i is against the concentration gradient.

In summary:

-The driving force for any mass flux is not the concentration gradient, but the gradient in the chemical potential.

-In phase separation processes, the components are transported against their concentration gradient because the activity coefficient is increased to such an extent that the product of $f_i^s X_i$ is larger than unity.

- The activity coefficient of a component can be changed by changing the temperature, or the composition of the mixture. A typical example is the so-called "salting-out" effect, where the activity of the salt in an aqueous solution is raised by adding an organic solvent to such an extent that the salt precipitates from the solution.

2.2 Preparation of Integrally Skinned Membranes

An integrally skinned asymmetric membrane consists of a top skin layer and a porous sublayer. The top layer has about the same properties as a homogeneous film.

The skin layer of an asymmetric membrane is formed when the concentration at the surface of the cast polymer solution film is increased. The following different techniques explain how the polymer concentration in the skin layer determines the skin formation (Broens et al., 1980).

-Precipitation by the intrusion of nonsolvent .

-Immersion precipitation.

In the first method, the precipitation is accomplished by the intrusion of nonsolvent from the vapour phase. In this case, polymer concentration at the top of the cast film is effectively unchanged even after the exposure of the film surface to the nonsolvent vapour, since the vapour phase is saturated with the solvent and solvent evaporation from the cast film is very slow. Then, the polymer concentration will become the same from the top to the bottom of the membrane, which results in a symmetric membrane without any skin layer.

In immersion precipitation, the nonsolvent is added to the casting solution by immersing the cast polymer film in a bath of the nonsolvent fluid (Figure 2.2). When the cast polymer film is immersed into the gelation bath, the solvent leaves, and nonsolvent enters the film. At the film surface, the concentration of the nonsolvent soon reaches such a value that phase separation is resulted. In the interior of the film, however, the polymer concentration is still far below the limiting concentration for phase separation. Phase separation therefore occurs at the surface of the film, where, due to the very steep gradient of the polymer chemical potential on a macroscopic scale, there is a net movement of the polymer in direction perpendicular to the surface layer. It is the concentrated surface layer, which forms the skin of the asymmetric membrane

(Strathmann and Kock, 1977). The formation of this skin will increase the barrier for the diffusion of solvent out and nonsolvent into the sublayer of the polymer solution (Broens et al., 1980). In the film below the skin, phase separation will take place at lower polymer concentration compared to that in the skin. In the former region, two types of structures have been mentioned in the literature, sponge-like structure and finger-like structure.

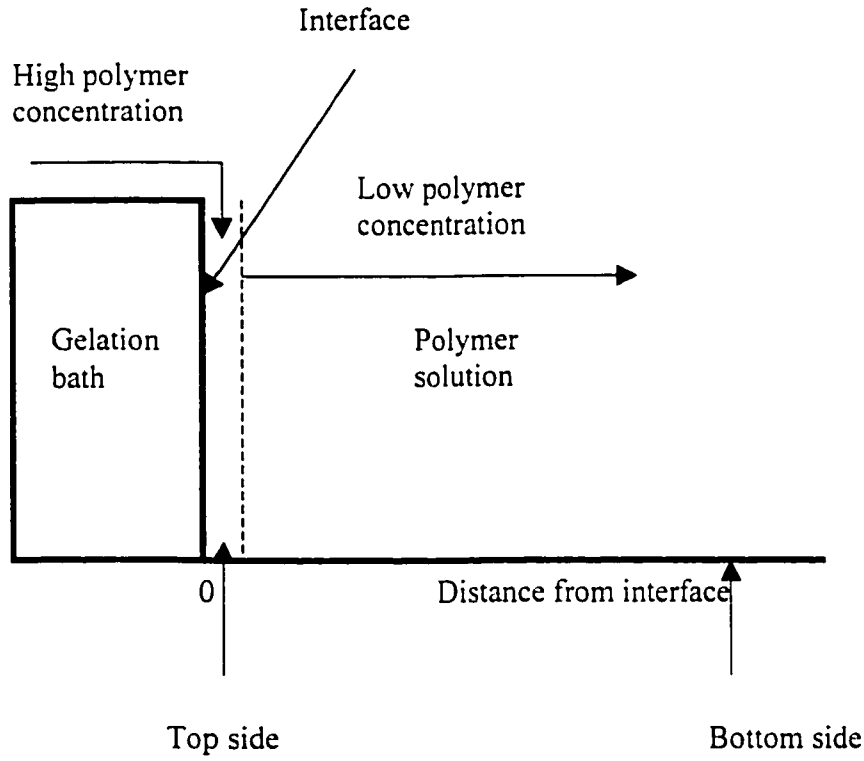

Figure 2.2. Schematic drawing of the polymer concentration in the casting solution after immersion in gelation bath.

Broens et al. (1980) and Tweddle and Sourirajan (1978) discussed the factors, which affect the formation of the skin layer:

-The concentration of the polymer in the casting solution. A higher concentration of the polymer solution will favour the formation of a denser skin. This also observed by Singh et al. (1998).

-The composition of the nonsolvent gelation bath. Adding a proper additive to the gelation bath, will decrease the tendency of the nonsolvet to enter the cast solution film and delay the precipitation until a high concentration of polymer is attained at the top layer.

-The temperature of the gelation bath. Lowering the temperature of the gelation bath will increase the supersaturation, while at the same time it will decrease the growth kinetics of nuclei; a denser skin will result.

2.3 Nodular Structure of the Skin

From the microscopic scanning of RO and UF membranes, it has been observed that the skin of asymmetric membranes consists of nodules. The nodule is an aggregate of the macromolecular spheres (Matsuura, 1993). These nodules vary in size from 200 to 2000 A (Broens et al., 1980). The nodules can aggregate themselves, forming aggregates of nodules, which are called supernodular aggregates. The pores on the surface of RO membranes are void spaces between macromolecular spheres, while those on the surface of UF membranes are void spaces between nodules (Matsuura, 1993).

2.4 Interfacial Phenomena of Surfactant Solution

The term "interfacial phenomena" is very general in nature and refers to any activity, which either originates in the interface or is specific to it. An "interface" is, as the name suggests, a boundary between phases. Because interfaces are very thin, in most cases only a few molecular diameters thick, we sometimes tend to think of them as two-dimensional surfaces and neglect their thickness. But the third dimension is of great significance as well. Indeed, the rapid changes in density and/or composition across interfaces give them their most important property, an excess free energy or lateral stress which is usually called interfacial tension.

Interfacial tension is a key factor influencing the shape of fluid interfaces, and it controls their deformability. In multicomponent systems composition in the interfacial region can differ dramatically from that of either bulk phase. This difference is especially striking when surface-active materials or 'surfactants" are present. As their name implies, these substances find it energetically favorable to be located at the interface rather than in the bulk phases. As described in Chapter 1, surfactants produce significant decreases in interfacial tensions and alter wetting properties as well, the latter property being of particular importance in detergency. Moreover, surfactant molecules tend to aggregate in solution, forming phases such as micellar solutions, microemulsions, and lyotropic liquid crystals with interesting and unusual properties. Surfactants and the phases they form are a major factor influencing the stability and behavior of some colloidal dispersions such as emulsions and foams. (Miller and Neogi, 1985).

2.4.1 Thermodynamics of Surfactant Solutions

The molecules at the surface of a liquid have potential energies greater than those of similar molecules in the interior of the liquid. This is because attractive interactions of molecules at the surface with those in the interior of the liquid are greater than those with widely separated molecules in the gas phase. Because the potential energies of molecules at the surface are greater than those in the interior of the phase, an amount of work equal to this difference in potential energy must be expended to bring a molecule from the interior to the surface. The surface free energy per unit area, or surface tension, is a measure of this work. It is the minimum amount of work required to bring sufficient molecules to the surface from the interior to expand it by unit area.

$$\gamma = \frac{dw}{dA} \tag{2.12}$$

where γ is the surface tension and w is the work needed to form the surface.

When a new surface area dA, is created, there is a possibility that a number of molecules, dN, move to or from the surface region. This movement introduces the concept of surface excess or deficiency of component i:

$$\Gamma_i = \frac{dN_i}{dA} = \text{surface excess of component i.} \tag{2.13}$$

The process of forming a new surface can be divided into two parts (Davies and Rideal, 1963):

- The phase must be displaced to expose the new surface.
- Atoms in the surface plane rearrange to assume their equilibrium positions.

In liquids, parts one and two happen almost instantaneously, and the creation of the new surface produces γ, the reversible work to form the new surface. In solids, part two may

occur slowly or not at all. Due to low atomic mobility, a solid can be stretched or compressed without changing the number of atoms at the surface; however, the distance of separation between atoms is altered, resulting in surface stress. In a multi-component system, part two can be combined with the migration of atoms to or from the interface, (i.e., the development of surface excesses or deficiencies, Γ_i). In a single-component system, $\Gamma_i = 0$, unless there is a change in density near the surface.

From basic thermodynamics, using either the Gibbs or Guggenheim treatment of interfaces, it can be shown that

$$d\gamma = -\sum_i \Gamma_i d\mu_i \qquad (2.14)$$

where the surface excess of component i, $\Gamma_i = N_i/A$. Eq. 2.14 is the Gibbs adsorption equation, a fundamental equation of surface chemistry which relates the surface excess of components with the change in surface energy. If, $\Gamma_i > 0$, i is concentrated at the surface zone and the phenomenon is called adsorption. If $\Gamma_i < 0$, there is a deficiency of i at the surface and is referred to as negative adsorption.

The energy necessary to create a new surface is always positive (Gibbs, 1928). This means that a solid or a liquid would have a lower total energy if there were no surface.

2.4.2 Solubility in Surfactant Solution

One reason that surfactants are useful in a wide variety of applications is that, under suitable conditions, their aqueous solutions are able to dissolve substantial amounts of compounds that have very low solubilities in water. Similarly, surfactants can greatly increase the solubility of water and other polar compounds in hydrocarbons and other liquids of low polarity. This phenomenon, which involves incorporation of the solute (the

dissolved phase) by aggregates of surfactant molecules, is known as solubilization. It occurs not only for small surfactant aggregates such as (nearly) spherical micelles but also for larger aggregates such as microemulsion drops, vesicles, and cylindrical and plate-like micelles. Lyotropic liquid crystals containing regular arrays of surfactant aggregates are also effective media for solubilization (Miller, 1997).

A Simple Model of Solubilization

This model is presented as presented by Miller (1997) "We begin with a relatively simple model, which was suggested some years ago by Mukeijee and provides considerable insight on solubilization of small amounts of solutes in spherical micelles. Suppose that an aqueous micellar solution has reached its solubilization limit and is in equilibrium with an excess liquid phase of a pure hydrocarbon or some other compound of low polarity. Equating the chemical potentials μ_b^o and μ_m of the solute in the bulk organic phase and the micelles, we have

$$\mu_b^o = \mu_m = \mu_m^o + RT \ln X_m \tag{2.15}$$

where X_m is the mole fraction of the solute in the micelles and where ideal mixing in the micelles has been assumed. μ_m^o is the standard chemical potential inside the micelles. If we assume that we can treat the surface of a spherical micelle like an interface between bulk fluids, the pressure in the nonpolar interior of the spherical micelle is higher than that in the surrounding water by an amount $(2\gamma/r)$, where γ is the interfacial tension and r the micelle radius. Since μ_m^o must be evaluated at this higher pressure, we have

$$\mu_m^o = \mu_b^o + (2\gamma v/r) \tag{2.16}$$

where v is the molar volume of the solute. Also, pressure in the bulk oil phase has been taken equal to that in the water, a reasonable assumption here since the radii of curvature of the oil-water interface greatly exceed the micelle radius, r, which is only 2 to 3 nm. Substituting this expression into Eq. 2.15, we obtain

$$X_m = \exp[-(2\gamma v/rRT)] \tag{2.17}$$

According to Eq. 2.17, solubilization should increase with decreasing interfacial tension γ between the micelles and water. It is known that interfacial tension decreases as surfactant's hydrophilic and lipophilic properties become more nearly balanced, for instance as salinity or hardness of the aqueous phase increases in the case of ionic surfactants. Solubilization increases under these conditions as well, so that the prediction is in qualitative agreement with experimental data.

Eq. 2.17 is satisfactory only when micelles are small and spherical and solubilization is relatively low. While the above derivation can apply either to nonpolar species solubilized in the micelle interior or to amphiphilic species such as alcohols, which basically form mixed micelles with the surfactant, caution should be used in the latter case. The reason is that alcohols that are less hydrophilic than the surfactant can cause the micelles to become rod-like, thus violating the assumption of spherical micelles employed in the analysis.

The above analysis can be extended in various ways to provide insight, though not necessarily useful quantitative predictions, for other situations. For example, long, cylindrical micelles can be considered, in which case the factor of 2 disappears from Eq. 2.17. Indeed, surfactant bilayers can also be considered if one includes a surface energy term in writing the free energy change, ΔG, for transfering δn moles of solute from the

bulk oil phase into a bilayer of fixed half-thickness, d, as

$$\Delta G = [-\mu_b^o + \mu_m^o + RT \ln X_m \gamma(\partial A/\partial N)]\, \delta N \qquad (2.18)$$

where A is bilayer area and N is the number of moles of solubilized solute. Since r is infinite, $\mu_b^o = \mu_m^o$, according to Eq. 2.16. Moreover, $(\partial A/\partial N) = (v/d)$. Hence, setting $\Delta G = 0$ yields Eq. 2.17 without the factor of 2 and with r replaced by d".

2.4.3 Solubility and Surfactant Concentration

Solubility of a solute in surfactant or micellar solution may be presented as the mole fraction, X_m of solute in the solution or the micelle, as in Eq. 2.18. More commonly, however, one finds a plot of the moles of solute dissolved in the micellar solution as a function of surfactant concentration. As it is shown in Figure 2.3, below the CMC, the amount solubilized is usually constant and equal to the solute solubility in water. Above CMC, the solubility increases approximately linearly with the concentration of the surfactant (Rosen, 1989 and Miller, 1997).

2.5 Surfactants and Solvent Extraction

Adding the surfactant to water will have effect on the interfacial area and the mass transfer coefficient. The interfacial area increase is evident from Gibbs equation where the increase in the surfactant concentration will result in an increase in surface excess. In general, it is assumed that the process of interphase mass transfer in liquid-liquid systems consists of three steps: Diffusion of the solute molecules from the bulk of the raffinate phase to the interface, crossing of the interface and the diffusion away from it to the bulk of the extract solvent (Sawistowski, 1971).

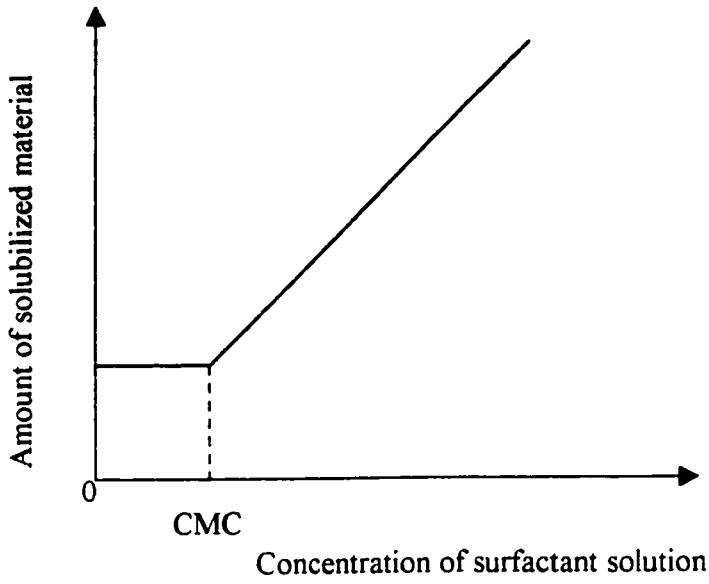

Figure 2.3. Plot of the amount of material solubilized as a function of concentration of the surfactant solution.

In this work, the cast polymer solution can be considered as the raffinate phase and the gelation bath as the extract solvent. The gelation bath that consists of water or aqueous solution is called phase 2. The cast solution is called phase 1.The solute is extracted from phase 1 to phase 2 in analogy to liquid-liquid extraction. However, in this case, the solute to be extracted is in fact the solvent (NMP) in the cast polymer solution. The rate of mass transfer in solvent extraction dE/dt is proportional to the mass transfer coefficient, the interfacial area and the driving force.

$$\frac{dE}{dt} = K_{01} A\left(C_1 - C_1^*\right) = K_{02} A\left(C_2^* - C_2\right) \tag{2.19}$$

Where K_{01},K_{02} are the overall mass transfer coefficients based on phases 1 and 2 respectively; A is the interfacial area; C_1, C_2 are the concentrations of the solvent (NMP)

in phases 1 and 2, respectively. The asterisk denotes the equilibrium value with respect to the concentration of the solvent (NMP) in the adjoining phase.

The introduction of surfactants in phase equilibrium will affect the properties of the interface in several ways. In addition, surface viscosity will increase slowing down any movements in the interface (Sawistowski, 1971).

2.6 Reverse Osmosis Fundamentals

Nanofiltration and reverse osmosis are used when low molecular weight solutes such as inorganic salts or small organic molecules have to be separated from a solvent. Both processes are considered as one process since the basic principles are the same (Mulder, 1996).

Reverse osmosis is a process in which pressure is used to reverse the osmotic flow of water across a semipermeable membrane. The normal direction of water flow across a membrane is from a solution of lower solute concentration to a solution of higher solute concentration. If a pressure (Δp) is applied to the concentrated solution just equal to the osmotic pressure difference between the two solutions ($\Delta\pi$), water flow ceases, and we have osmotic equilibrium. At a higher pressure ($\Delta p > \Delta\pi$), water will flow from the concentrated to the dilute solution. If the membrane is sufficiently semipermeable, this process can be used to desalt the concentrated solution. Most waters treated by reverse osmosis have a substantial osmotic pressure. For seawater, $\pi \cong 2.5 \times 10^3$ kPa, while for most brackish waters $\pi \cong 0.1 \times 10^3 - 0.4 \times 10^3$ kPa. Even tap water containing 500 ppm total dissolved solids has an osmotic pressure of about 40 kPa (Lonsdale, 1983). Furthermore, as water is removed from these solutions, the osmotic pressure increases. A

simple relationship between π and c_j (salt concentration) is the van't Hoff equation:

$$\pi = c_j RT/M \tag{2.20}$$

The water flow can be represented by Eq. 2.21 if it is assumed that no solute permeates through the membrane:

$$J_w = A\,(\Delta p - \Delta\pi) \tag{2.21}$$

Where J_w is the water flux through the membrane, and A is the water permeability coefficient.

In practice, the membrane may be slightly permeable to low molecular weight solutes. In such a case, $\sigma\,\Delta\pi$ should be used for the osmotic pressure term instead of $\Delta\pi$, where σ is the reflection coefficient of the membrane towards that particular solute.

Eq. 2.21 now becomes

$$J_w = A\,(\Delta p - \sigma\,\Delta\pi) \tag{2.22}$$

However, for a membrane of high selectivity σ can be approximated by unity.

According to the solution-diffusion model, the water permeability coefficient A (also defined as the hydrodynamic permeability coefficient) is a constant for a given membrane and contains the following parameters.

$$A = \frac{D_w c_w v_w}{RT\Delta x} \tag{2.23}$$

where, D_w is water diffusivty in the membrane, c_w is water concentration in the membrane, v_w is water molar volume, and Δx is the membrane thickness.

The solute flux can be described by

$$J_s = B\,\Delta c_s \tag{2.24}$$

where B is the solute permeability coefficient and Δc_s is the solute concentration

difference across the membrane ($\Delta c_s = c_f - c_p$). The value of B lies in the range 5×10^{-3} – 10^{-4}m.h^{-1} for reverse osmosis with NaCl as a solute, with the lowest value for high rejection membranes. For nanofiltration membranes the retention for the various salts may vary considerably. For example, the retention for NaCl may range from about 5 to 95%. For this reason, it is not very useful to give a range for the solute permeability coefficient for this process. The solute permeability coefficient B is a function of the diffusivity and the distribution coefficient k_s as given by Eq. 2.25

$$B = \frac{D_s k_s}{\Delta x} \tag{2.25}$$

From Eq. 2.21 it can be seen that when the applied pressure is increased the water flux increases linearly. According to Eq. 2.24 the solute flux is hardly affected by the pressure difference and is only determined by the concentration difference across the membrane.

The selectivity of a membrane for a given solute is expressed by the retention coefficient or rejection coefficient R:

$$R = \frac{c_f - c_p}{c_p} = 1 - \frac{c_p}{c_f} \tag{2.26}$$

Consequently, as the pressure increases the selectivity also increases because the solute concentration in the permeate decreases. The limiting case R_{max} is reached as Δp approaches infinity.

With $c_p = J_s/J_w$ and combining Eqs. 2.21, 2.24 and 2.26, the rejection coefficient can be written as:

$$R = \frac{A(\Delta p - \Delta \pi)}{A(\Delta p - \Delta \pi) + B} \tag{2.27}$$

Eq. 2.27 is very illustrative since the only variable, which appears in this equation, is Δp

assuming that the constants A and B are independent of the pressure.

The pressures used in reverse osmosis range from 2×10^3 kPa to 10^4 kPa and in nanofiltration from 10^3 kPa to 2×10^3 kPa , which are much higher than those used in ultrafiltration. In contrast to ultrafiltration and microfiltration, the choice of material directly influences the separation efficiency of reverse osmosis through the constants A and B (Eq. 2.27). In simple terms, this means that the constant A must be as high as possible whereas the constant B must be as low as possible to obtain an efficient separation. In other words, the membrane (material) must have a high affinity for the solvent (mostly water) and a low affinity for the solute. This implies that the choice of material is very important because it determines the intrinsic membrane properties. On the other hand, in the case of ultrafiltration and microfiltration, where the dimensions of the pores in the membrane determine the separation properties and the choice is mainly based upon chemical resistance.

CHAPTER 3

3. EXPERIMENTS AND METHODS

3.1 Overview

In the integrally skinned membranes, the skin and substructure are composed of the same material. The skin layer determines both the permeability and selectivity in membranes for gas separation and reverse osmosis. The skin layer determines the flux and rejection characteristics of an ultrafiltration or microfiltration membrane (Fritzche et al., 1992). The flux depends on the pore density and the skin layer thickness, and the selectivity depends on the pore size. A porous sublayer acts mainly as a mechanical support. Molecular weight cut-off (MWCO, molecular weight of a solute for which the rejection coefficient is 90%) and the mean pore size alone are not sufficient to predict the membrane selectivity. The pore size distribution is also needed to predict the selectivity of a membrane with a significant confidence. Hirose et al. (1996) have noted that, apart from the mean pore size and pore size distribution, roughness of the skin layer seems to have an effect on the permeate flux.

The relation between the solute separation and the size of solute has been the subject of many studies in an attempt to obtain information about the pore size and the pore size distribution of the membrane. According to Michaels (1980), when the rejection coefficient is plotted versus molecular size, a log-normal probability distribution describes the resulting curve for a number of ultrafiltration membranes. Kassotis et al. (1985) used dextrans to measure the rejection coefficient of polyacrylonitrile membranes in order to find the pore size distribution. Amir et al. (1990) measured the rejection coefficient of membranes with dextrans and the data were fitted to a log-normal pore size distribution. Singh et al. (1998) used polyethylene glycols (PEG) to determine the pore size and the pore size distribution of polyethersulfone (PES) membranes by using the solute transport technique and the results were compared to those obtained from atomic force microscopic technique (AFM). They found that a log-normal distribution was very appropriate for describing pore size distribution both from solute transport and from AFM.

In this work a technique based on the solute transport was used to determine the mean pore size and the pore size distribution and the AFM technique was used to determine the surface roughness of a number of PES membranes.

3.2 Experiments and Methods

3.2.1 Membrane Materials and Preparation

Polyethersulfone (PES, Victrex 4100P), supplied by Imperical Chemical Industries, was dried at 150°C without further purification. Polyvinylpyrrolidone (PVP) of molecular weight 10,000, supplied by Sigma Chemicals Co., was dried at 60°C and used as an additive to the casting solution. N-methylpyrrolidone (NMP), supplied by Sigma

Chemicals Co., was used as solvent. The composition of the casting solution, by weight percent (wt %), was as follows:

Polyethersulfone (PES)	20 %
Polyvinylpyrrolidone (PVP)	20 %
N-methylpyrrolidone (NMP)	60 %

Asymmetric membranes were made by the phase inversion technique. Membranes were cast by pouring the casting solution, at room temperature, on to a glass plate and spreading it by a casting rod at a uniform speed. The wet thickness (gap between the glass plate and the casting rod) was maintained at 0.25mm for all membranes. Immediately after casting, the glass plate was immersed into a gelatin bath. Membranes were stored in distilled water allowing the water soluble components in the membrane to be leached out.

3.2.2 Preparation of Gelation Media

Gelation medium was either distilled water or a sodium dodecyl sulfate (SDS) aqueous solution. SDS solutions were prepared by dissolving SDS supplied by Sigma Chemicals Co., in 5L distilled water. The solutions were kept at room temperature for one hour to be used at room temperature. Some of the solutions were placed in a refrigerator until their temperature became 4°C.

3.2.3 Characterization of Gelation Media

3.2.3.1 Measurements of Surface Tension

The surface tensions of sodium dodecyl sulfate (SDS) solutions (concentration range from 0 to 3.0 g/L) were measured at room temperature and 4°C. The drop weight method

was adopted for its accuracy. A multichannel syringe pump (79000 series; Cole-Parmer Instrument Company) was used to pump the solution from a 2.5 mL glass syringe to a glass bottle on a balance (Mettler AJ 150) at a flow rate of 0.1 mL/min through a capillary Teflon tip with outside diameter of 0.275cm. By this way, drop volume and corresponding drop weight could be obtained at different times. The surface tension was calculated by

$$W = 2\pi r_B \gamma F(r_B/V^{1/3})$$

where,

W = drop weight (g)

r_B = capillary tip diameter (cm)

γ = surface tension (dynes / cm)

V = drop volume (mL)

$F(r_B/V^{1/3})$ is a correction factor that depends on the ratio of capillary tip radius to the cubic root of the drop volume. Values of $F(r_B/V^{1/3})$ are tabulated elsewhere (Padday,1969). An average of seven to eight drops was taken.

3.2.3.2 Measurements of Conductivity

Ionic conductivity for the gelation baths was measured by conductivity meter (CDM 80; Radiometer Copenhagen).

3.2.4 Reverse Osmosis Experiment

Polyethylene glycols of molecular weight 2,000-8,000 were supplied by Sigma Chemicals. Polyethylene glycols of molecular weight 10,000-35,000 were supplied by Fluka Co. Polyethylene oxide (PEO) was supplied by Sigma Chemicals Co. They were

dissolved in distilled water to prepare feed solutions for reverse osmosis experiments. The solute concentration was kept at 200 ppm by weight.

Reverse osmosis (RO) experiments were carried out using conventional continuous flow cells (Figure 3.1). The cell is made of stainless steel, and consists of two detachable parts. The lower part is a high-pressure chamber provided with an inlet and an outlet for the flow of the feed solution under pressure. The upper part is provided with an outlet opening for the withdrawal of the membrane permeated product solution.

The wet membrane is mounted on a stainless steel porous plate embedded in the upper part of the cell such that the surface layer of the asymmetric membrane faces the feed solution. A Whatman filter paper is placed between the membrane and the porous plate to protect the membrane from abrasion and also aid the flow of the product solution through the porous plate. Under the operating conditions of RO, the porous plate and the filter paper offer practically no resistance to fluid flow. The lower and upper parts of the cell are set in proper alignment with rubber O-ring contacts between the high pressure chamber and the wet membrane. A pressure tight seal is obtained by clamping the two parts of the cell tightly between two thick end plates.

The experimental setup is shown in Figure 3.2. Six cells with an effective average area of 12.28 cm^2, were connected in series. A pump was used to let the feed solution flow under pressure through the cells. The operating pressure was measured at both ends of the cell series. The purge valve was used to drain the system whenever necessary. A stainless steel pressure valve was used to control the operating pressure in the cells.

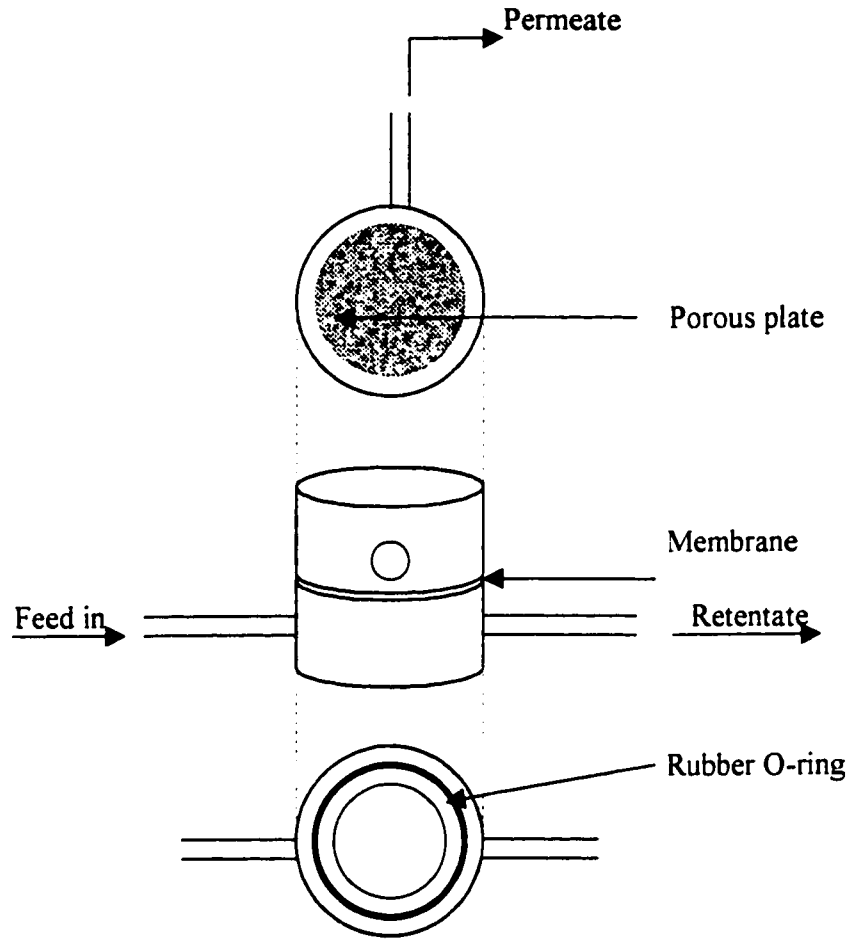

Figure 3.1. Sketch of laboratory cross-flow permeation cell for flat reverse osmosis membrane.

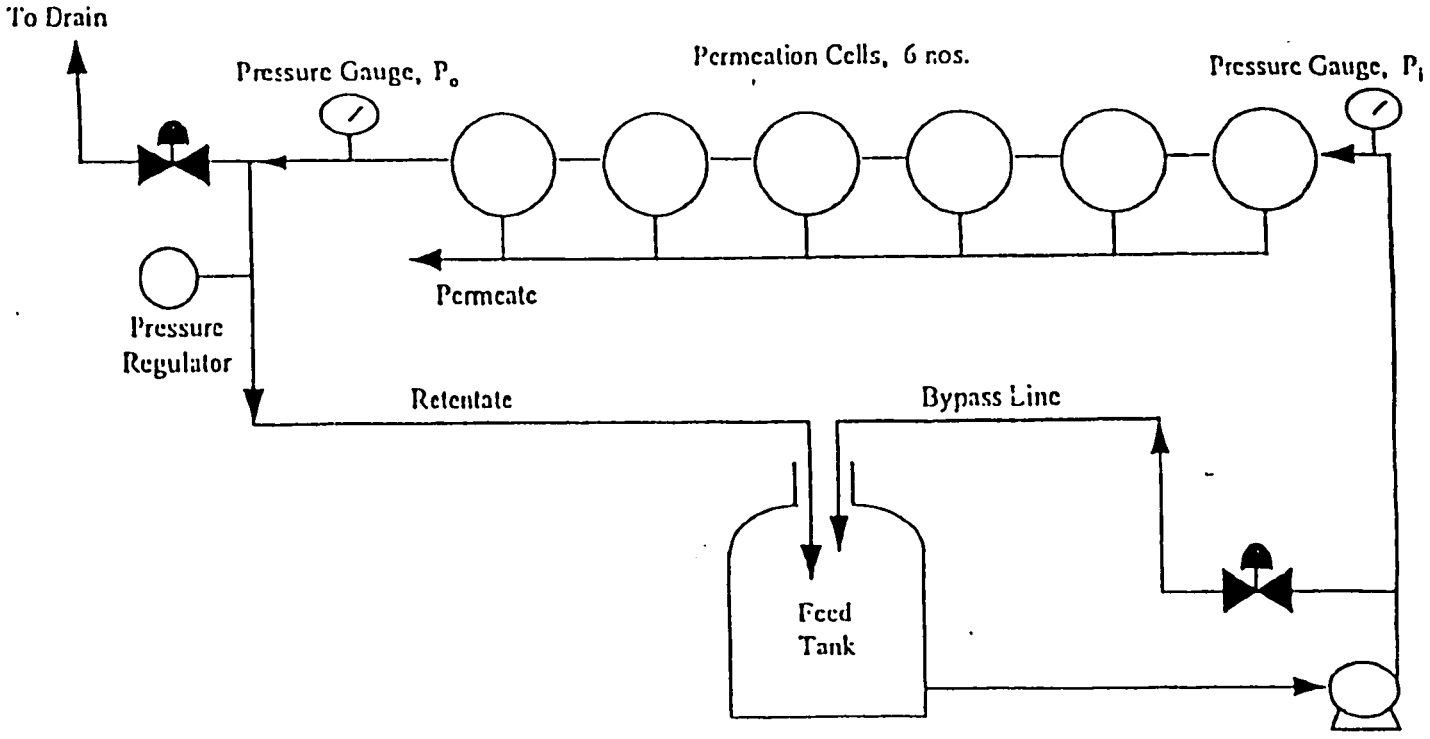

Figure 3.2. Schematic layout of the Reverse Osmosis/Ultrafiltration experiment.

Each membrane was initially subjected to pure water pressurization under 1.7×10^3 kPa (250 psig) for 5 hours prior to subsequent reverse osmosis experiments. The operating pressure and the feed flow rate were kept at 1.03×10^3 kPa (150 psig) and 800 mL/min, respectively. The pure water permeation rate (PWP) data were obtained after membranes were under operating pressure (1.03×10^3 kPa) for two hours. Then, the feed was switched to a PEG/PEO aqueous solution of 200 ppm and the permeate sample collected after the feed solution was circulated for one hour and half. Both the feed and permeate samples were subjected to total organic carbon analysis (DC-190; Folio Instruments) by which PEG and PEO concentrations were determined in terms of total organic carbon (TOC). The separation of PEG and PEO, f, was obtained by

$$f = \frac{\text{TOC in feed - TOC in product}}{\text{TOC in feed}}$$

The system was flushed with distilled water between runs with PEG/PEO of different molecular weights PWP data were collected after two hours of pure water circulation.

3.2.5 Measurement of Membrane Surface Roughness by Atomic Force Microscopy

In previous works, the surface roughness has been related to the performance of the membrane. Singh et al. (1998) found that PES membranes prepared from a higher polymer concentration solution have a smaller pore size and smoother surface than membranes prepared from a low polymer concentration solution. The small pore size and the smooth surface could be ascribed to the high polymer concentration in the skin layer. Similar results have been observed by Fritsche et al. (1992b). They used the AFM technique to measure the roughness parameters for PES membranes with different MWCOs (10,000,

35,000 and 100,000). The results showed that the roughness increased when the MWCO increased.

Generally, in the nineties, the AFM technique became very popular in the study of the membrane morphology, and that is because of the advantages of this technique over other techniques. Most of the latter techniques, like scanning electron microscope (SEM) and transmission electron microscope (TEM), need a tedious process of sample preparation. Heavy metal coating required in SEM and TEM might give some artifacts. High beam energy as required in SEM for high resolution tends to damage polymeric membranes.

Atom force microscopy (AFM) relies on the precise scanning of a probe on a sample surface to produce the topography of the surface. An extremely sharp tip is brought into contact with a sample as shown in Figure 3.3. The tip is attached to a cantilever that induces forces smaller than inter-atomic forces, allowing the topography of the sample to be measured without displacing the atoms. The sample, which is set on the top of a piezoelectric scanner, is scanned under the tip in an X-Y raster pattern. Features on the sample surface deflect the cantilever, which in turn changes the position of a laser beam on the photodiodes (Figure 3.3). As the tip encounters a raised feature, the cantilever is pushed up, deflecting the laser beam upward and as the tip encounters a low feature, the laser beam will be deflected downward. The change in the beam position will result in a change in the voltage, which is set at zero when the beam reflection at the center of the photodiode.

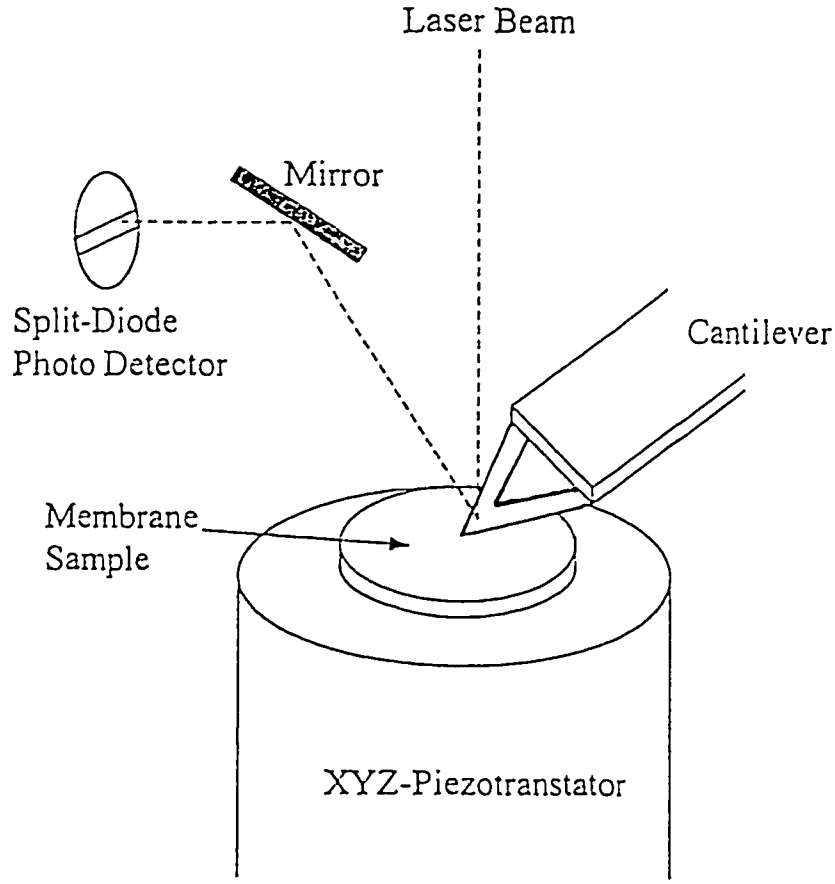

Figure 3.3. Schematic diagram of atomic force microscope for surface imaging.

The voltage differential is sensed by the feedback electronics, causing a change in the Z piezo, the piezo moves in the Z direction and the cantilever recenters the laser beam onto the photodiodes. These changes in Z values will be in both positive and negative. These values of Z will determine the roughness parameters. A mean value will be calculated, by software connected to the hardware of the equipment, and taken as Z equal to zero.

3.2.5.1 Preparation of Samples

Small pieces were cut from the cast membrane and left in a 30 wt % glycerin for 12 hours. The membranes were then dried in air for two days. Small squares of approximately 0.5 cm^2 area were cut from each prepared sample and glued on a metal disk.

3.2.5.2 Microscopic Observations

The AFM images were obtained using a Nanoscope III equipped with a 1553D scanner (Digital Instruments, Santa Barbara, CA). The membrane surfaces were imaged in a scan size of 0.5 × 0.5 μm. Four readings for four areas of 0.25 × 0.25 μm were taken for every sample (0.5 × 0.5 μm) and the average was reported.

3.3 Data Analysis

3.3.1 Membrane Characterization Based on Solute Transport Data

3.3.1.1 Mean Pore Size and Pore Size Distribution

Solute separation, f, in percent is defined as

$$f = \frac{\text{TOC in feed - TOC in product}}{\text{TOC in feed}} \times 100\ \% \qquad (3.3.1)$$

When the solute separation (%) of an ultrafiltration membrane is plotted versus the solute diameter on a log-normal probability paper, a straight line is often found (Micheals, 1980). If solute separation correlates with solute diameter according to the log-normal probability function, the relationship can be expressed as

$$f = \text{erf}(z) = \frac{1}{\sqrt{2\pi}} \int_{-\infty}^{z} e^{-\frac{u^2}{2}} du \qquad (3.3.2)$$

where $$z = \frac{\ln d_s - \ln \mu_s}{\ln \sigma_g} \qquad (3.3.3)$$

and d_s is the solute diameter, μ_s is the geometric mean diameter of a solute which corresponds to solute separation f = 50% and σ_g is the geometric standard deviation about the mean diameter. According to Eqs. 3.3.2 and 3.3.3, a straight line in the form of

$$F(f) = A_0 + A_1 (\ln d_s) \qquad (3.3.4)$$

will be found between f (solute separation in %) and d_s (solute diameter) on a log-normal probability paper. A_0 and A_1 are the intercept and the slope, respectively. From this log-normal plot, mean solute size (μ_s) can be calculated as d_s corresponding to f = 50%. σ_g can be determined from the ratio of d_s at f = 84.13% and at 50%. By ignoring the dependence of solute separation on the steric and hydrodynamic interaction between the solute and the pore (Michaels , 1980; Cooper and Derver, 1979; Ishiguro et al., 1996 and Singh et al., 1998), the mean pore size (μ_p) and the geometric standard deviation (σ_p) of the membrane will be the same as solute mean size and solute geometric standard deviation. From μ_p and

σ_p , the pore size distribution of an ultrafiltration membrane can be expressed by the following probability density function (Youm and Kim, 1991).

$$\frac{df(d_p)}{dd_p} = \frac{1}{d_p \ln\sigma_p \sqrt{2\pi}} \exp\left[-\frac{(\ln d_p - \ln\mu_p)^2}{2(\ln\sigma_p)^2}\right] \tag{3.3.5}$$

where d_p is the pore size.

3.3.1.2 Pore Density and the Surface Porosity

The number of pores per unit area, known as pore density, can be calculated from the permeability data of the membrane using the Hagen-Poiseuille equation. Based on this equation, solvent flux (J_i) through the pores of diameter d_i can be expressed as

$$J_i = \frac{N_i \pi d_i^4 \Delta P}{128\eta\delta} \tag{3.3.6}$$

where N_i is the number of pores (per unit area) having diameter of d_i, δ is the length of the pores, η is the solvent viscosity and ΔP is the pressure difference across the pores. Total flux J through the membrane can be calculated by adding all the fluxes through the pores of different sizes as

$$J = \sum J_i$$

$$J = \frac{\pi\Delta P}{128\eta\delta}\left[N_1 d_1^4 + N_2 d_2^4 + N_3 d_3^4 + \text{----------}\right] \tag{3.3.7}$$

Equation 3.3.7 can be written in terms of total number of pores N and the fraction f_i of pore size d_i

$$J = \frac{\pi\Delta P}{128\eta\delta}\left[f_1 N_1 d_1^4 + f_1 N_2 d_2^4 + f_1 N_3 d_3^4 + \text{------}\right]$$

$$J = \frac{\pi \Delta P N}{128 \eta \delta} \sum_{d_{min}}^{d_{max}} f_i d_i^4 \tag{3.3.8}$$

From Eq. 3.3.8, the total number of pores (N) per unit area can be calculated as

$$N = \frac{128 \eta \delta J}{\pi \Delta P \sum_{d_{min}}^{d_{max}} f_i d_i^4} \tag{3.3.9}$$

The pore length δ is considered equivalent to the skin layer thickness of an asymmetric ultrafiltration membrane.

Similarly, the expression for surface porosity (S_p), which is defined as the ratio between the area of pores to the total membrane surface area, can be derived as

$$S_p = \left(\frac{N \pi}{4} \sum_{d_{min}}^{d_{max}} f_i d_i^2 \right) \tag{3.3.10}$$

3.3.1.3 Stokes Radius of Polyethylene Glycol and Polyethylene Oxide Molecules

The Stokes radius of a macromolecule can be obtained from its diffusivity in a solution by using the following Stokes-Einstein equation

$$D_{AB} = \frac{kT}{6 \pi \eta a} \tag{3.3.11}$$

where D_{AB} is the diffusivity, k is Boltzmann's constant, η is the solvent viscosity and a is the Stokes radius. The diffusivity can also be calculated by the following equation (Hsiehet al.,1979)

$$D_{AB} = \frac{2.5 \times 10^6 kT}{\left\{ \eta \left(M[\eta] \right)^{1/3} \right\}} \tag{3.3.12}$$

where M and [η] are the molecular weight and the intrinsic viscosity of the polymer, respectively. By combining (3.3.11) and (3.3.12) we obtain

$$a = 2.122 \times 10^{-8}(M[\eta])^{1/3} \qquad (3.3.13)$$

where a is in cm, M is in g/mol and [η] is in dL/g. Intrinsic viscosity of a polyethylene glycol (PEG) and a polyethylene oxide (PEO) of known molecular weight can be calculated from the following equations

for PEG (Meireles et al, 1995)

$$[\eta] = 4.9 \times 10^{-4} M^{0.672} \qquad (3.3.14)$$

for PEO (Nabi, 1968)

$$[\eta] = 1.192 \times 10^{-4} M^{0.76} \qquad (3.3.15)$$

Intrinsic viscosities of PEGs of various molecular weights calculated from the empirical equation (Eq. 3.3.14) are in very good agreement with the values determined experimentally by Hsieh et al. (1979). Intrinsic viscosities for some of the PEG are given by (Bessieres et al., 1996), and they are also in very good agreement with the values calculated from empirical equation (Eq. 3.3.14). By substituting the expression for [η] in Eq 3.3.13, we obtain the following equation.

for PEG (Singh et al., 1998)

$$a = 16.73 \times 10^{-10} M^{0.557} \qquad (3.3.16)$$

for PEO (Singh et al., 1998)

$$a = 10.44 \times 10^{-10} M^{0.587} \qquad (3.3.17)$$

From the above empirical equation (Eqs. 3.3.16 and 3.3.17) Stokes radii , in cm, of PEG and PEO molecules can be obtained from their molecular weights.

3.3.2 Membrane Characterization by Atomic Force Microscopy

Surfaces of membranes were compared in terms of the roughness parameters, such as the mean roughness (R_a), the root mean square of the Z data (R_q), and the mean difference in height between the five highest peaks and the five lowest valleys (R_z). Z value is the vertical distance the piezoelectric scanner moves. The mean roughness is the mean value of surface relative to the center plane, the plane for which the volume enclosed by the image above and below this plane are equal, and is calculated as

$$R_a = \frac{1}{L_x L_y} \int_0^{L_x} \int_0^{L_y} |f(x,y)| \, dx \, dy \tag{3.3.18}$$

where f(x, y) is the displacement of the surface relative to the centre plane and L_x and L_y are the dimensions of the surface.

The root mean square of Z values (R_q) is the standard deviation of the Z values within the given area and is calculated as

$$R_q = \sqrt{\frac{\Sigma (Z_i - Z_{avg})^2}{N_p}} \tag{3.3.19}$$

where Z_i is the current Z value, Z_{avg} is the average of the Z values within the given area, and N_p, is the number of points within given area. N_p was set at 256 × 256, which is the number of observations of Z value taken on the sample surface fore.

The average difference in height (R_z) between the five highest and five lowest valleys is calculated relative to the mean plane, which is a plane about which the image data has a minimum variance.

CHAPTER 4

4. RESULTS AND DISCUSSION

The results of this research work will be presented starting with the surface tension and conductivity measurements of the gelation media, followed by the characterization of the membranes by the solute separation technique, and, finally, the membrane characterization by roughness measurements using the AFM technique.

In the discussion, it is intended to discuss the effect of the gelation medium composition and temperature on PES membrane performance and morphology. In particular, the focus will be on the effect of the interfacial phenomena of the surfactant solution on the solvent-nonsolvent exchange, which takes place in the gelation bath and subsequently on the membrane performance and morphology.

4.1. Characterization of Gelation Media

4.1.1. Measurements of Surface Tension

Surface tension data were obtained for SDS aqueous solutions that were used as gelation media in the preparation of PES membranes. The surface tension measurements were carried out at two different temperatures, 4°C and 20°C. The concentration of SDS

in the gelation bath was in a range of 0 to 3.0 g/L. The experiments were carried out at flow rate of 0.1 mL/min.

Figure 4.1 shows surface tension data plotted as a function of sodium dodecyl sulfate (SDS) concentration at 4°C and at 20°C. The surface tension decreased with an increase in SDS concentration until the concentration reached a certain value then levelled off. This concentration corresponds to the CMC, which was 1.2 g/L (8.27×10^{-3}M) for solutions measured at 20°C. The CMC was 1.4 g/L (9.6×10^{-3}M) at 4°C. The lowest surface tension occurred at 4°C, which was higher than that recorded at 20°C.

As indicated in section 2.3.1, the measurement of the surface tension of a surfactant solution is a common physical technique to characterise the surfactant. The maximum reduction in surface tension that can be achieved by the addition of any quantity of surfactant is known as surfactant "effectiveness" (Myers, 1988). The results in this work showed that the temperature affects the effectiveness of SDS especially at concentrations higher than 0.2 g/L.

4.1.2. Measurements of Conductivity

Figure 4.2 shows the results of conductivity measurements for SDS aqueous solutions at 4°C and 20°C. The conductivity at 20°C is higher than the conductivity at 4°C. The results at 20°C show a bigger change after 1.2 g/L, which is the CMC, than before it. The change is more significant after 1.4 g/L. The significant change in the conductivity at 4°C occurs after 1.4 g/L, which is the CMC.

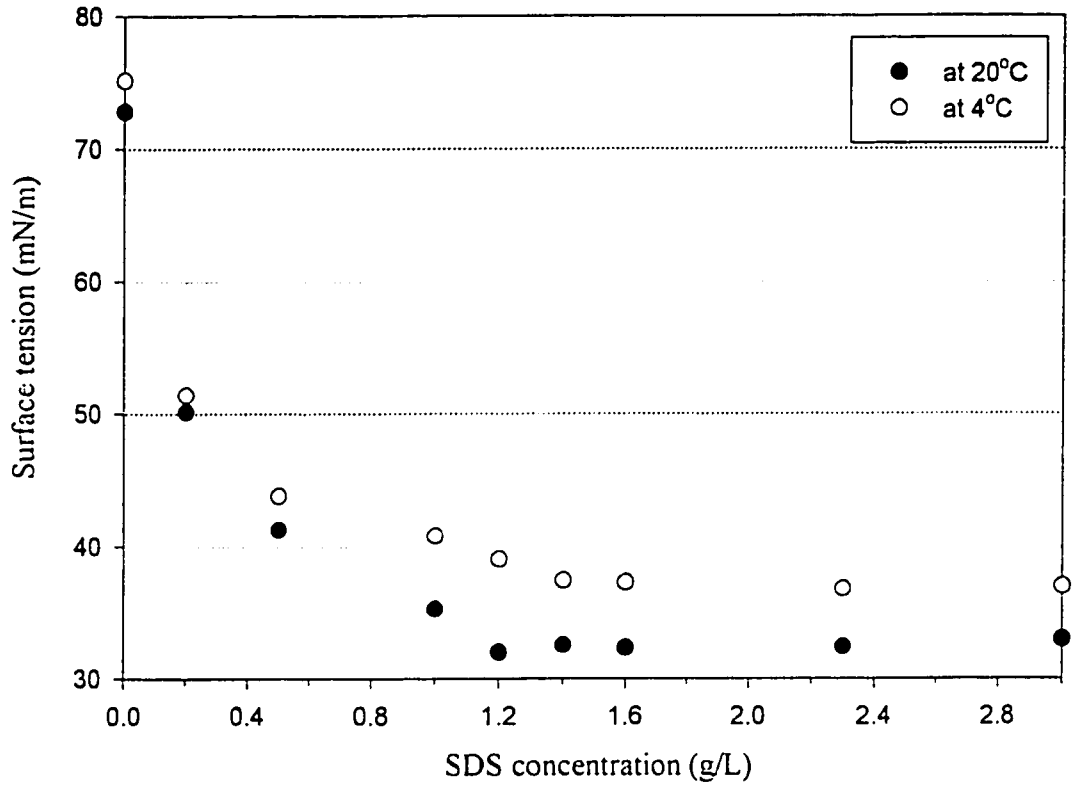

Figure 4.1. Surface tension of SDS aqueous solutions as a function of SDS concentration.

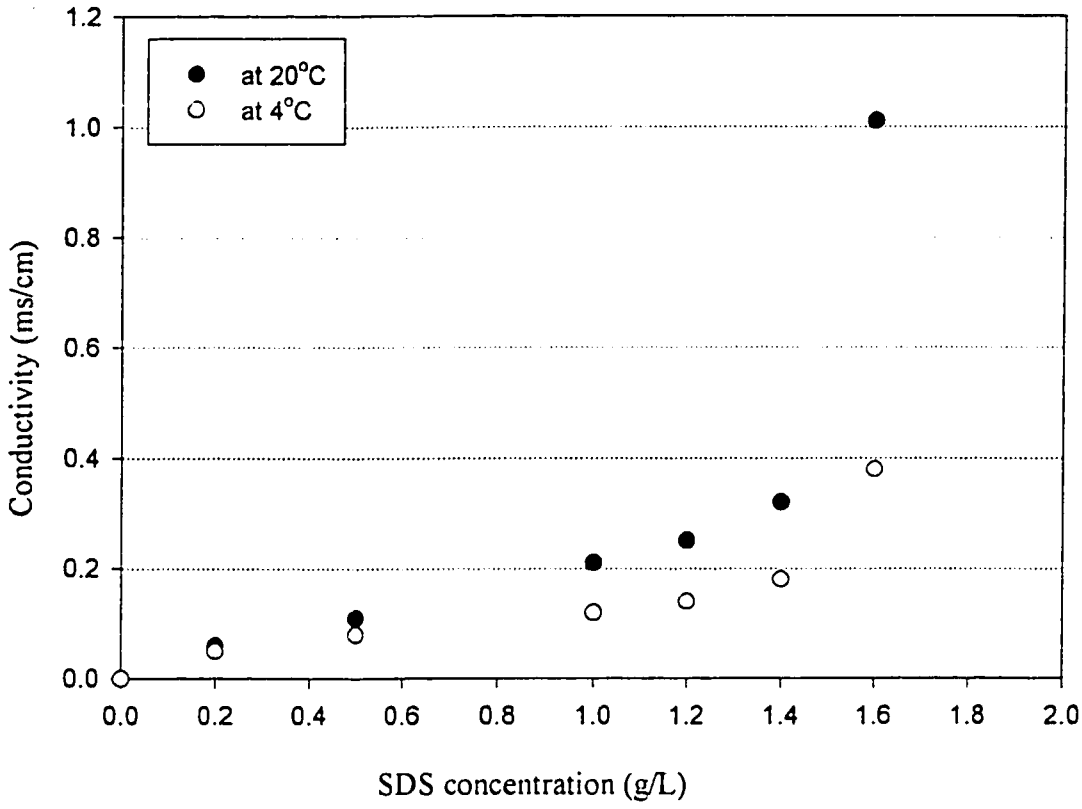

Figure 4.2. Conductivity of SDS aqueous solutions as a function of SDS concentration.

But, most important, the difference in the conductivity between both temperatures increases until CMC was reached. The difference became much larger at the concentration above CMC.

As it is mentioned in Chapter 2, the sharp turn in conductivity indicates micelle formation at CMC. The temperature affects the number of formed micelles by affecting the shape of the surfactant molecules. The molecules at higher temperature are more flexible, and micelles can form more easily (Miller, 1997). As a result, more and bigger micelles will be formed at high temperature than at lower temperature. The solubility in micelle solution increases with an increase in the number and the size of the formed micelles. Therefore, the solubility in SDS solutions at 20°C solutions should be higher than that at 4°C.

4.2. Effect of SDS Concentration on the Membrane Performance

4.2.1 Effect of SDS concentration on Molecular Weight Cut-off and Mean Pore Size

Molecular weight cut-offs (MWCO) (molecular weight of the solute at which 90% separation can be achieved), pore sizes and their distributions within the tested membranes were calculated from the separation data using PEG and PEO of various molecular weights as solutes. A straight line was obtained with a correlation coefficient (r^2) ranging from 0.8 to 0.97, while plotting the percent separation of PEG/PEO solutes versus their diameters on a log-normal probability paper as depicted in Figures 4.3 and 4.4. The percent separation data from each cell were plotted in these graphs.

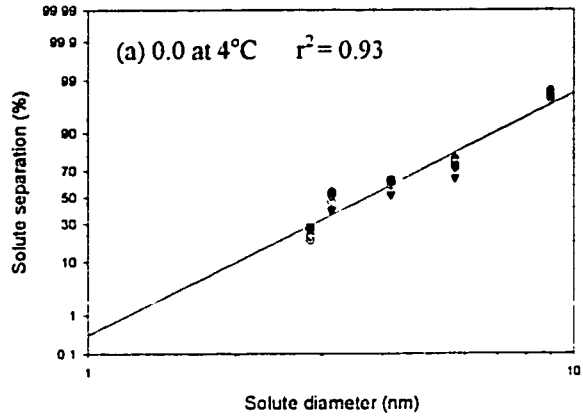

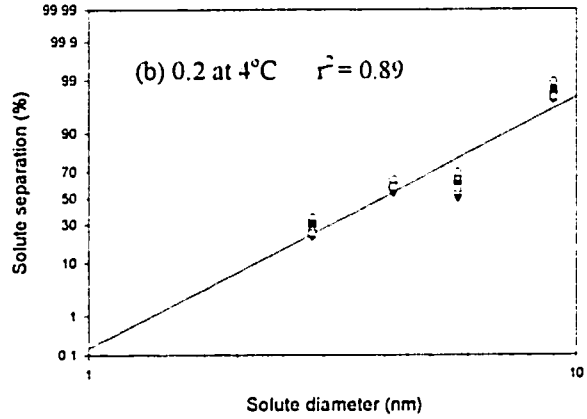

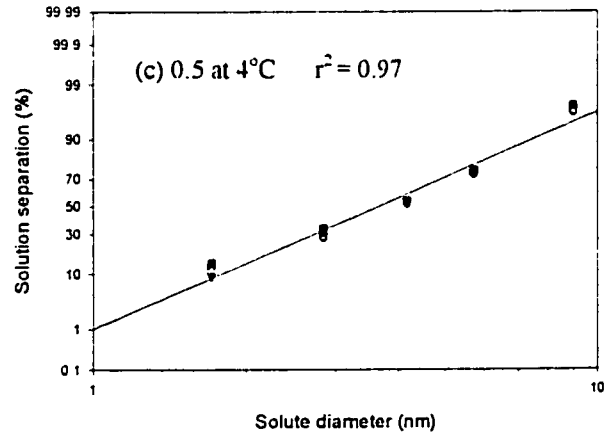

Figure 4.3. Solute separation versus solute diameter for membranes gelled at 4°C plotted on log-normal probability paper (• cell 1, o cell 2, ▼ cell 3, ▽ cell 4, ■ cell 5, □ cell 6). SDS concentration, (a) 0.0 g/L (b) 0.2 g/L (c) 0.5 g/L.

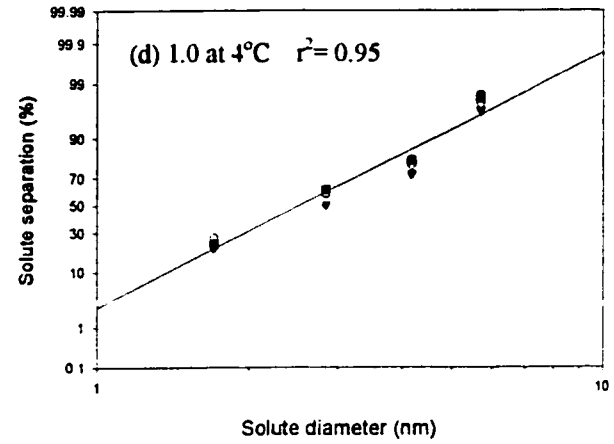

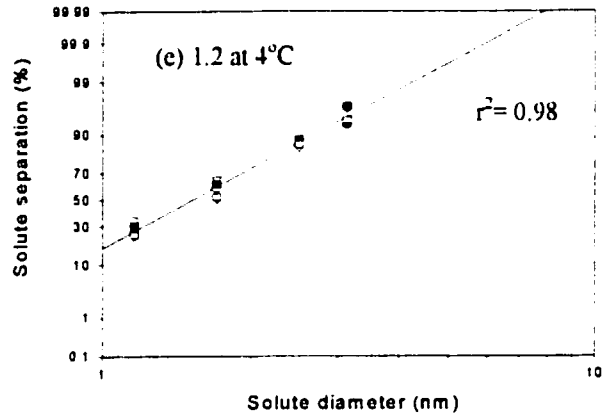

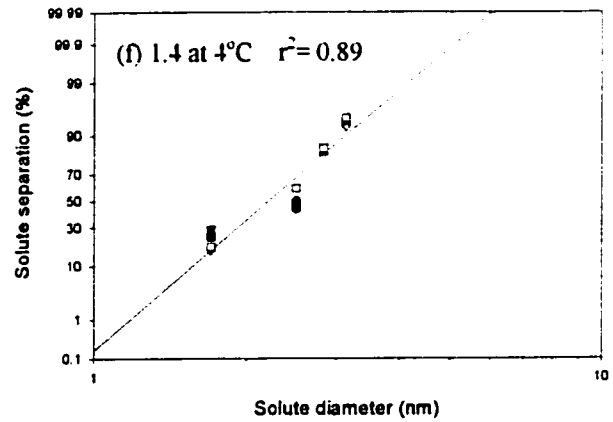

Figure 4.3. (cont'd) Solute separation versus solute diameter for membranes gelled at 4°C plotted on log-normal probability paper (• cell 1, o cell 2, ▼ cell 3, ▽ cell 4, ■ cell 5, □ cell 6). SDS concentration, (d) 1.0 g/L (e) 1.2 g/L (f) 1.4 g/L.

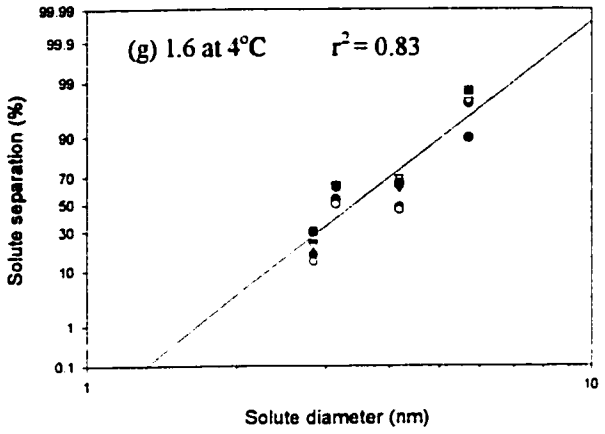

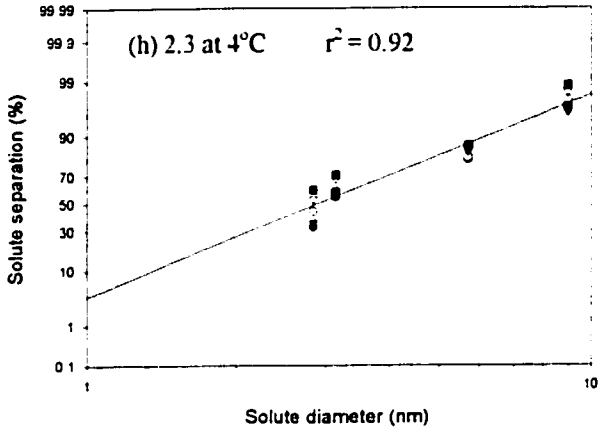

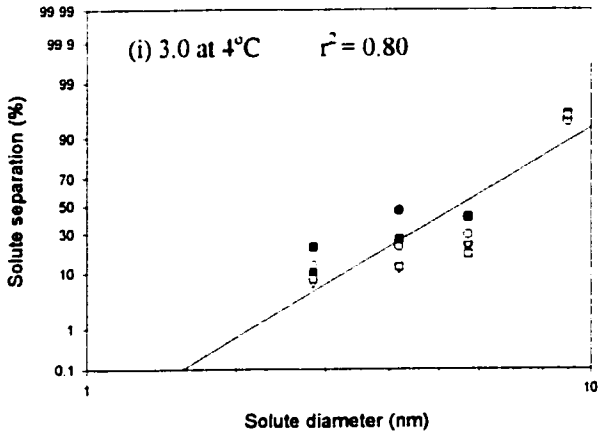

Figure 4.3. (cont'd) Solute separation versus solute diameter for membranes gelled at 4°C plotted on log-normal probability paper (• cell 1, o cell 2, ▼ cell 3, ▽ cell 4, ■ cell 5, □ cell 6). SDS concentration, (g) 1.6 g/L (h) 2.3 g/L (i) 3.0 g/L.

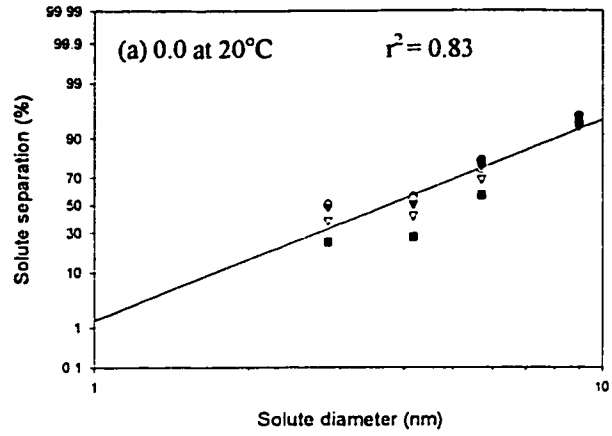

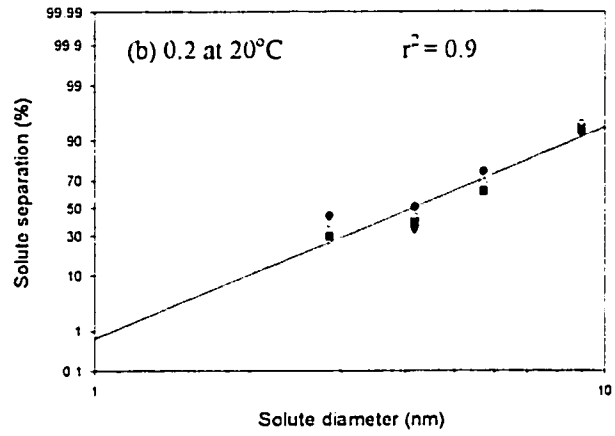

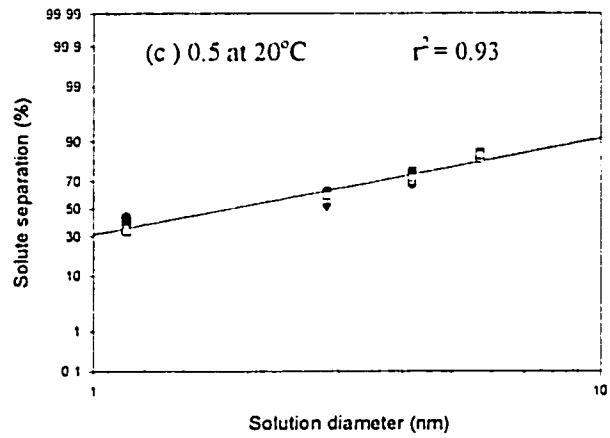

Figure 4.4. Solute separation versus solute diameter for membranes gelled at 20°C plotted on log-normal probability paper (• cell 1, o cell 2, ▼ cell 3, ▽ cell 4, ■ cell 5, □ cell 6). SDS concentration, (a) 0.0 g/L (b) 0.2 g/L (c) 0.5 g/L.

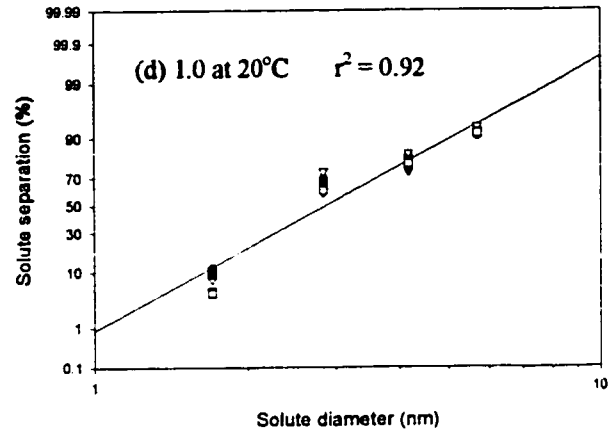

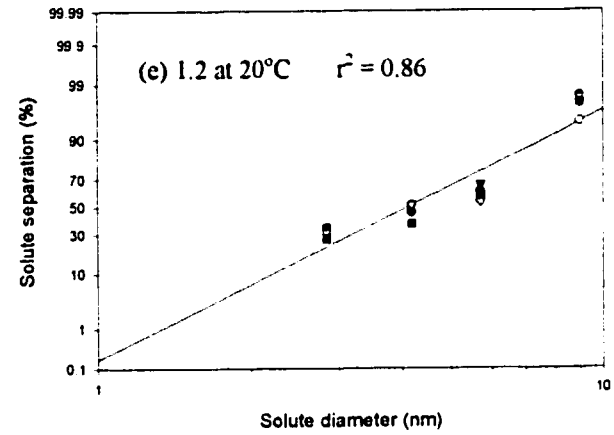

Figure 4.4. (cont'd) Solute separation versus solute diameter for membranes gelled at 20°C plotted on log-normal probability paper (• cell 1, o cell 2, ▼ cell 3, ▽ cell 4, ■ cell 5, □ cell 6). SDS concentration, (d) 1.0 g/L (e) 1.2 g/L.

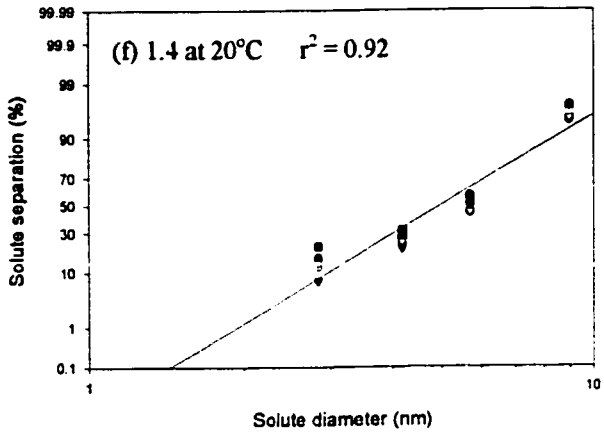

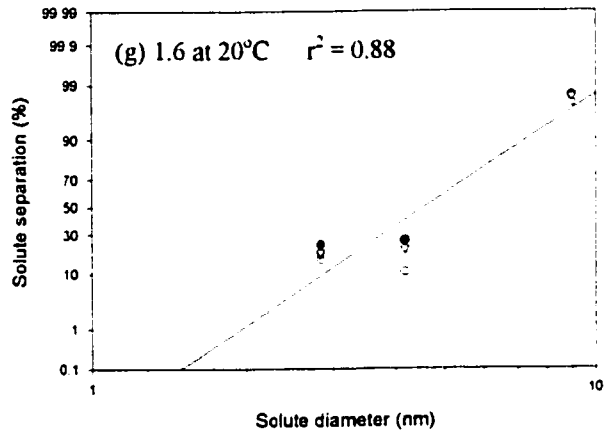

Figure 4.4. (cont'd) Solute separation versus solute diameter for membranes gelled at 20°C plotted on log-normal probability paper (• cell 1, o cell 2, ▼ cell 3, ▽ cell 4, ■ cell 5, □ cell 6). SDS concentration, (f) 1.4 g/L (g) 1.6 g/L.

The values of the molecular weight cut-off (MWCO), the geometric mean pore size (μ_p) and the geometric standard deviation (σ_p) around the mean were determined from Figure 4.3 and Figure 4.4 according to the method described in Chapter 3. These values are summarised in Table 4.1. Sample calculation of the MWCO, the geometric mean pore size and the geometric standard deviation is provided in Appendix B.

Figure 4.5 shows the effect of SDS concentration in the gelation bath on MWCO of the tested membranes. Each data point represents a membrane that was prepared by using a gelation bath of the given concentration. The effect of temperature is also shown in Figure 4.5. The approximate error bars in Figure 4.5 were generated in the following way. The standard deviation in solute separation around 90% is ±2%. Therefore, the molecular weights that correspond to 88% and 92%, respectively, were taken as the lower and upper end for each bar. It is obvious from the figure that the correlation curve can be divided into two regions. Region 1 is from 0 to 1.2 g/L for 4°C, and from 0 to 1.0 g/L for 20°C.

In region 1, MWCO decreases progressively with an increase in SDS concentration. In region 2, MWCO increases progressively with an increase in SDS in the gelation bath. The only exception in this region was membranes gelled in 0.2 g/L. Even if the MWCOs of membranes gelled in 0 g/L, 0.2 g/L and 0.5 g/L looks similar by considering the error bars, the mean values of MWCOs showed difference. The SDS concentration ranges in the gelation bath corresponding to region 2 are (1.2 - 3.0 g/L) for 4°C and (1.0 - 1.6 g/L) for 20°C.

Table 4.1. Geometric mean pore size (μ_p), geometric standard deviation (σ_p) and MWCO values for various SDS concentrations in the gelation bath at 4°C and 20°C.

SDS conc.in the gelation bath (g/L)	Temperature of gelation media, 4°C			Temperature of gelation media, 20°C		
	MWCO, (kDa♣)	Mean pore size, μ_p(nm)	Geometric Std. Dev.,σ_p	MWCO, (kDa♣)	Mean pore size, μ_p(nm)	Geometric Std. Dev.,σ_p
0	49.83* ± 5.16**	7.43	1.62	65.19 ± 5.62	7.47	1.82
0.2	56.41 ± 6.21	7.09	1.69	73.79 ± 6.11	8.20	1.78
0.5	50.02 ± 5.37	7.09	1.76	58.97 ± 8.69	4.53	2.45
1.0	23.68 ± 2.27	5.02	1.60	28.52 ± 2.09	5.70	1.56
1.2	9.15 ± 0.03	3.06	1.53	60.02 ± 7.27	7.96	1.67
1.4	11.97 ± 0.74	4.42	1.30	70.81 ± 5.68	7.09	1.49
1.6	28.52 ± 1.77	6.77	1.36	88.89 ± 7.35	10.99	1.57
2.3	42.24 ± 5.25	5.83	1.80			
3.0	83.54 ± 6.11	10.99	1.51			

♣kilodaltons. * Mean value. **Standard deviation.

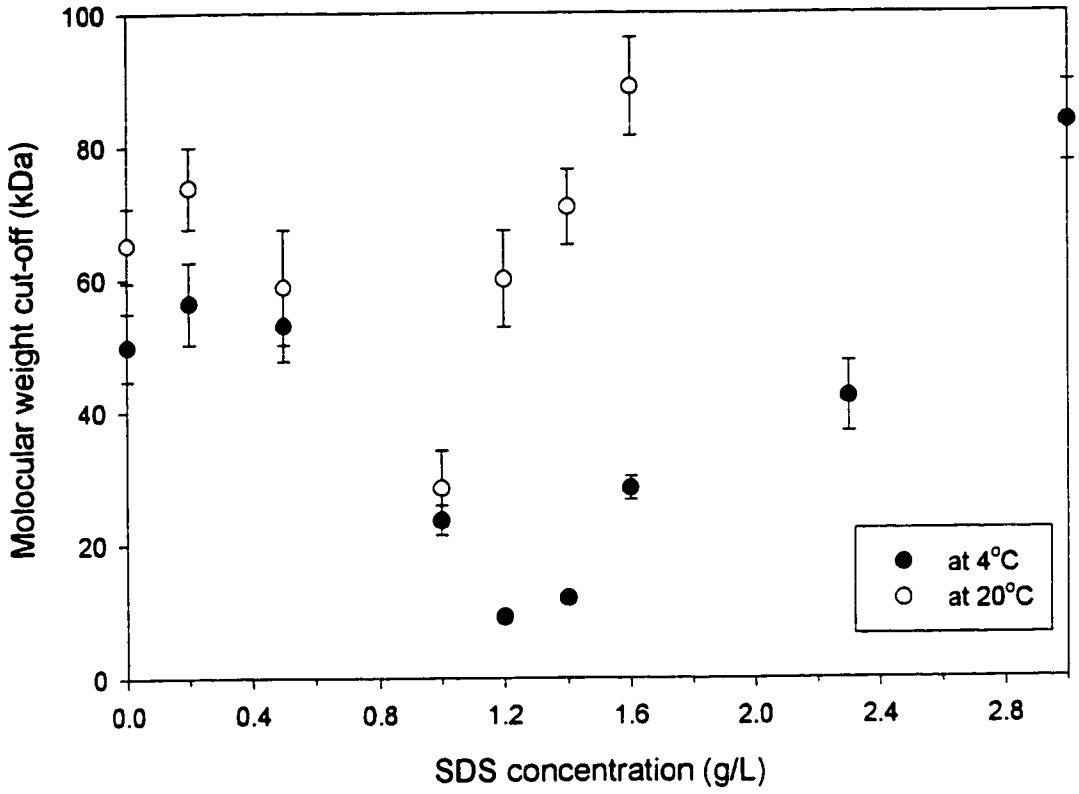

Figure 4.5. Effect of SDS concentration in the gelation bath on the molecular weight cut-off (MWCO) of PES membranes (error bars represent the standard deviation around the mean value).

The MWCO, at 4°C, drops from 49.83 kDa, when the SDS concentration is 0 g/L, to 9.15 kDa, when the SDS concentration is 1.2 g/L and then increases again to 83.54 kDa, when the SDS concentration is 3.0 g/L. The MWCO at 20°C drops from 65.19 kDa, at SDS concentration of 0 g/L, to 28.52 kDa, at SDS concentration of 1.0 g/L and then increases to 88.89 kDa, at SDS concentration of 1.6 g/L. From Figure 4.15 and Table 4.1, it is shown that when the CMC increased, by decreasing the temperature, the decrease in the MWCO continued, and therefore, 1.0 g/L is considered the minimum at 20°C and 1.2 g/L is considered the minimum at 4°C.

The mean pore size, similar to the MWCO, decreased with a progressive increase in SDS concentration in region 1 and then increased with an increase in SDS concentration in region 2. The smallest pore sizes were obtained at 1.2 g/L and 0.5 g/L for 4°C and 20°C, respectively. The smallest pore size was 3.06 nm for 4°C and 4.53 nm for 20°C. In general, the mean pore size (μ_p) has the same trend as the MWCO. The mean pore size was higher for membranes having higher molecular weight cut-offs (Table 4.1).

The presence of two regions in the plot of pore size (represented by molecular weight cut-off in Figure 4.5) versus SDS concentration in the gelation bath can be explained in the following way. When a cast polymer solution is immersed in a gelation medium (water or SDS solution in this case), one side of the film is brought into contact with the gelation medium. The exchange of solvent and nonsolvent starts to occur at the gelation medium/polymer solution interface, that is, the solvent moves from inside the cast film into the gelation medium and the nonsolvent (water in this study) moves from the gelation medium into the cast film (Figure 4.6,a).

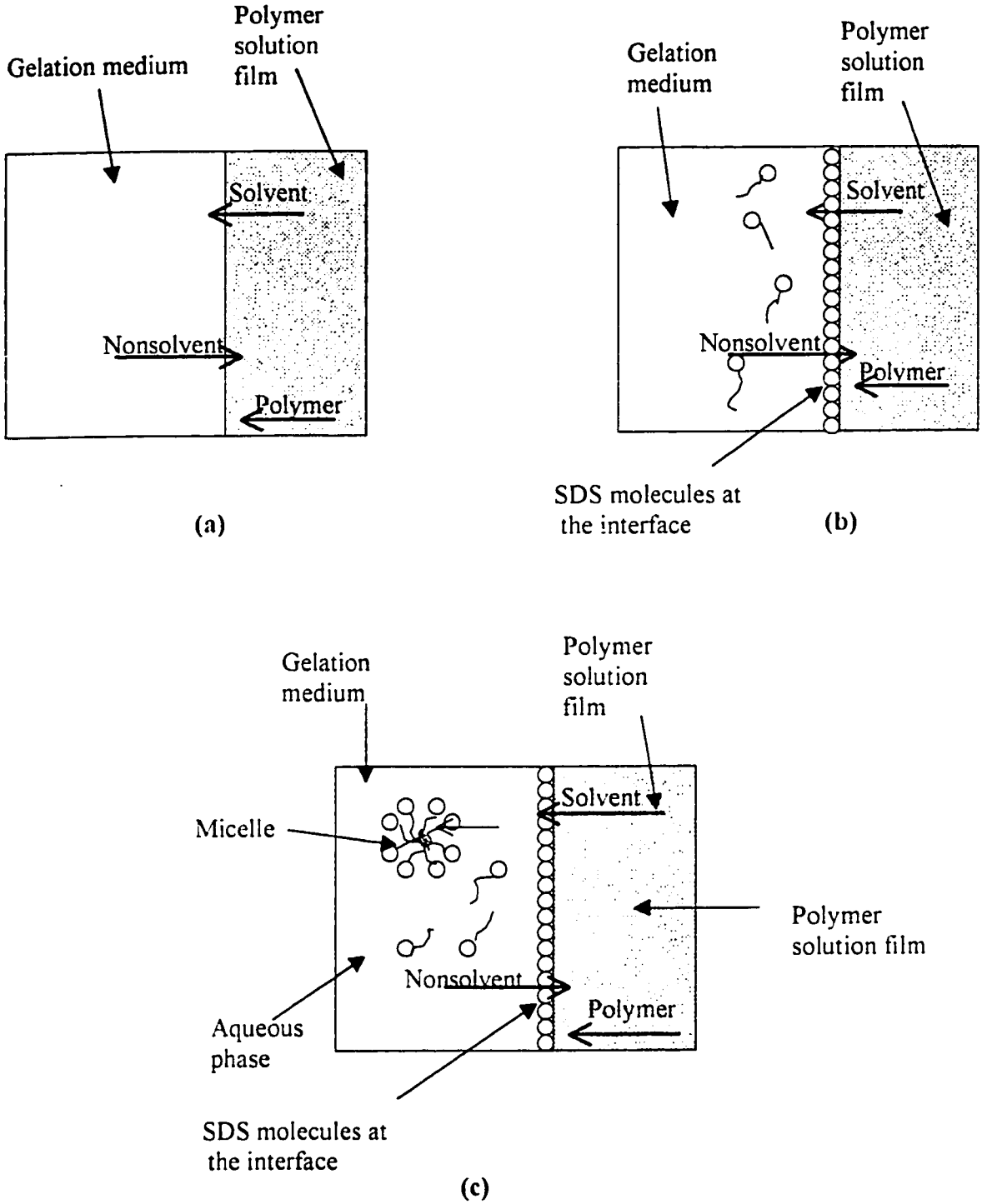

Figure 4.6. Schematic drawing of nonsolvent/solvent exchange process at the gelation media/polymer solution interface. Gelation bath has different SDS concentration, (a) pure water (b) SDS concentration, CMC (c) SDS concentration, higher than CMC.

As a result of this exchange, the ratio of nonsolvent to solvent in the polymer solution film starts to increase. When the ratio reaches a critical value, the nonsolvent/solvent mixture can not hold polymer any longer and polymer precipitates. Precipitation of polymer occurs first at the interface, since the nonsolvent/solvent ratio change is the fastest at the interface, and gradually propagates into the polymer solution film. As it is described in Chapter 2, not only solvent and nonsolvent but also the polymer in the solution film keeps moving towards the interface during the gelation procedure (Strathmann and Koch, 1977).

The movement of the polymer is, however, restricted to the inside of the polymer solution film. It should be noted that the movement of the polymer continues as long as the polymer stays in a fluid state. The longer the polymer moves, the higher its concentration becomes at the interface.

In the presence of SDS in gelation medium, the SDS molecules are adsorbed at the interface. The SDS molecules accumulate at the interface, forming a barrier layer against the mass transfer through the interface (Figure 4.6,b). According to Sawistowski (1971), the presence of the surfactant at the interface will reduce the mass transfer through it. This slows down the process of nonsolvent/solvent exchange at the interface and delays the time at which polymer precipitates. As a result, the polymer concentration at the interface becomes higher and a denser polymer layer is formed. Since the latter polymer layer will become the skin layer of an asymmetric membrane, when the gelation process is completed, the pore size of the skin layer becomes smaller. The decrease in pore size is enhanced as the SDS concentration in the gelation medium increases. This explains

region 1, where pore size decreases with an increase in the SDS concentration and particularly, when the SDS concentration is below CMC.

The exception in region 1is the increase in the MWCO at 0.2 g/L, which does not go with the previous assumption for region 1. The behavior of this membrane can be ascribed to the effect of the surface tension on the interfacial area. Decreasing the surface tension increases the interfacial area, which in turn increases the extraction rate of the solvent (NMP). The effect of the surface tension decrease on the contact interfacial area is stronger than the effect of the presence of the surfactant molecules on the overall mass transfer. In other words, the driving force acts more effectively, in favour of faster transfer of NMP from the casting solution film than the resistance, which is caused by the presence of SDS molecules at the interface. The decrease in the MWCO and the pore size start clearly from SDS concentration of 0.5 g/L. The increase in the interfacial area continues side by side with the decrease in the surface tension. By looking back in Figure 4.1, it can be noticed that the effect of SDS concentration on surface tension generally diminishes as SDS concentration increases. This effect is the strongest when the first 0.2 g/L are added. This explains why the effect of interfacial area increase surpassed the effect of the barrier formation at this concentration. The increase in the SDS concentration, beyond 0.2 g/L, increases the resistance more than increasing the interfacial contact area. This favors slower transfer of NMP and consequently increases the polymer concentration in the skin layer.

In region 2, where the concentration of SDS is higher than CMC, its concentration in the aqueous phase of the gelation media remains constant, since the aqueous phase has

been already saturated with SDS. SDS molecules that can not be dissolved in the aqueous phase start to form micelles in the gelation medium (Figure 4.6,c). These micelles have a capacity to accommodate solvent molecules. Therefore, solvent molecules after they transfer from the polymer solution film to the gelation medium, they further transfer from the aqueous phase of the gelation medium to the inside of the micelles. The result is a decrease in solvent concentration in the aqueous phase. The driving force, which is the concentration difference, for the transfer of the solvent (NMP) from the polymer solution film to the gelation medium is thus increased. The resistance of the interfacial SDS barrier layer, on the other hand, remains constant, since the SDS concentration in the aqueous phase remains constant when SDS concentration is above CMC. In other words, the resistance remains the same and the driving force for the solvent (NMP) transfer, which takes form of concentration difference, increases with the increase in the SDS concentration. As a result, solvent transport rate is increased. Therefore, the critical nonsolvent/solvent ratio is achieved more quickly when SDS concentration surpasses the CMC, resulting in a less dense solid polymer layer at the interface. As SDS concentration keeps increasing, the polymer layer becomes progressively less dense, resulting in an increase in the pore size at the skin layer of the asymmetric membrane.

The geometric standard deviations around the mean pore sizes (σ_p) was determined from Figures 4.3 and 4.4. Their range is from 1.30 to 2.45. Micheals (1980) found that the values of σ_p for different ultrafiltration membranes, both biological and synthetic, were very close to each other (from 1.2 to 1.66). On this basis, it was said that virtually all the membrane ultrafilters, irrespective of their origin, were quite similar in their

microstructure. Singh et al. (1998) found that σ_p of different PES membranes covered a much wider range (from 1.68 to 3.31). The range of σ_p obtained in this study is slightly higher than that obtained by Micheals (1980), which means that the membranes used in this study have wider pore size distribution.

The cumulative pore size distributions for membranes gelled at 4°C and 20°C are shown in Figure 4.7 and Figure 4.8. From Figure 4.7,a, the pore size distribution shifts to the left with an increase in the SDS concentration in the gelation bath. These membranes belong to region 1, where the pore size decreases with an increase in SDS concentration in the gelation bath. The shift to the left in the pore size distribution means a decrease in the pore size. On the other hand, the pore size shifts to the right with the increase in SDS concentration in the gelation bath as shown in Figure 4.7,b. These membranes belong to region 2. In Figure 4.8,a, the pore size distribution shifts to the left with the increase in SDS concentration in the gelation bath. In figure 4.8,b, the pore size distribution shifts to the right with the increase in SDS concentration.

Probability density function curves were also generated from Eq. 3.3.5 by using the values of mean pore size and geometrical standard deviation for all the membranes under study. As shown in Figure 4.9,a and Figure 4.10,a, the leftward shifts of the probability density function curves were observed as the SDS concentration increased in the gelation bath. In Figures 4.9,b and 4.10,b, the probability density function curves shifted to the right as the SDS concentration increased in the gelation bath.

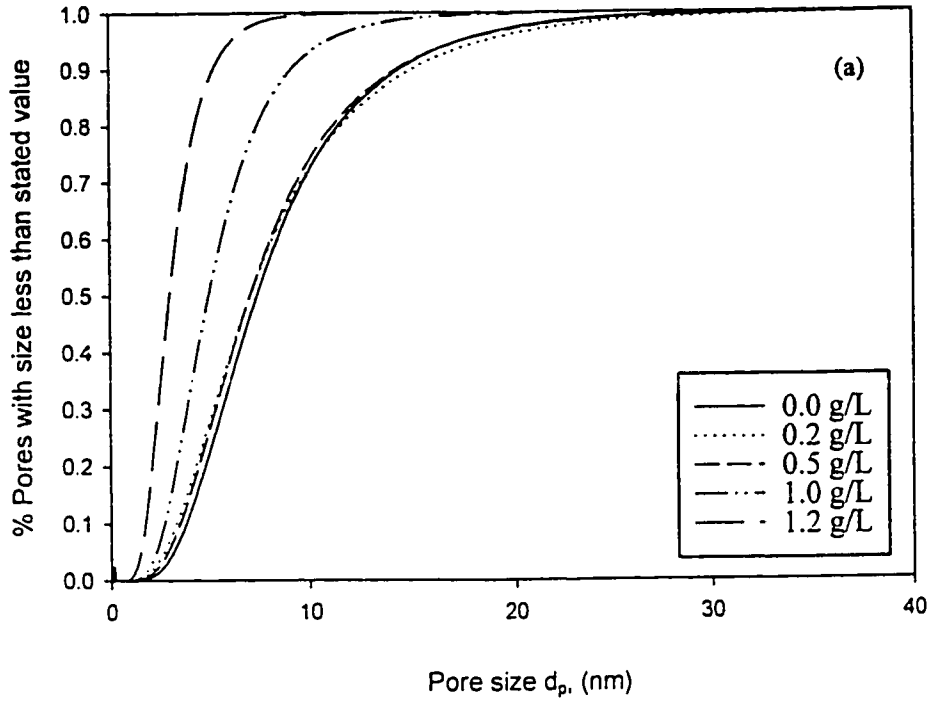

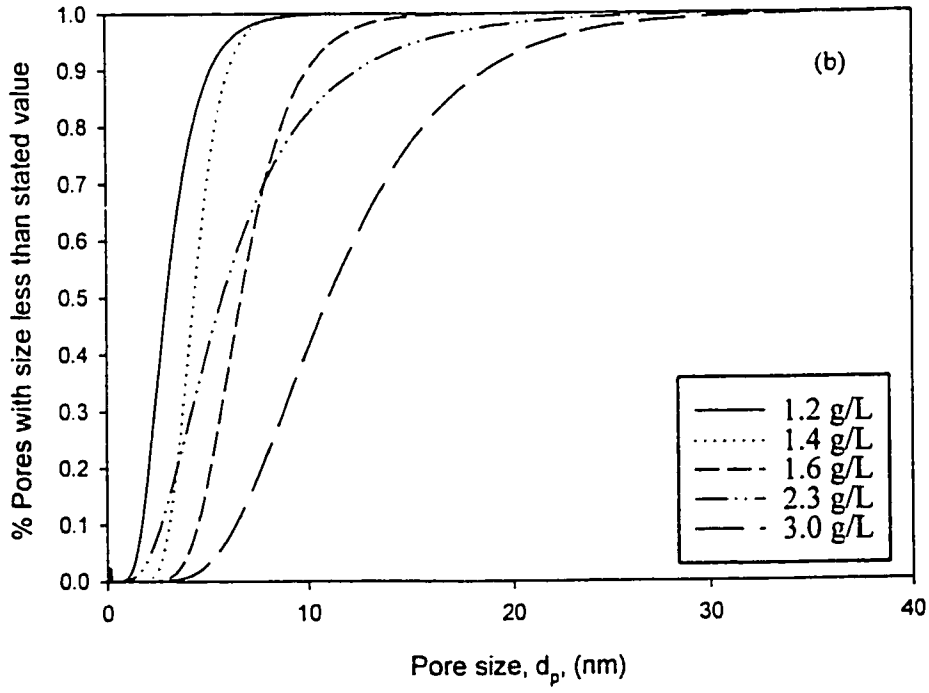

Figure 4.7. Cumulative pore size distribution for membranes gelled at 4°C gelation baths (a) SDS concentration, below CMC (b) SDS concentration, CMC and higher.

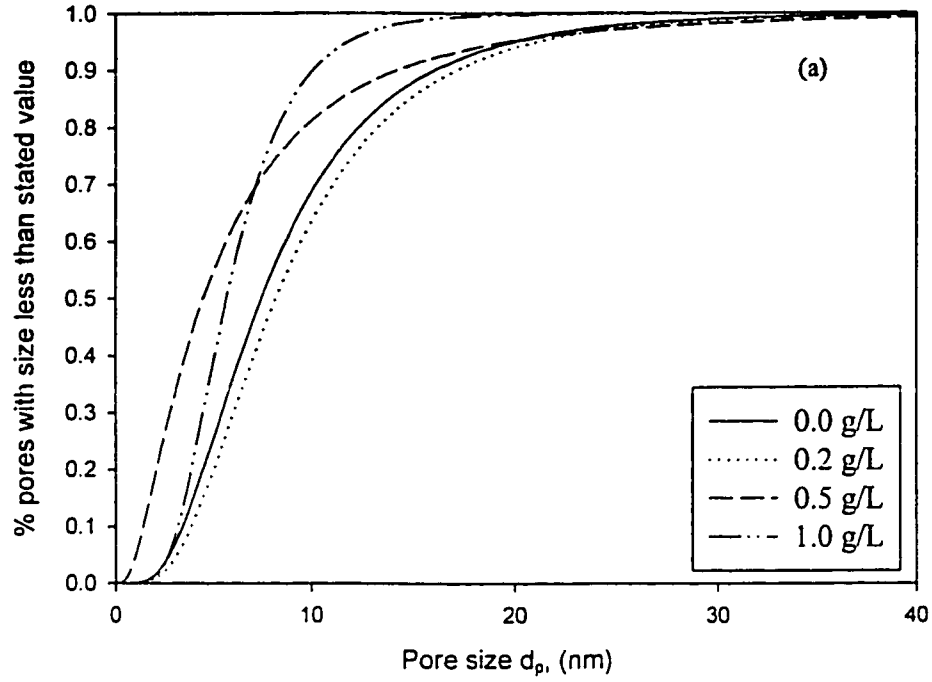

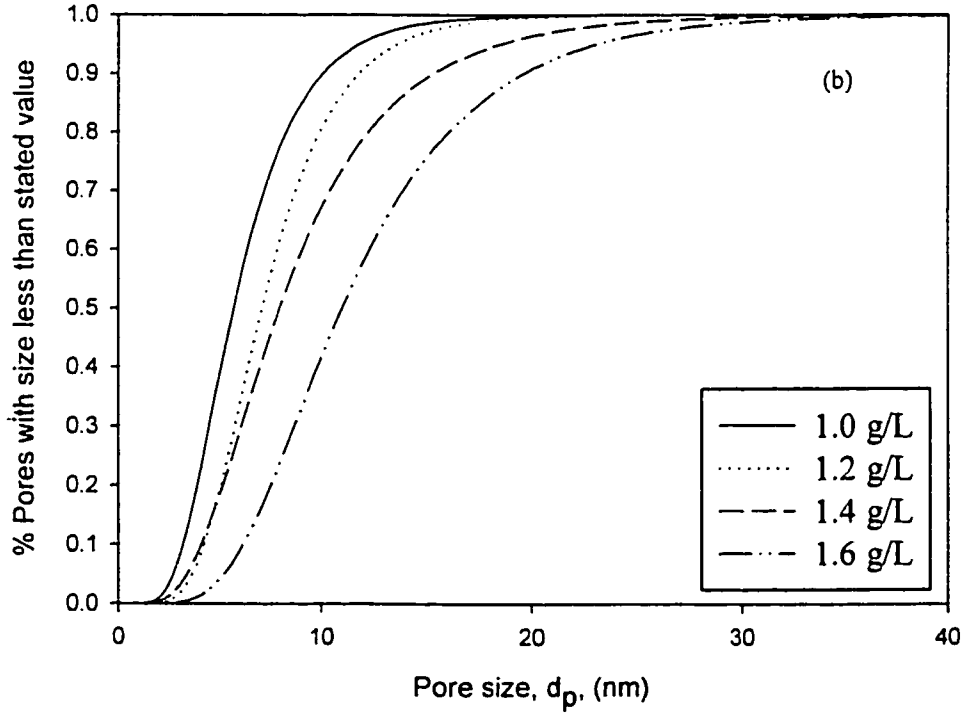

Figure 4.8. Cumulative pore size distribution for membranes gelled at 20°C gelation baths (a) SDS concentration, below CMC (b) SDS concentration, CMC and higher.

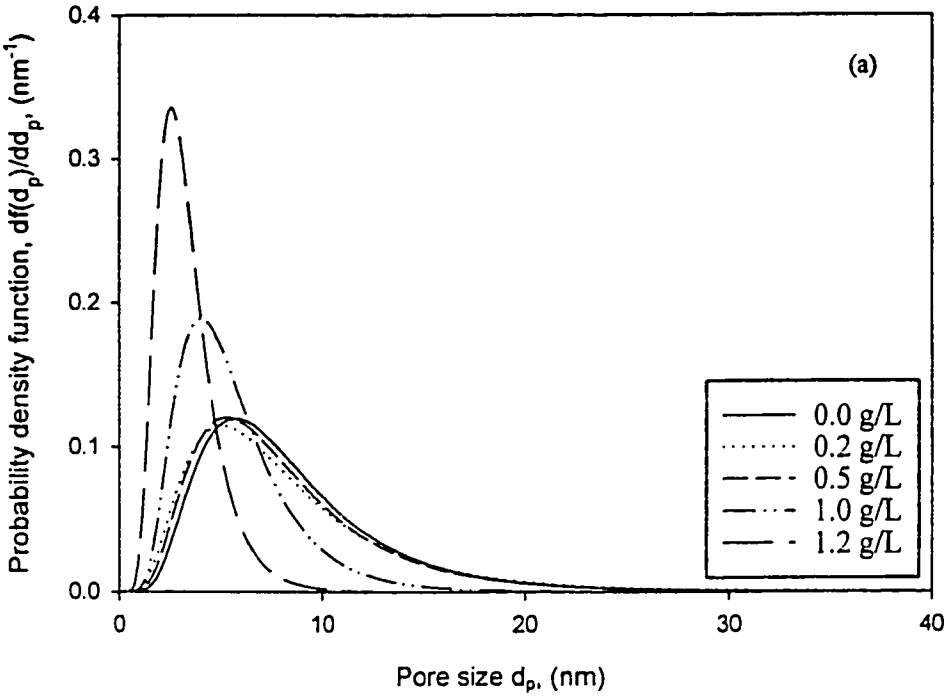

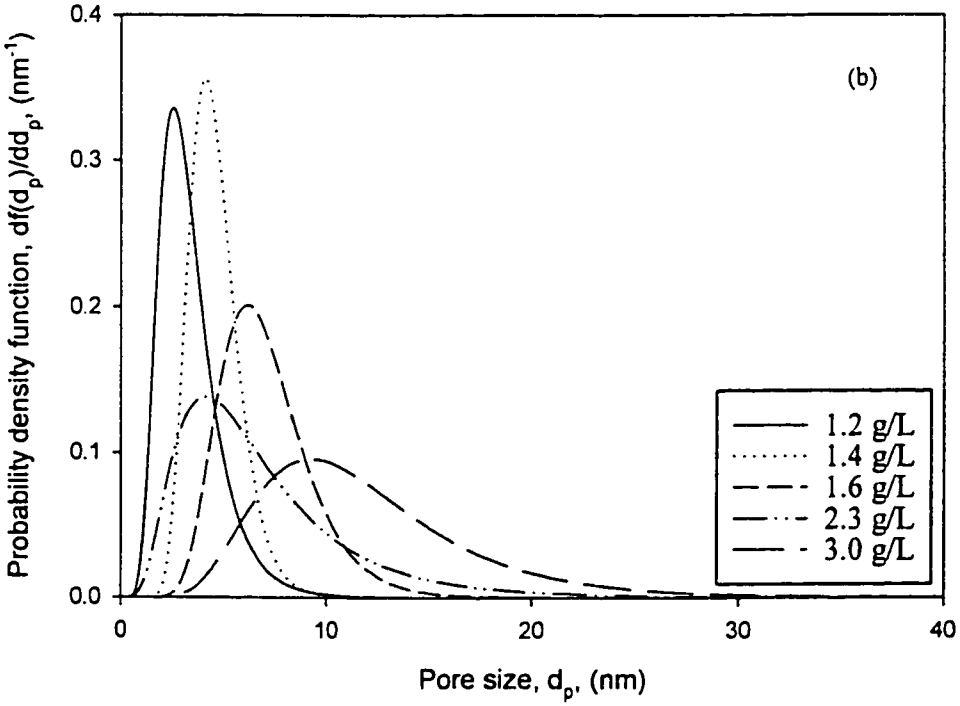

Figure 4.9. Probability density function curves for membranes gelled at 4°C (a) SDS concentration, below CMC (b) SDS concentration, CMC and higher.

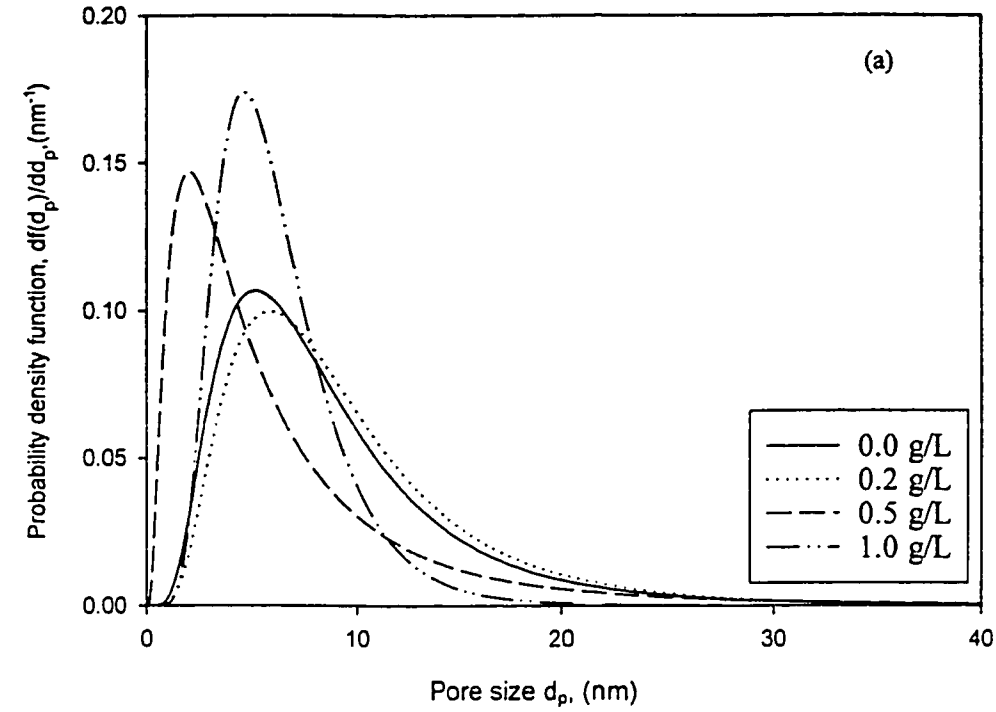

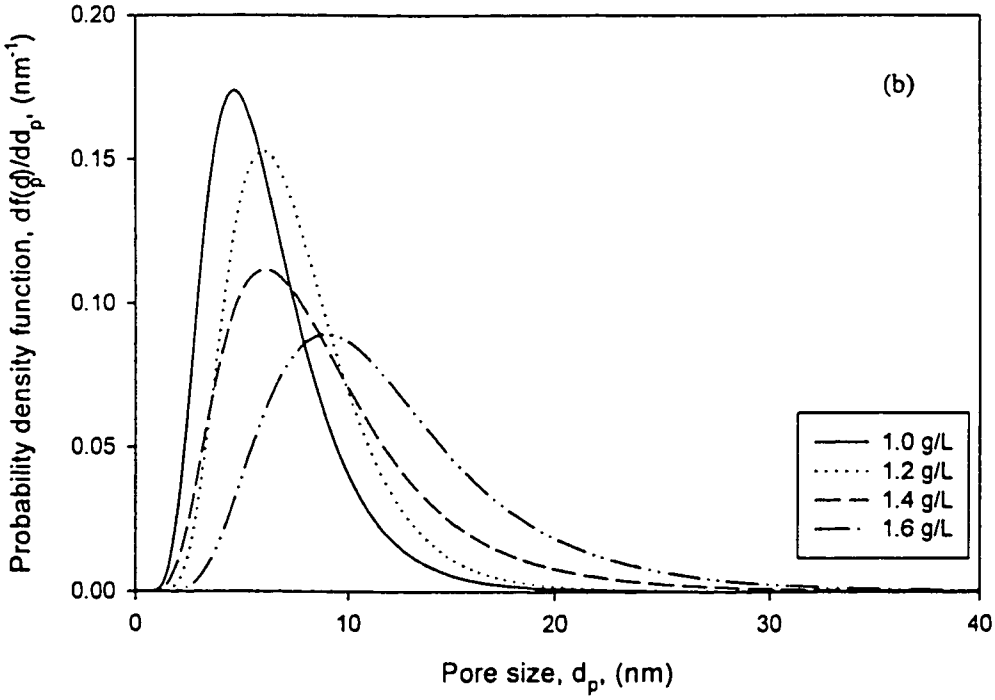

Figure 4.10. Probability density function curves for membranes gelled at 20°C (a) SDS concentration, below CMC (b) SDS concentration, CMC and higher.

4.2.2 Effect of SDS Concentration on Pore Density and Surface Porosity

Pore density and surface porosity were calculated from Eqs. 3.3.8 and 3.3.9, respectively, and the results are summarised in Table 4.2. The skin layer thickness was assumed to be 0.2 μm, which was well within the range of the skin layer thickness mentioned by other researchers (Strathmann et al., 1975 and Singh et al., 1998) for ultrafiltration membranes made of various materials. Sample calculation of pore density and surface porosity is provided in Appendix B. The membrane gelled in an aqueous solution of 1.2 g/L SDS concentration has the highest pore density of 998.2 pores/μm^2 among membranes gelled at 4°C. However, for membranes gelled at 20°C, the membrane gelled in an aqueous solution of 1.0 g/L SDS concentration has the highest pore density of 126.6 pores/μm^2. In general, the pore density increases with an increase in SDS concentration in the gelation bath in region 1, and decreases with an increase in SDS concentration in region 2.

Surface porosities of membranes gelled at 4°C were between 0.14 to 1.22 %, while those for membranes gelled at 20°C were between 0.09 to 0.54 %. The surface porosity, in general, increases with an increase in pore density and decreases with a decrease in pore density.

The pore density and surface porosity of the tested membranes were plotted against the gelation media concentration as shown in Figures 4.11 and 4.12. Two regions similar to the ones resulted from Figure 4.5 appeared. In region 1, the pore density and the surface porosity increase with the increase in the SDS concentration in the gelation media, which is the result of the high polymer concentration in the skin layer. The high

Table 4.2. Pore densities and surface porosities of various membranes gelled in aqueous solutions with various SDS concentrations.

SDS conc. in gelation bath (g/L)	Gelation baths at 4°C		Gelation baths at 20°C	
	Pore density (Pores/μm^2)	Surface porosity (%)	Pore density (Pores/μm^2)	Surface porosity (%)
0	29.5	0.23	9.3	0.09
0.2	15.8	0.14	9.7	0.12
0.5	28	0.23	15.0	0.12
1.0	164.6	0.58	126.6	0.54
1.2	998.3	1.22	17.3	0.16
1.4	558.7	1.10	16.4	0.20
1.6	141.2	0.69	10.9	0.17
2.3	54.7	0.31		
3.0	11.1	0.16		

In region 2, the surface porosity and the pore density decrease with the increase in the SDS in the gelation media. As it is explained earlier for the pore size and the MWCO, the decrease in the porosity and pore density resulted from the decrease in the polymer concentration in the skin layer. The polymer concentration decreases because of the acceleration in the transfer rate of NMP as the SDS concentration increased in the gelation media (Figure 6,b).

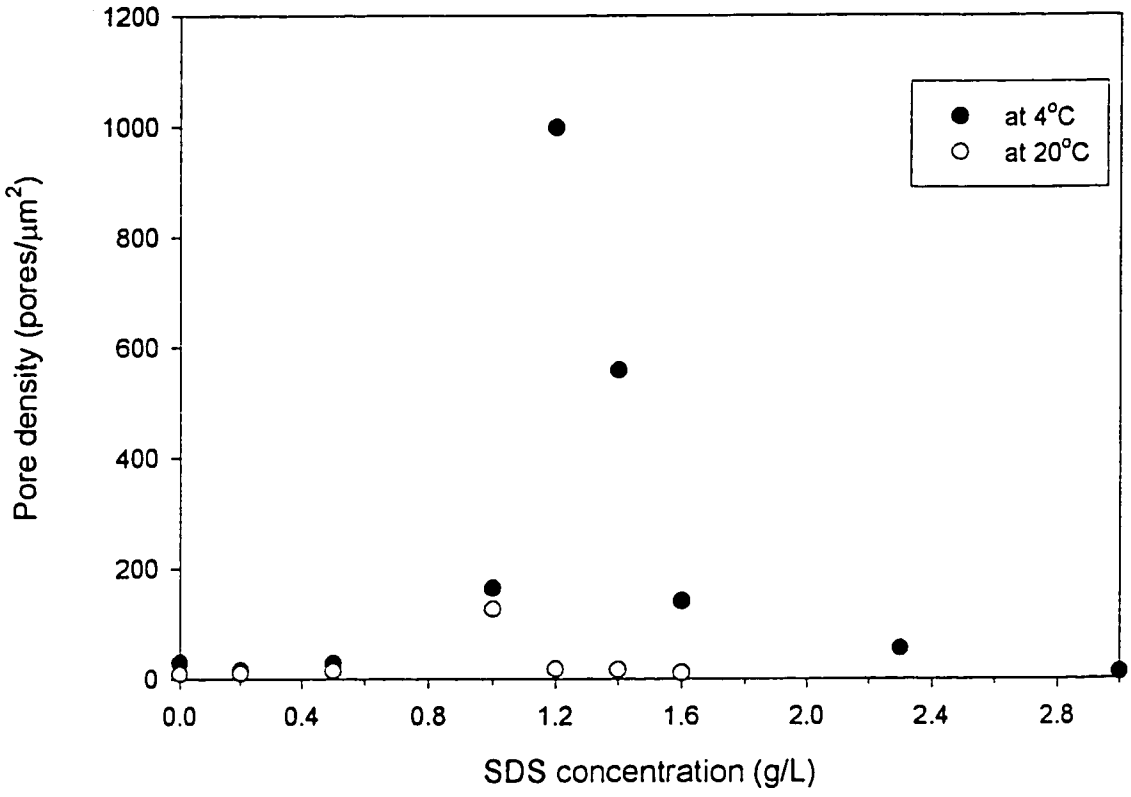

Figure 4.11. Effect of SDS concentration in the gelation bath on the pore density of PES membrans

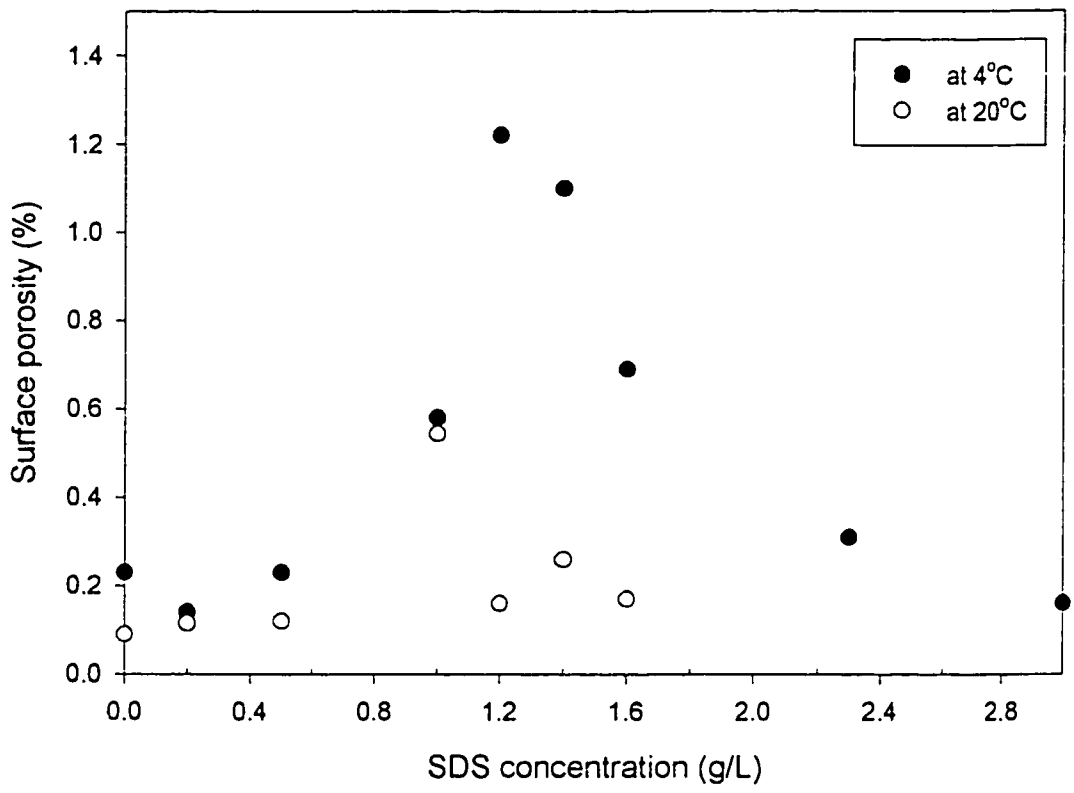

Figure 4.12. Effect of SDS concentration in the gelation bath on the surface porosity of PES membrans

4.3 Effect of Gelation Media Temperature on the Membrane Performance

In the previous section, the effect of SDS concentration in the gelation media was discussed. This effect was the same, as a trend, at the two applied temperatures. However, by looking in Table 4.1 and Figures 4.5, 4.11 and 4.12, the effect of temperature on the values of MWCO, mean pore size, pore density and surface porosity can be noticed. The effect of the temperature in region 1 is different from that effect in region 2.

In region 1, a decrease in temperature will decrease the tendency of the penetration of the nonsolvent to the polymer casting film (Broens et. al, 1980). This slowing of the nonsolvent delays the precipitation of the polymer by delaying the achievement of the solvent/nonsolvent critical value in the casting film. This causes the polymer to concentrate more at the surface and a smaller pore size will be the result. This effect is more pronounced at 0 g/L and 0.2 g/L than at 0.5 g/L and 1.0 g/L. At 0.5 g/L, the MWCOs at both temperatures become close. At 1.0 g/L, the MWCO, the mean pore size, the pore density and the surface porosity become very close to each other, at both temperatures. At 0.5 g/L and 1.0 g/L, the effect of the temperature is less effective because the effect of the SDS concentration becomes stronger and more in control of the nonsolvent/solvent exchange rate. At 1.2 g/L, the difference becomes very big and that is, simply, because these membranes are not in the same region. 1.2 g/L SDS concentration at 4°C is less than CMC, while it is in the CMC range at 20°C. So that, at 4°C more SDS molecules at the interface causes more delay in the solvent/nonsolvent exchange rate and consequently higher polymer solution in the skin layer. The result is a membrane with smaller pore size and higher pore density.

In region 2, on the other hand, a decrease in the temperature causes an increase in SDS molecules stiffness. As SDS molecules become stiffer, the formation of micelles become more difficult (Miller, 1997). The number and the size of the formed micelles will decrease. This is an evident from Figure 4.2, where the conductivity is a measurement of micelles formation. At 4°C, the conductivity is less than that at 20°C. This means that a less number of micelles formed at 4°C. As a result of less formed micelles, the transfer of NMP is slows down, causing a delay in polymer precipitation and small pore size.

4.4 Pure Water Permeation Flux (PWP)

Pure water permeation flux (PWP) is the water flux through the membrane when the feed is distilled water. Figures 4.13 and 4.14 show the effect of SDS concentration in the gelation bath on PWP. The PWP for each membrane is the mean of PWP of five to six cells and the error bars represent the standard deviation around the mean. It is a characteristic of membranes that the flux decreases as the pore size decreases, and what is usually expected is a trend similar to the MWCO (Figure 4.5). If the membranes are taken individually in Figures 4.13 and 4.14, there is no clear trend similar to the one obtained in Figure 4.5, and that is because PWP is not only governed by pore size of the membrane but also by the porosity. The change in the pore size and the porosity do not happen with the same intensity, and that is why the change in PWP does not show a clear trend as the trend in the change in MWCO, pore size and porosity.

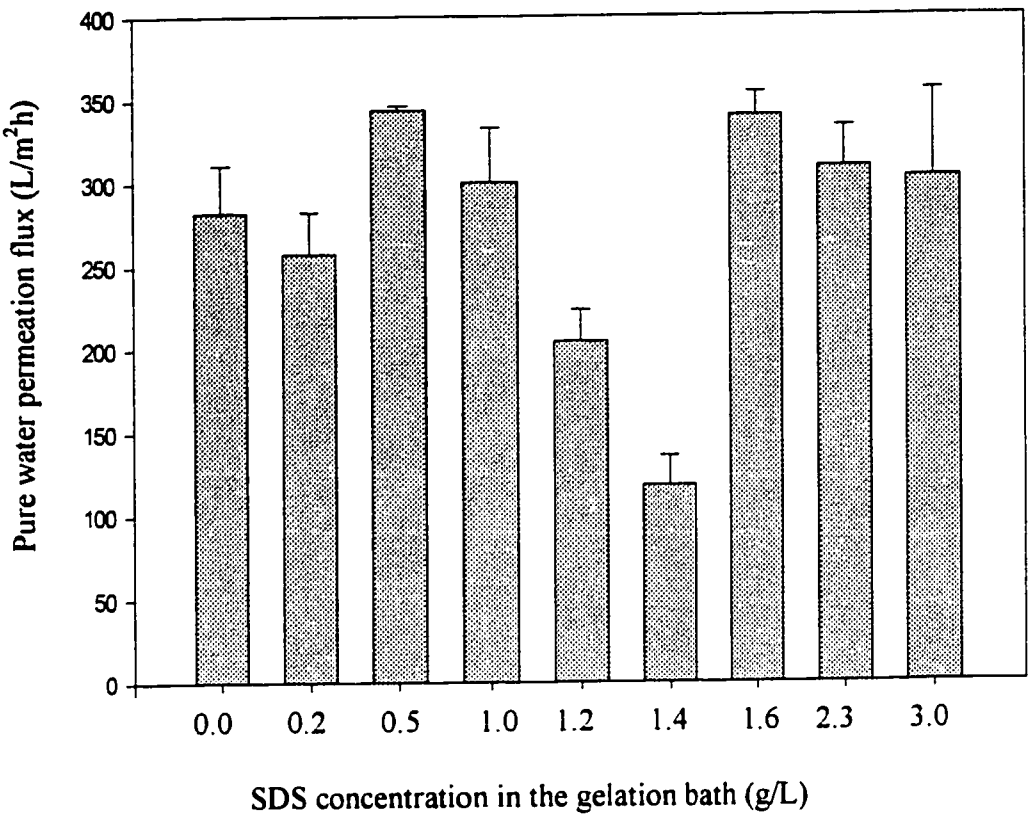

Figure 4.13. Effect of SDS concentration in the gelation bath on the pure water permeation flux of membranes gelled at 4°C (Error bars represent the standard deviation around the mean value).

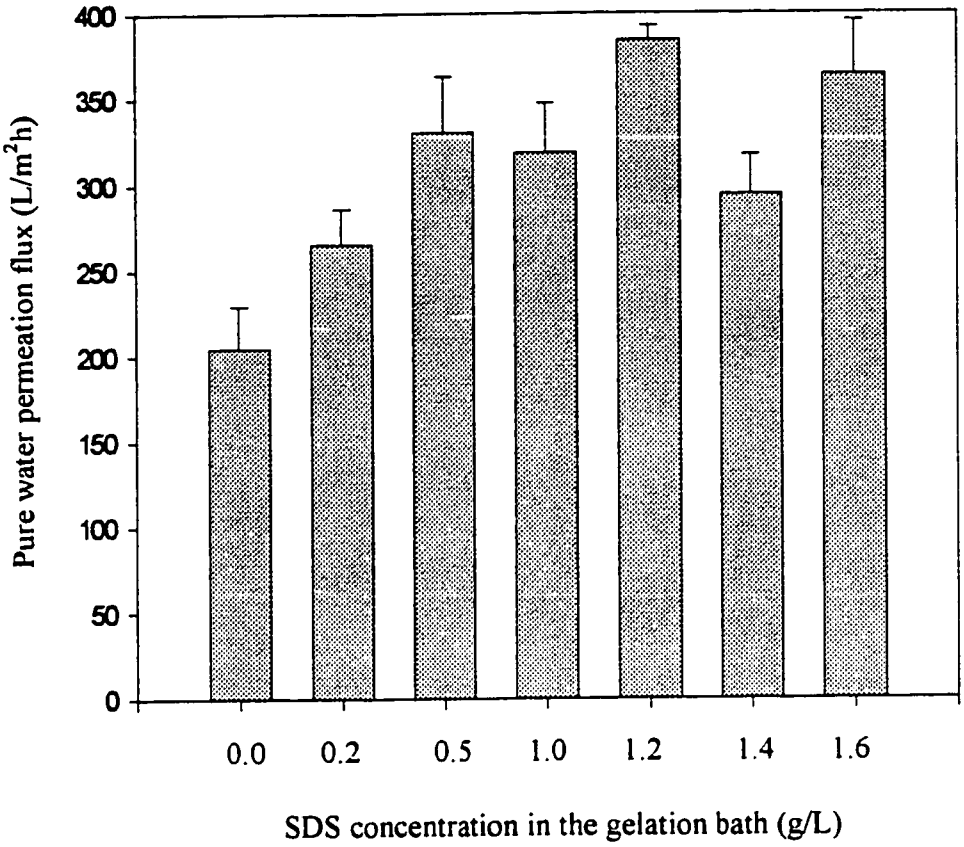

Figure 4.14. Effect of SDS concentration in the gelation bath on the pure water permeation flux of membranes gelled at 20°C (Error bars represent the standard deviation around the mean value).

4.5 Effect of SDS Concentration on Surface Morphology

Figures 4.15 and 4.16 show the representative surface images of membranes gelled in different gelation media. Membrane codes are given below each image. For example, (1.6-20C) indicates a membrane, which was gelled in a gelation medium with SDS concentration of 1.6 g/L at 20°C. The images are presented in 500 nm × 500 nm scanning area with a 15nm Z range. To show the surface variability of a membrane, four different spots on the surface of two different membranes (2.3-4C and 1.0-20C) have been captioned, as examples, and shown in Appendix C.

Surface roughness of membranes was given in terms of the mean roughness (R_a), the root mean square of the Z data (R_q) and the mean difference between the five highest peaks and the five lowest valleys (R_z) which were obtained by using AFM technique. The images in Figures 4.15 and 4.16 were analysed. Each image was divided into four areas of 250 nm × 250 nm. The average values, of the four areas on the surveyed samples, were taken for each roughness parameter and the corresponding standard deviation values were calculated. These results are presented in Table 4.3. These roughness parameters are calculated by software connected to the hardware system of the Nanoscope III.

4.5.1 Comparison of Membrane Roughness Parameters and AFM Images at 4°C

Roughness parameters represent quantification of surface images. The definitions of roughness parameters used in this study were provided in Chapter 3. Considering the data presented in Table 4.3, it can be noticed that roughness parameters for membranes gelled at 4°C decrease with an increase in SDS concentration in the gelation bath, in region 1, and increase with an increase in SDS concentration in the gelation bath, in region 2.

Table 4.3. Various roughness parameters measured from the AFM images of 500 nm × 500 nm for different membranes

SDS percent in the gelation bath (g/L)	Gelation baths at 4°C			Gelation baths at 20°C		
	Roughness parameters					
	R_a (nm)	R_q (nm)	R_z (nm)	R_a (nm)	R_q (nm)	R_z (nm)
0	1.97* ± 0.52**	1.55 ± 0.45	7.93 ± 0.73	0.65 ± 0.21	0.44 ± 0.08	2.30 ± 0.18
0.2	0.76 ± 0.22	0.58 ± 0.17	3.90 ± 0.79	0.53 ± 0.13	0.38 ± 0.02	2.12 ± 0.35
0.5	0.63 ± 0.04	0.51 ± 0.04	2.66 ± 0.23	0.55 ± 0.06	0.41 ± 0.05	2.22 ± 0.30
1.0	0.45 ± 0.07	0.41± 0.18	1.82 ± 0.33	0.58 ± 0.14	0.46 ± 0.10	2.79 ± 0.35
1.2	0.38 ± 0.06	0.31 ± 0.06	1.46 ± 0.28	0.72 ± 0.11	0.59 ± 0.09	3.04 ± 0.24
1.4	0.65 ± 0.12	0.52 ± 0.09	2.84 ± 0.82	0.37 ± 0.27	0.29 ± 0.02	2.17 ± 0.25
1.6	0.57 ± 0.05	0.45 ± 0.04	3.78 ± 0.43	0.63 ± 0.04	0.51 ± 0.04	2.66 ± 0.23
2.3	0.64 ± 0.11	0.50 ± 0.07	3.74 ± 0.53			
3.0	5.05 ± 1.68	3.73 ± 1.16	27.3 ± 12.3			

*Mean value. **Standard deviation.

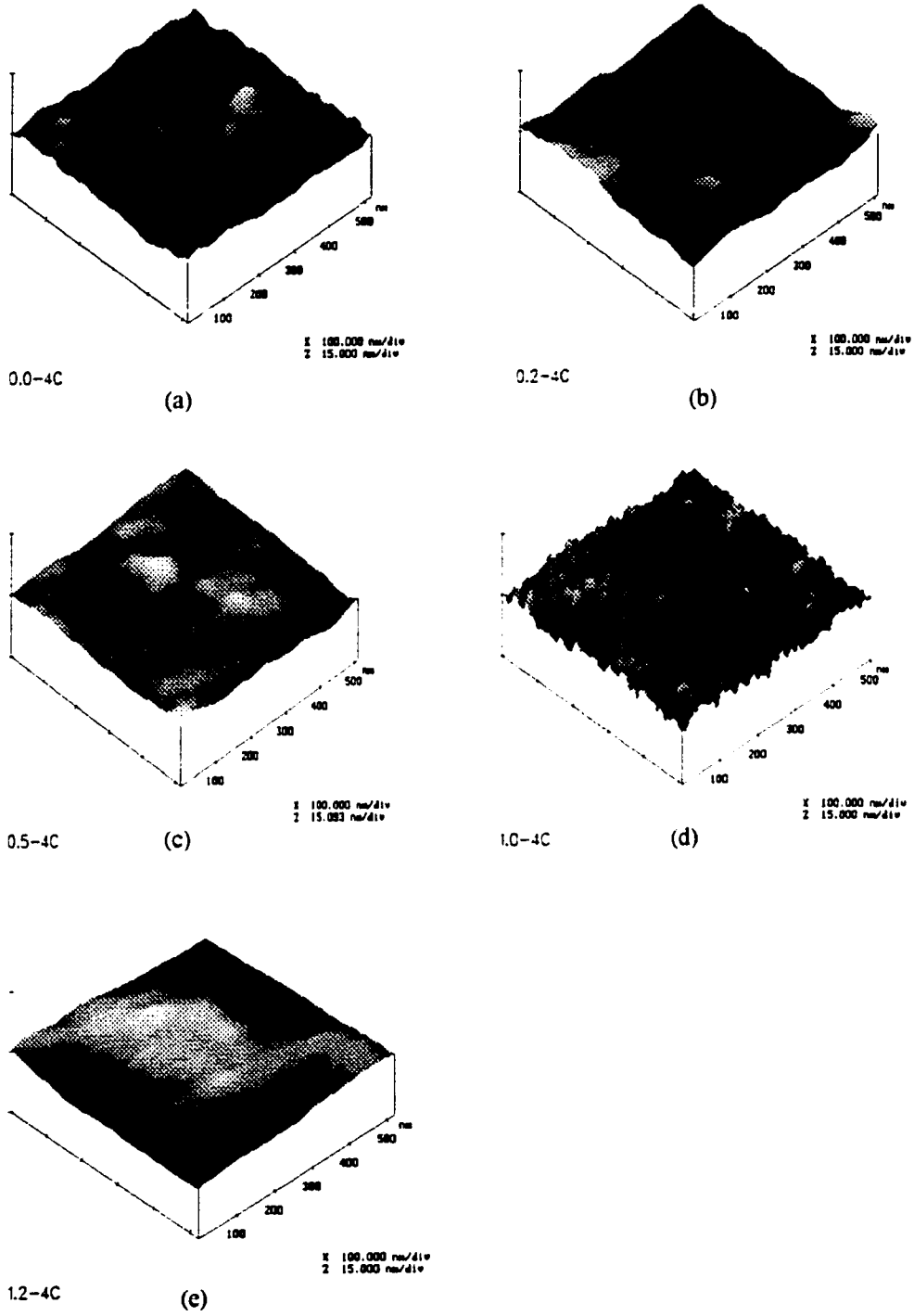

Figure 4.15. Atomic force microscopic images of the top (skin) side of membranes gelled at 4°C. SDS concentrations, (a)0 g/L (b)0.2 g/L (c)0.5 g/L (d)1.0 g/L (e)1.2 g/L.

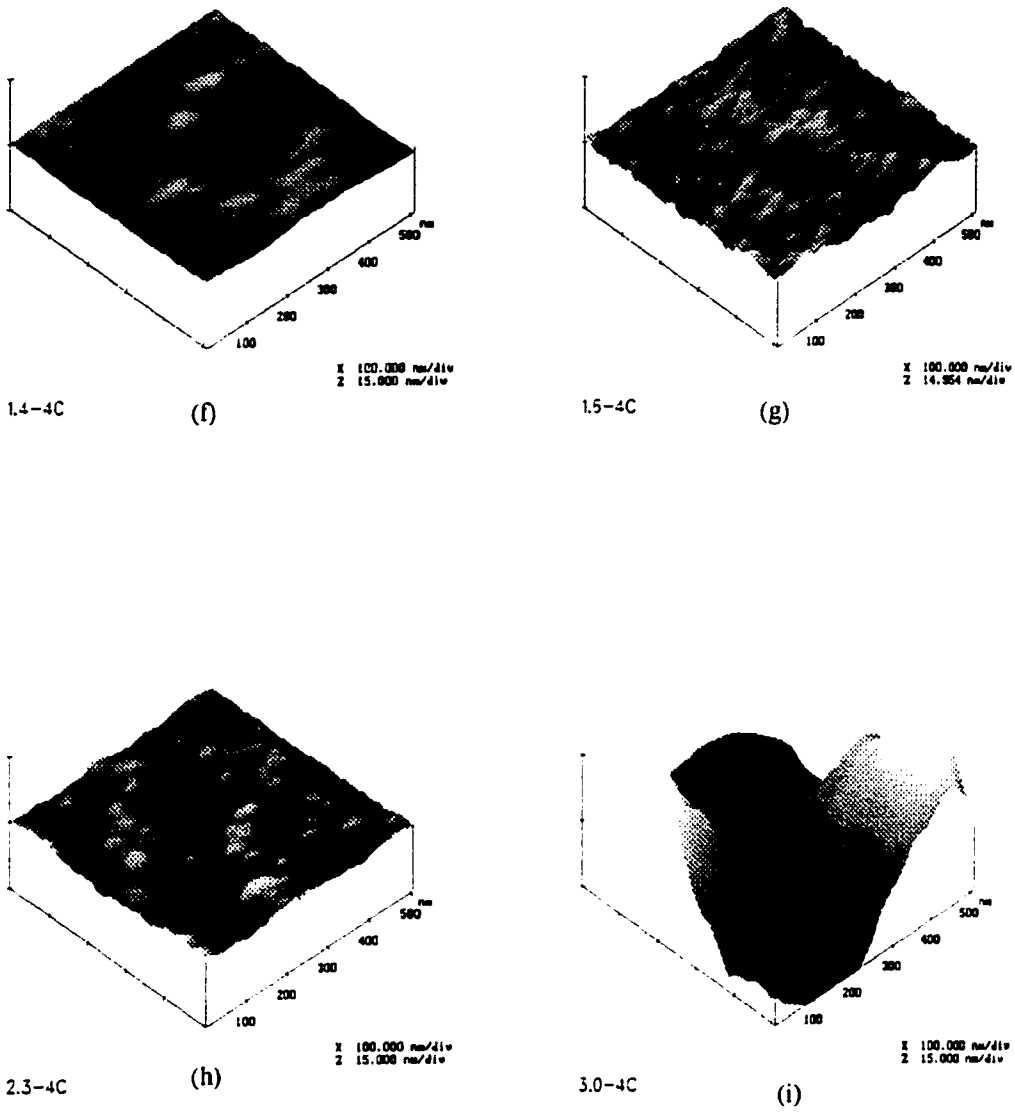

Figure 4.15. Atomic force microscopic images of the top (skin) side of membranes gelled at 4°C. SDS concentrations, (f)1.4 g/L (g)1.6 g/L (h)2.3 g/L (i)3.0 g/L

The change in the roughness parameters goes side by side with the change in MWCO and pore size. The same correlation between MWCO and roughness parameter was also observed by Fritzsche et al. (1992c) Bessieres et al. (1996) and Singh et al. (1998). This change is expected, because the roughness parameters depend on the Z value, which is the vertical distance that the piezoelectric scanner moves. As described in Chapter 3, the movement of the scanner is proportional to the distance that the tip moves up or down on the membrane surface so that, when the surface consists of big depressions (pores) and big peaks (nodules), the tip moves up and down over a high range (high Z values) and the result should be high roughness.

In Figure 4.15 it is shown that the features on the membrane surface change from big peaks and depressions at 0 g/L to smaller ones at 1.0 g/L and then they, completely, disappear at 1.2 g/L. The disappearance of the features does not indicate their absence but is because they become so small that the tip can not sense them.

The features start to show up again, as the roughness increases, by increasing the SDS concentration in the gelation bath in region 2. In the image of the membrane gelled in the bath with 1.6 g/L SDS concentration, the features look like the ones on the membrane gelled in 1.0 g/L SDS concentration. At SDS concentration of 2.3 g/L, the pores look bigger and then they become very big at 3.0 g/L, SDS concentration. The highest roughness parameters were obtained for the membrane gelled in the bath with 3.0 g/L, SDS concentration, which has the highest MWCO and mean pore size. The lowest roughness parameters were obtained for the membrane gelled at 1.2 g/L SDS concentration, which has the lowest MWCO and mean pore size.

4.5.2 Comparison of Membrane Roughness Parameters and AFM Images at 20°C

In Table 4.3, the roughness parameters of membranes gelled at 20°C did not show any significant change and no trend was clear, even though the images in Figure 4.16 showed a different picture. In the images, it is a clear to the naked eye that nodules and pores size change by changing the SDS concentration in the gelation bath. At 0 g/L, the nodules look big and the pores are well characterised by big depressions. Similar to the MWCO, the images of membranes gelled at 0.2 g/L and 0.5 g/L looked similar to the one at 0 g/L. As the concentration of SDS increases to 1.0 g/L, the nodules and the pores become more and smaller. More interestingly, the images at 1.0 g/L at both temperatures look similar, as their MWCO, mean pore size and porosity. As the SDS concentration is increased, in region 2, the depressions become bigger. The only difference that can be noticed in the membranes gelled at 20°C is the shape of the peaks. The tops of the peaks in the images of these membranes look smoother than those in the images of membranes gelled at 4°C. As it is mentioned earlier, the Z value is due to the transfer of the tip vertically on the membrane surface, and because of the softened nodules tops, the change in Z value is not significant to make a difference in the roughness values.

The effect of the temperature could be explained as follows: after the gelation takes place and the pores formed, the nodules are formed in a shape similar to the nodules appearing in 4°C images. At 4°C, the nodules keep their shape because they freeze directly, but at 20°C they melt in a way like the melting of an ice cream cone on a warm day. The melting affects the tops only because the solubility of PES in water is very low.

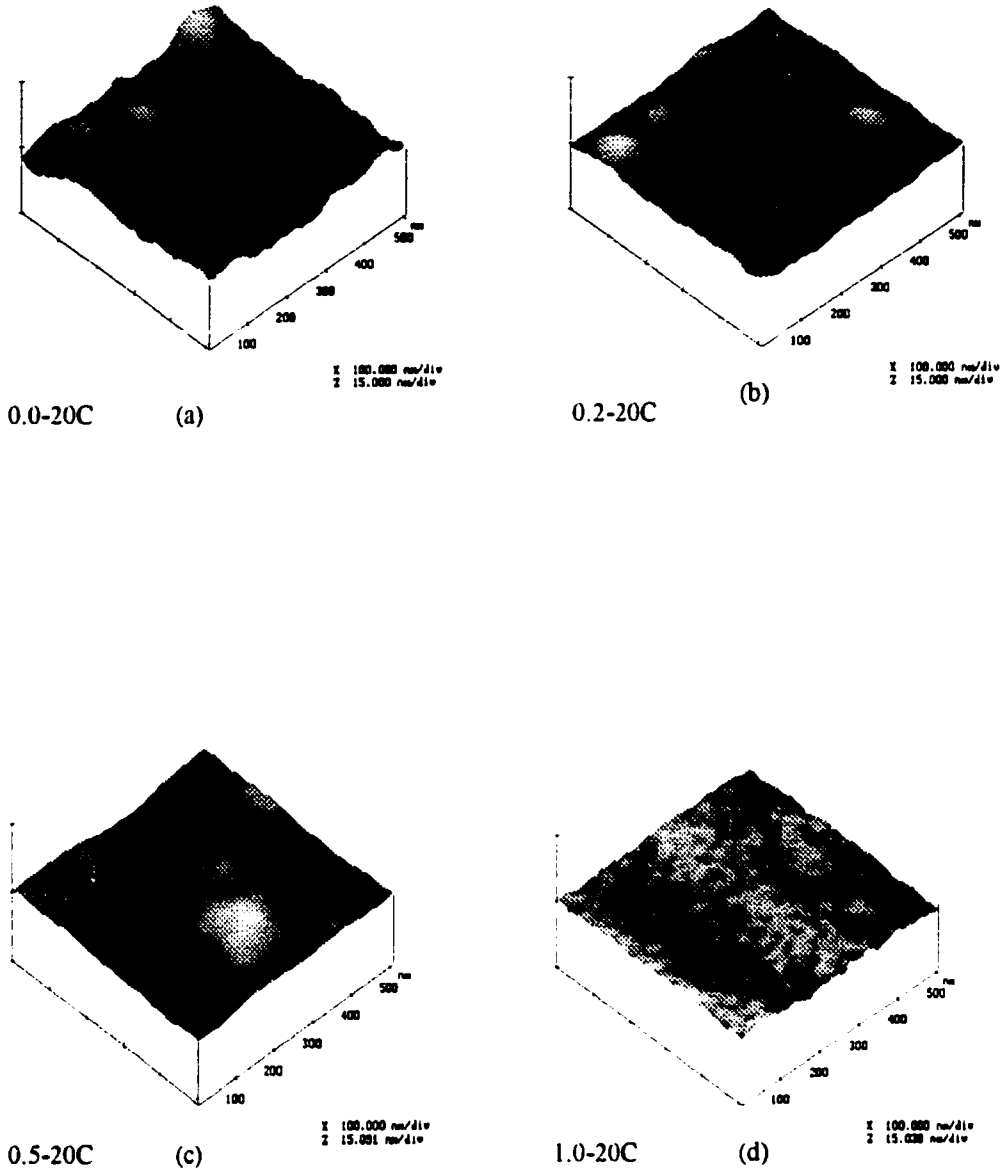

Figure 4.16. Atomic force microscopic images of the top (skin) side of membranes gelled at 20°C. SDS concentrations, (a)0 g/L (b)0.2 g/L (c)0.5 g/L (d)1.0 g/L.

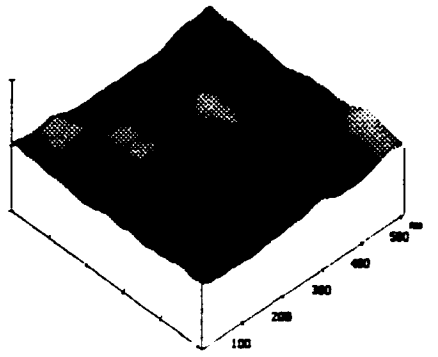

1.2-20C (e)

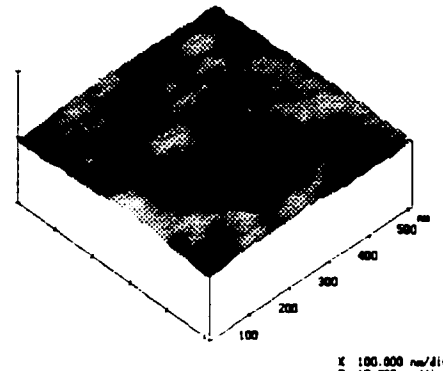

1.4-20C (f)

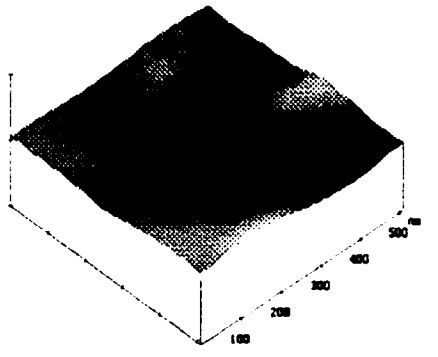

1.6-20C (g)

Figure 4.16. Atomic force microscopic images of the top (skin) side of membranes gelled at 20°C. SDS concentrations, (e)1.2 g/L (f)1.4 g/L (g)1.6 g/L

In general, parallel relations were found between the membrane morphology and the membrane performance (MWCO, mean pore size and porosity) obtained by the solute transport approach. It is most obvious at 4°C that the roughness parameters decreased with an increase in SDS concentration in region 1, while they tend to increase in region 2. This is exactly the same trend, which was found for the MWCO and the mean pore size.

In summary, it can be concluded that the membrane surface becomes rougher as the pore size increases. In addition, the delay, in achieving the critical solvent/nonsolvent ratio, at the interface of the gelation medium and polymer solution renders the membrane surface to become smoother.

CHAPTER 5

5. CONCLUSIONS AND RECOMMENDATIONS

5.1 Conclusions

Gelation media with different concentrations of sodium dodecyl sulfate (SDS) were used in the preparation of polyethersulphone (PES) membranes at two different temperatures. Based on available results, the following conclusions were drawn:

1. The presence of SDS in the gelation medium has an effect on the membranes morphology as well as on the membrane performance. The mean pore size of PES membranes decreased with an increase in SDS concentration in the gelation bath when SDS concentration was below CMC, and increased with an increase in SDS concentration when SDS concentration was above CMC.

2. Comparing the two temperatures at which membranes were gelled, the effect of SDS concentration on the membrane morphology and membrane performance was more pronounced at 4°C than at 20°C.

3. The surface of the membrane became rougher as the pore size increased.

4. Studying the interfacial phenomena of SDS solutions used as gelation media contributes to the understanding of nonsolvent/solvent exchange at the interface and consequently the mechanism of the skin layer formation of asymmetric membranes prepared by the phase inversion technique.

5.2 Recommendations

The following recommendations are formulated based on the results and discussion of this work:

1. To add a surfactant of the same class (alcohol sulfates) but with a higher CMC value to the gelation medium, which shall result in membranes with a smaller pore size. Because of the low efficiency of such surfactant in lowering the surface tension, a big amount of this surfactant is needed to reach the CMC. The big amount of the surfactant at the interface increases the barrier that slows the nonsolvent/solvent exchange rate and as a result increases the polymer concentration in the skin layer. One of such surfactants is $C_8H_{17}SO_4Na$.

2. To use scanning electron microscopic (SEM) technique to obtain a clearer picture of the density of the skin-layer of asymmetric membranes prepared by the phase inversion technique.

CHAPTER 6

6. REFERENCES

Akita, S., Yang, L., and Takeuchi, H., "Micellar-enhanced ultrafiltration of gold(III) with nonionic surfactant", J. Membrane Sci., 133, 189(1997).

Amir, P., Meireles, M., and Sanchez, F., "A contribution to the translation of retention curves into pore size distribution for sieving membranes", J. Membrane Sci., 54, 321(1990).

Bessieres, A., Meireles, M., Cortager, R., Beauvillian, J., and Sanchez, V., "Investigations of surface properties of polymeric membranes by near field microscopy", J. Membrane Sci., 109, 271(1996).

Bindal, R.C., Hanra, M.S., and Misra, B.M., "Novel solvent exchange cum immersion precipitation technique for the preparation of asymmetric polymeric membrane", J. Membrane Sci., 118, 23(1996).

Binning, G., Quate, C.F., and Greber, C., "Atomic force microscope", Phys. Rev. Lett., 56, 930(1986).

Bowen, W.R., Mohammad, A.W., and Hilal, N., "Characterization of nanofiltration membrane for predictive purpose – use os salts, uncharged solutes and atomic force microscopy", J. Membrane. Sci., 126, 91(1997).

Broens, L., Altena, F.W., and Smolders, C.A., "Asymmetric membrane structures as a result of phase separation phenomena", Desalination., 32, 33(1980).

Calvo, J.I., Pradanos, P., Hernandez, A., Bowen, W.R., Hilal, N., Robert, W., and Williams, P.M., "Bulk and surface characterization of composite UF membranes. Atomic force microscopy, gas adsorption-desorption and liquid displacement techniques", J. Membrane Sci., 128, 7(1997).

Cheryan, M., "Ultrafiltration Handbook", Technomic Publishing Company, Inc., Lancaster, (1986).

Cooper , A.R., and Van Derver, D.S., " Characterization of ultrafiltration membranes by polymer transport measurement", Sep. Sci. Technol., 14, 551(1979).

Cox, M., and Flett, D.S., "The significance of surface activity in solvent extraction reagents" ISEC 77, 21, 63(1977).

Darcovich, K., and Kutowy, O., "Surface tension consideration for membrane casting systems", J. Appl. Polym. Sci., 35, 1769(1988).

Davies, J.J and Rideal, E.K., "Interfacial phenomena", 2nd Ed., Academic Press, New York (1963).

Franken, A.C.M., and Fane, A. G., "Environmental management using membranes" in CHEMECA. 90, Australasian Chemical Engineering Conference, Univ,, of Aukland School of Engineering, Aukland, NZ, 754 (1990).

Fritzche, A.K., Arevalo, A.R., Moor, M.D., Elings, V.B., Kjoller, K., and Wu, M.C., "The surface structure and morphology of polyvinylidene fluoride microfiltration membranes by atomic force microscopy", J. Appl. Polym. Sci., 68, 65(1992a).

Fritzche, A.K., Arevalo, A.R., Connolly, A.R., Moor, M.D., Elings, V.B., and Wu, M.C., "The structure and morphology of the skin of polyethersulfone ultrafiltration membranes: a comparative atomic force microscope and scanning electron microscope study", J. Appl. Polym. Sci., 45, 1945(1992b).

Fritzche, A.K., Arevalo, A.R., Moor, M.D., Weber, C.J., Elings, V.B., Kjoller, K., and Wu, M.C., "Image enhancement of polyethersulfone ultrafiltration membrane surface structure for atomic force microscopy" J. Appl. Polym. Sci., 46, 167(1992c).

Frommer, M.A., Reuven, M., and Rosenthal, U., "Mechanism of formation of reverse osmosis membranes" Ind. Chem. Prod. Res. Develop., 10. 193(1971).

Gibbs, J.W., "Collected works, Vol. 1", Longmans-Green, New York, 1928.

Gildert, G.R., Matsuura, T., and Sourirajan, S., "Effect of different alcohol-water mixtures as gelation mediums during formation of cellulose acetate reverse osmosis membranes", J. Appl. Polym. Sci., 24, 305(1979)...

Gourley, L., Britten, M., Gauthier, S.F., and Pouliot, Y., "Characterization of adsorptive fouling on ultrafiltration membranes by peptides mixtures using contact angle measurements" , J. Membrane Sci., 97, 283(1994).

Hirose, M., Ito, H., and Kamiyama, Y., "Effect of surface layer structure on the flux behaviour of RO membranes", J. Membrane Sci., 121, 209(1996).

Hsieh, F.U., Matsuura, T., and Sourirajan, S., "Reverse osmosis separations of polyethylene glycols in dilute aqueous solutions using porous cellulose acetate membranes", J. Appl. Polym. Sci., 23, 561(1979).

Ishguro, M., Matsuura, T., and Detellier, C., "A study on the solute separation and the pore size distribution of montmorillonite membrane", Sep. Sci. Technol., 31, 545(1996).

Jonsson, A., and Jonsson, B., "The influence of nonionic and ionic surfactants on hydrophobic and hydrophilic ultrafiltration membranees", J. Membrane Sci., 56, 49(1991).

Kai, M., Ishii, K., Tsugaya, H., and Miyano, T., "Development of polyether sulfone ultrafiltration membranes", in Reverse osmosis and ultrafiltration, eds. Sourirajan, S., and Matsuura, T., American Chemical Society, Washington, D.C, 1985.

Kassotis, J., Shmidt, J., Hodgins, L.T., and Gregor, H.P., "Modeling of the pore size distribution of ultrafiltration membranes", J. Membrane. Sci., 22, 61(1985).

Kesting, R.E., "Synthetic polymeric membranes: a structural prospective", John Wiley & Sons, Inc., New York, NY, 1985.

Kesting, R.E., and Fritzsche, A.K., "Polymeric gas separation membranes", John Wiley & Sons, Inc., New York, NY, 1993.

Khulbe, K.C., Kruczek, B., Chowdhury, G., and Matsuura, T., "Surface morphology of homogeneous and asymmetric membranes from poly(phenylene oxide) by tapping mode atomic force microscopy", J. Appl. Polym. Sci., 59, 1151(1996).

Lafreniere, L.Y., Talbot, D.F., Matsuura, T., and Sourirajan, S., "Effect of polyvinylpyrrolidone additive on the performance of polyethersulfone ultrafiltration membranes", Ind. Eng. Chem. Res., 26, 2385(1987).

Lau, W.W.Y., Guiver, M.D., and Matsuura, T., "Phase separation in carboxylated polysulphone/solvent/water systems", J. Appl. Polym. Sci., 42, 3215(1991).

Leypoldt, J., "Determining pore size distribution of ultrafiltration membranes by solute sieving – Mathmatical limitations", J. Membrane. Sci., 31, 289(1987).

Liu, T., Xu, S., Zhang, D., Sourirajan, S., and Matsuura,T., "Pore size and pore size distribution on the surface of polyethersulfone hollow fiber membranes", Desalination, 85, 1(1991).

Lonsdale, H.K., "Reverse osmosis" in Synthetic membranes: science, engineering and applications, Bungay, P.M., Lonsdale, H.K and Pinho, M.N., eds., D. Reidel Publishing Company, Dordrecht, Holland, 1983.

Loyen, K., Iliopoulos, I., Audebert, R., and Olsson, U., "Reversible thermal gelation in polymer/surfactant system. Control of the gelation temperature", Langmuir, 11, 1053(1995).

Lui, A., Talbot, F.D.F., Fouda, A., Matsuura, T., and Sourirajan, S., "Studies on solvent exchange technique for making dry cellulose acetate membranes for the separation of gaseous mixtures", J. Appl. Polym. Sci., 36, 1089(1988).

Manne, S., Butt, H.J., Gold, S.A.C and Hansma, P.K., "Imaging metal atoms in air and water using the atomic force microscope", Appl. Phys. Lett., 56, 18(1990).

Matsuura, T., "Synthetic membranes and membrane separation process", CRC Press, Inc., (1993).

McHugh, A.J., and Tsay, C.S., "Dynamic of the phase inversion process", J. Appl. Polym. Sci., 46, 2011(1992).

McLean, D.D and Burn, N.J "Data collection and interpretation", course notes, July (1992).

Meireles, M., Bessieres, A., Rogissart, I., Aimar, P., and Sanchez, V., "An appropriate molecular size parameter for porous membranes calibration", J. Membrane. Sci., 103, 105(1995).

Micheals, A.S., "Analysis and prediction of sieving curves for ultrafiltration membranes: A universal correlation", Sep. Sci. Technol., 15, 1305(1980).

Miller, C. A., "Micellar systems and micromulsions: Solubilization aspects", in Handbook surface and colloid chemistry, Birdi, K. S., ed., CRC Press, Boca Raton, Florida, 1997.

Miller, C., A., and Neogi, P., "Interfacial phenomena : equilibrium and dynamic effects", Marcel Dekker, Inc., New York, 1985.

Miyano, T., Matsuura, T., Carlsson, D.J., and Sourirajan, S., "Retention of polyvinylpyrrolidone swelling agent in the poly(ether p-phenylenesulfone) ultrafiltration membranes", J. Appl. Polym. Sci., 41, 407(1990).

Miyano, T., Matsuura, T., and Sourirajan, S., "Effect of polymer, solvent and casting solution composition on the pore size and the pore size distribution of polyethersulfone (victrex) membranes", Chem. Eng. Comm., 95, 11(1990).

Miyano, T., Matsuura, T., and Sourirajan, S., "Effect of polyvinylpyrrolidone additive on the pore size and the pore size distribution of polyethersulfone (victrex) membranes", Chem. Eng. Comm., 119, 23(1990).

Mulder, M., "Basic principles of membrane technology", 2nd Ed., KluwerAcademic, Dordocht, Boston, (1996).

Myers, D., "Surfactant science and technology", VCH Publishers, Inc., New York, (1988).

Mysels, K.J., "Surface tension of solutions of pure sodium dodecyl sulphate", Langmuir., 2, 423(1986).

Nakao, S., and Kimura, S., "Analysis of solutes rejection in ultrafiltration", J. Chem. Eng. Japan., 14, 32(1981).

Okada, T., and Matsuura, T., " Pattern formation on the surface of cellulose membranes prepared by the phase inversion technique", Ind. Eng. Chem. Res., 27, 1335(1988).

Padday, J.F, in Surface and colloid science, Matijevic, E., ed., Wiley Interscience, New York (1969).

Porter M.R., "Handbook of surfactants", Blackie Academic & Professional, Glasgow, (1994).

Purcell, L.P., Lu, R.J., Thomas, R.K., Howe, M.A., and Penfold, J., " Adsorption of sodium dodecyl sulfate at the surface of aqueous solutions of poly(vinylpyrrolidone) studied by neutron reflection", Langmuir, 14, 1637(1998).

Rosen, M.J., "Surfactants and interfacial phenomena", John Wiley & Sons, Canada, (1989).

Sawistowski, H., "Interfacial phenomena" in Hanson, C. ed., "Recent advances in liquid-liquid extraction", Pergamon Press, Oxford, 1971.

Singh, S., Khulbe, K.C., Matsuura, T., and Ramamurthy, P., "Membrane characterization by solute transport and atomic force microscopy", J. Membrane. Sci., 142, 111(1998).

Smolders, C.A., Reuvers, A.J., Boom, R.M., and Wienk, I.M., "Microstructure in phase inversion membranes. Part1. Formation of macrovoids", J. Membrane. Sci., 73, 259(1992).

Strathmann, H., Kock, K., Amar, P., and Baker, R.W., "The formation mechanism of asymmetric membranes", Desalination, 16, 179(1975).

Strathmann, H., and Kock, K., "The formation mechanism of phase inversion membranes", Desalination, 21, 241(1977).

Strathmann, H., "Synthetic membranes" in synthetic membranes: science, engineering and applications, Bungay, P.M., Lonsdale, H.K and Pinho, M.N., eds., D. Reidel Publishing Company, Dordrecht, Holland, 1983.

Strathmann, H., "Synthetic membranes and their preparation" in Porter, M. C., ed., "Handbook of industrial membrane technology", Noyes, Park Ridge, N.J, 1990.

Tam, C.M., Dal-Cin, M., and Guivar, M.D., "Polysulfone membranes. IV. Performance evaluation of radal A/PVP membranes", J. Membrane. Sci., 78, 123(1993).

Tanny, G.B., "The surface tension of polymer solutions and asymmetric membranes formation", J. Appli. Polym. Sci., 18, 2149(1974).

Tremblay, A.Y., "Finely porous models and radially averaged friction factors", J. Appli. Polym. Sci., 45, 159(1992).

Tsay, C.S., and McHugh, A.J., "The combined effects of evaporation and quench steps on asymmetric membrane formation by phase inversion", J. Polymer. Sci., Polym. Phys., 29, 1261(1991).

Tsay, C.S., and McHugh, A.J., "Mass transfer modelling of asymmetric membrane formation by phase inversion", J. Polymer. Sci., Polym. Phys., 28, 1327(1990).

Tweddle, T.A., and Sourirajan, S., "Effect of ethanol-water as gelation medium during formation of cellulose acetate reverse osmosis membranes", J. Appli. Polym. Sci., 22, 2265(1978).

Wijmans, J.G., and Smolders, C.A., "Preparation of asymmetric membranes by the phase inversion process" in Synthetic membranes: science, engineering and applications, Bungay, P.M., Lonsdale, H.K., and Pinho, M.N., eds., D. Reidel Publishing Company, Dordrecht, Holland, 1983.

Youm, K.H., and Kim, W.S., "Prediction of intrinsic pore properties of ultrafiltration membrane by solute rejection curves: effect of operating conditions on pore properties", J. Chem. Eng. Japan, 24, 1(1991).

Young, T., Lai, J., You, W., and Cheng, L., "Equilibrium phase of the membrane forming water-DMSO-EVAL copolymer system", J. Membrane. Sci., 128, 55(1997).

Zhenxin, Z., "Some factors affecting structure in RO/UF membranes – The result using surface tension measurements" in Matsuura, T., and Sourirajan, S., ed.," Advances in RO and UF membranes", National Resource Council of Canada, Ottawa, 1989.

Appendix A: Raw Data

Separation data, resulted from every used cell, of the testes membranes in this study.

Table A.1: Membranes gelled at 4°C

A.1.a 0 g/L

PEG/PEO Molecular Weight (Da)	Separation (%)					
	Cell 1	Cell 2	Cell 3	Cell 4	Cell 5	Cell 6
10000	26.11	19.72	21.74	21.68	27.46	
12000	54.12	4.35	40.19	51.04	53.43	
20000	62.76	59.36	51.92	1.47	2.85	
35000	77.68	75.4	64.6	71.59	73.1	
100000	98.2	97.6	97.48	97.19	97.62	

A.1.b 0.2 g/L

PEG/PEO Molecular Weight (Da)	Separation (%)					
	Cell 1	Cell 2	Cell 3	Cell 4	Cell 5	Cell 6
10000	32.24	34.56	22.68	27.35	30.51	24.37
20000	58.43	64.23	54.67	58.24	58.64	58.64
35000	62.35	69.25	50.16	64.37	60.35	57.23
100000	97.38	98.87	97.6	97.85	98.34	97.7

A.1.c 0.5 g/L

PEG/PEO Molecular Weight (Da)	Separation (%)					
	Cell 1	Cell 2	Cell 3	Cell 4	Cell 5	Cell 6
4000	12.20	10.67	9.17	12.43	13.90	
10000	27.25	28.63	34.14	32.54	30.70	
20000	52.38	51.62	52.05	53.4	53.78	
35000	73.23	72.94	73	74.01	75.1	
100000	97.7	97.24	97.86	98.51	98.27	

A.1.d 1.0 g/L

PEG/PEO Molecular Weight (Da)	Separation (%)					
	Cell 1	Cell 2	Cell 3	Cell 4	Cell 5	Cell 6
4000	26.30	26.30	20.85	22.80	22.9	
10000	58.28	58.68	50.46	61.95	61.82	
20000	80.60	78.27	72.70	77.08	80.23	
35000	98.20	97.64	9.51	97.18	98.11	

A.1.e 1.2 g/L

PEG/PEO Molecular Weight (Da)	Separation (%)					
	Cell 1	Cell 2	Cell 3	Cell 4	Cell 5	Cell 6
2000	26.32	34.16	23.9	29.81	30.4	24.58
4000	58.28	58.68	50.46	65.46	61.9	52.29
80000	86.21	86.6	88.59	84.61	86.93	86.14
12000	93.08	96.5	96.47	94.35	96.72	94.18

A.1.f 1.4 g/L

PEG/PEO Molecular Weight (Da)	Separation (%)					
	Cell 1	Cell 2	Cell 3	Cell 4	Cell 5	Cell 6
4000	25.43	17.41	29.03	16.57	24	18.21
8000	49.61	45.71	46.57	43.58	44.37	59.43
10000	83.9	84.51	85.66	84.72	83.49	84.69
12000	93.08	94.23	94.30	92.79	94.18	94.78

A.1.g 1.6 g/L

PEG/PEO Molecular Weight (Da)	Separation (%)					
	Cell 1	Cell 2	Cell 3	Cell 4	Cell 5	Cell 6
10000	16.58	13.6	22.87	21.56	30	
12000	53.49	49.9	62.8	64.4	65.33	
20000	47.29	45.39	62.48	68.63	65.33	
35000	96.69	97.26	97.27	97.5	98.44	

A.1.h 2.3 g/L

PEG/PEO Molecular Weight (Da)	Separation (%)					
	Cell 1	Cell 2	Cell 3	Cell 4	Cell 5	Cell 6
10000	32.38	43.45	35.35	53.39	60.02	
20000	54.81	58.92	58.9	67.87	70.38	
35000	79.8	80.55	84.13	85.41	86.33	
100000	96.72	97.46	95.8	98.25	98.74	

A.1.i 3.0 g/L

PEG/PEO Molecular Weight (Da)	Separation (%)					
	Cell 1	Cell 2	Cell 3	Cell 4	Cell 5	Cell 6
10000	10.24	12.72	7.54	7.11	21.5	8.3
20000	45.79	21.59	11.7	12.36	26.1	12.14
35000	41.2	28.9	21.42	22.53	41.23	17.72
100000	94.8	94.27	95.57	65.64	95.89	95.49

Table A.2: Membranes gelled at 20°C

A.2.a 0 g/L

PEG/PEO Molecular Weight (Da)	Separation (%)					
	Cell 1	Cell 2	Cell 3	Cell 4	Cell 5	Cell 6
10000	50.50	49.65	48.29	38.46	24.20	
20000	56.28	54.91	50.7	41.95	27.16	
35000	80.7	75.34	77.6	69.15	57.68	
100000	95.68	95.19	95.65	93.64	94.14	

A.2.b 0.2 g/L

PEG/PEO Molecular Weight (Da)	Separation (%)					
	Cell 1	Cell 2	Cell 3	Cell 4	Cell 5	Cell 6
10000	44.12	38.12	27.65	27.65	29.47	
12000	50.8	42.35	34.19	39.40	38.40	
20000	75.35	68.24	62.94	62.94	62.37	
35000	94.27	94.27	92.37	93.64	92.84	

A.2.c 0.5 g/L

PEG/PEO Molecular Weight (Da)	Separation (%)					
	Cell 1	Cell 2	Cell 3	Cell 4	Cell 5	Cell 6
4000	43.6	33	40.78	36.53	40.92	33.5
10000	62.76	59.36	51.92	61.47	62.85	59.71
20000	67.19	69.6	72.51	72.82	76.02	71.96
35000	83.17	82.71	96.23	84.72	85.64	84.70
100000	93.08	94.23	94.3	92.79	94.18	94.78

A.2.d 1.0 g/L

PEG/PEO Molecular Weight (Da)	Separation (%)					
	Cell 1	Cell 2	Cell 3	Cell 4	Cell 5	Cell 6
4000	11.43	9.20	5.24	7.90	9.37	4.60
10000	69.70	65.75	60.00	74.00	67.50	61.20
20000	81.90	78.28	74.28	83.70	78.70	78.70
35000	91.80	90.60	90.83	93.25	91.70	91.55

A.2.e 1.2 g/L

PEG/PEO Molecular Weight (Da)	Separation (%)					
	Cell 1	Cell 2	Cell 3	Cell 4	Cell 5	Cell 6
10000	30.97	33.9	34.97	30.75	26.73	
20000	45.2	50.7	45.4	51.1	37.16	
35000	60.57	53.8	66.03	53.34	58.37	
100000	98.2	94.6	97.54	97.96	97.65	

A.2.f 1.4 g/L

PEG/PEO Molecular Weight (Da)	Separation (%)					
	Cell 1	Cell 2	Cell 3	Cell 4	Cell 5	Cell 6
10000	15.73	11.86	7.57	13.53	21.51	
20000	26.78	22.37	20.6	24.16	31.3	
35000	56.51	43.47	48.33	44.67	52.06	
100000	97.04	94.62	94.6	95.11	97.02	

A.2.g 1.6 g/L

PEG/PEO Molecular Weight (Da)	Separation (%)					
	Cell 1	Cell 2	Cell 3	Cell 4	Cell 5	Cell 6
10000	23.41	15.7	18.14	19.1		
20000	25.47	10.51	20.81	22.02		
100000	98.26	97.53	98.19	96.86		

Table A.3 Pure water flow for membranes gelled at 4°C

SDS conc. in gelation bath (g/L)	Collected volume (mL) in one minute					
	Cell 1	Cell 2	Cell 3	Cell 4	Cell 5	Cell 6
0	6	5.5	5	5.625	6.75	
0.2	5.4	5.6	4.4	5	5.6	5.6
0.5	6.9	6.5	7.5	7	7	
1.0	6	6.25	5.4	7.2	5.9	
1.2	4.48	3.8	3.84	4.48	4.65	3.84
1.4	3.4	3.8	2.5	3.5	2.0	
1.6	7	7.25	6.75	7.25	6.5	
2.3	6	6.5	6	7.25	6	
3.0	5.5	6	5.25	6	8.25	6.5

Table A.4 Pure water flow for membranes gelled at 20°C

SDS conc. in gelation bath (g/L)	Collected volume (mL) in one minute					
	Cell 1	Cell 2	Cell 3	Cell 4	Cell 5	Cell 6
0	4.5	4.2	5	3.9	4.3	
0.2	5	5.7	6.5	4.8	5.7	
0.5	6.25	7.8	6.7	8	8.7	7.3
1.0	6.2	6.5	5.9	6.3	7.6	6.6
1.2	4.9	4.9	4.5	5.4	5.8	
1.4	6.5	6.8	5.7	7.2	6.6	
1.6	8.5	7.2	6.9	8		

Appendix B: Sample Calculation

Sample of calculation of MWCO, pore size, standard deviation, pore density and porosity by the solute transport technique:

By taking the membrane gelled in 1.0 g/L SDS concentration at 4°C, as an example in this calculation:

1- Use the equation 3.3.16, convert the MW of PEG to radius in cm.

$$a = 16.73 \times 10^{-10} M^{0.557}$$

2- Convert the radius units from cm to nm.

3- The data in Table A1.d will become radius (nm) and separation %:

Table B.1. Separation data of PEG solutions presented in Table A1.d.

Radius(nm)	Separation (%)				
1.70	26.30	26.30	20.85	22.85	22.90
2.84	58.28	58.68	50.46	61.95	61.95
4.17	80.60	78.27	72.70	77.08	80.23
5.70	98.20	97.60	96.50	97.20	98.10

4- Plot the data on a log-normal probability paper, as in Figures 3.3 and 3.4.

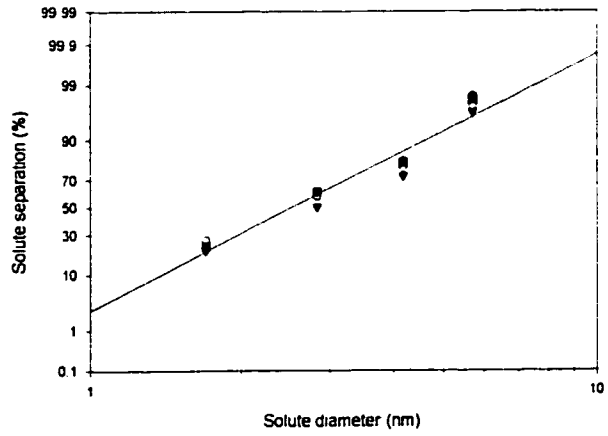

5- Take the radius at 90 % separation

$a = 4.57\ nm = 4.57 \times 10^{-7}\ cm$

and convert the radius to molecular weight by using the equation in step 1

That will be the **MWCO = 23.68 kDa**.

6- The diameter at 50 % is the mean pore size **(μ_p) = 5.02 nm**

7- Dividing the radius at 84.13 % by the radius at 50% will result in the standard deviation around the mean pore size **(σ) = 1.6 nm.**

8- By using equation 3.3.9, calculate number of pores/m^2.

$$N = \frac{128\eta\,\delta\,J}{\pi\Delta P \sum_{d_{min}}^{d_{max}} f_i d_i^4}$$

$\eta = 1 \times 10^{-3}$ kg/m.s

$\delta = 0.2 \times 10^{-6}$ m

$J = 1.12577 \times 10^{-4}$ m^3/m^2s (from table A3 and taking the average area for the used cells 12.27 cm^2).

$\Delta P = 1.0335 \times 10^{6}$ Pa

$f_i d_i^4 = 4.01 \times 10^{-33}$ (from the graph in step 4)

N = 164.6 pores/μm^2

9- By using equation 3.3.10, calculate porosity

$$S_p = \left(\frac{N\pi}{4} \sum_{d_{min}}^{d_{max}} f_i d_i^2 \right)$$

$f_i d_i^2 = 4.48 \times 10^{-17}$ (from the graph in step 4)

S_p = 0.58 %

Appendix C: AFM Images Variability

The following figures are surface images taken by AFM. Each figure shows four surface images for the same membrane, taken at four different spots.

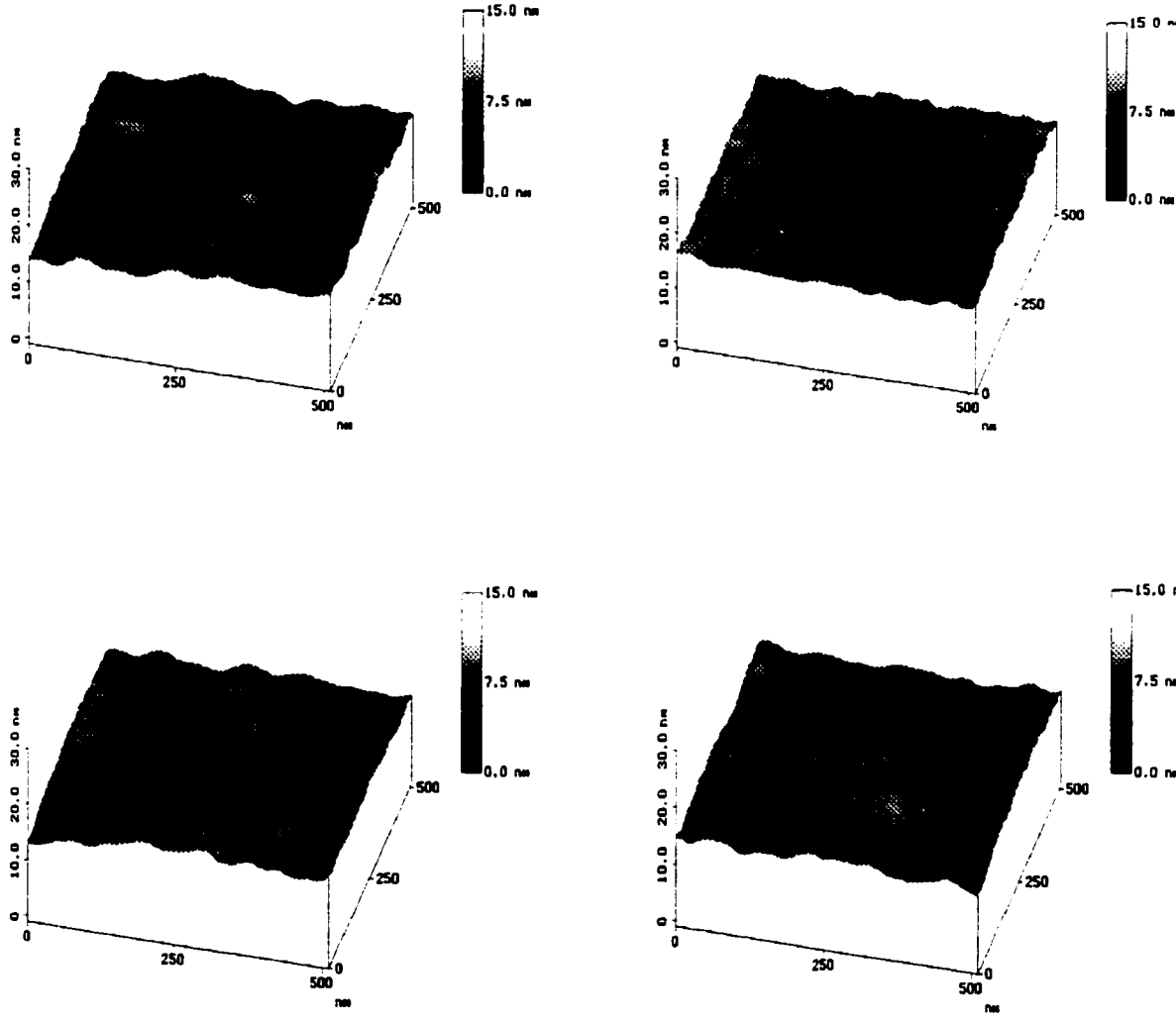

Figure C.1. AFM images for membrane gelled in 2.3 g/L SDS concentration at 4°C.

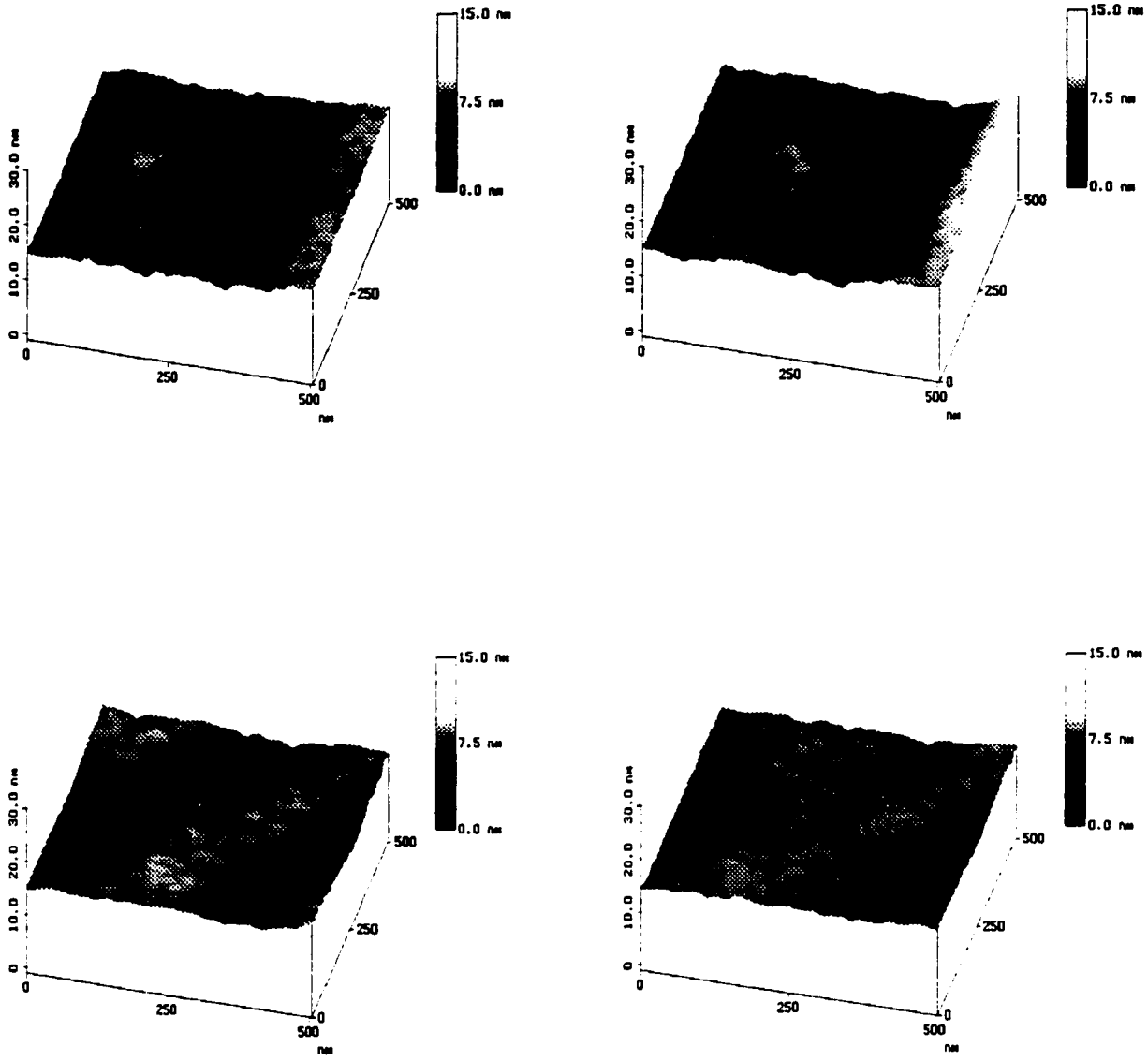

Figure C.2. AFM images for membrane gelled in 1.0 g/L SDS concentration at 20°C.